AN ABSTRACT OF THE THESIS OF

Michael Hoe for the degree of Master of Science in Sustainable Forest Management presented on September 9, 2016.

Title: Multi-temporal LiDAR analysis of landscape fire effects in southwestern Oregon

Abstract approved: ____

Temesgen Hailemariam

Quantitative assessments of post-fire effects are key to improving our understanding of ecosystem resilience. While remote sensing technology has allowed us to assess post-fire landscape effects, we are often limited by the lack of information related to pre-fire forest attributes. As a result, our ability to interpret fire effects in relation to landscape-scale canopy fuel distributions is severely inhibited. We used discrete-return multi-temporal Light Detection and Ranging (LiDAR) to quantify pre-fire basal area, basal area mortality, and post-fire basal area. Observed pre-fire basal area values were reconstructed from field measurements taken 2-years after fire. We modeled pre-fire basal area using a log-linear model, whereas, basal area mortality was modeled with beta regression and change estimation. Model performance was compared using bias, RMSE, RMSPE, AIC, and BIC. We also modeled basal area mortality using a combined approach, where we included RdNBR within the selection process. Intensity values were not used in combined models. In general, LiDAR models outperformed combined models (RMSPE of 0.1293 vs. 0.1347 with 3 and 4 variables, respectively) when quantifying basal area mortality. Intensity metrics improved pre-fire basal area models (reduction in AIC/BIC values ≈ 10-20; not shown). Lastly, we provide multiple examples of practical applications for renewed perspectives

by clearly defining fire effects, directly quantifying, and calibrating remotely sensed LiDAR information to field observations.

Multi-temporal LiDAR Analysis of Landscape Fire Effects in Southwestern Oregon

by
Michael Hoe

A THESIS

submitted to

Oregon State University

in partial fulfillment of
the requirements for the
degree of

Master of Science

Presented September 9, 2016
Commencement June 2017

Master of Science thesis of Michael Hoe presented on September 9, 2016

APPROVED:

Major Professor, representing Sustainable Forest Management

Co-Major Professor, representing Sustainable Forest Management

---

Head of the Department of Forest Engineering, Resources, and Management

---

Dean of the Graduate School

I understand that my thesis will become part of the permanent collection of Oregon State University libraries. My signature below authorizes release of my thesis to any reader upon request.

Michael Hoe, Author

ACKNOWLEDGEMENTS

I would like to thank my wife, mother, and children for their unconditional love, support, and understanding; the Bureau of Land Management and USDA Forest Service for their support and collaboration; Jason McCorkle, Jon Buzawa, and Amanda Gray for a great field season and high quality work; David Bell, David Woodruff, John Bailey, Harold Zald, Matt Reilly, Thomas Hilker, Jody Vogler, and Raymond Davis for their enthusiasm, support, and ideas; Elijah Allensworth, Krishna Poudel, Steven Huff, Joonghoon Shin, Karin Kralicek, Francisco Mauro, and Al Pancoast for their assistance, knowledge, and patience.

CONTRIBUTION OF AUTHORS

Temesgen Hailemariam assisted with interpreting results from data analysis, clarity, and formating for Chapters 2 & 3. Christopher Dunn assisted with sampling design, clarity, and formatting of Chapters 2 & 3.

TABLE OF CONTENTS

TABLE OF CONTENTS (Continued)

LIST OF FIGURES

LIST OF FIGURES (Continued)

LIST OF TABLES

To my wife, mother, & children

Without your strength, love, & support...

I would not be where I am today.

Multi-temporal LiDAR Analysis of Landscape Fire Effects in Southwestern Oregon

1 Chapter One

1.1 General Introduction

Improving our ability to assess landscape-scale fire effects has become increasingly important to land managers and research scientists for a multitude of reasons. For example, the wildland urban interface continues to expand as human populations grow, increasing the risk that fire will impact economic and social assets (Haas et al., 2013; Hammer et al., 2007).. Aggressive fire suppression and historical forest management increased fuel loading over broad landscapes and homogenized forest structures (Duren et al., 2012; Hessburg et al., 2007; Naficy et al., 2010). In addition, global climate projections are predicting longer fire seasons, increased drought conditions, and more frequent extreme fire weather events (Liu et al., 2013; Westerling et al., 2006). Many studies suggest that these conditions are not only unsustainable, but they pose great risk to valuable ecologic, economic, and social resources (Calkin et al., 2005; Jolly et al., 2015; Littell et al., 2009, 2010; Mallek et al., 2013; Marlon et al., 2012).

Approximately 1-2% of fires escaping initial attack account for >95% of annual area burned making remote sensing technology key to quantifying their impacts (Short, 2014; Thompson et al., 2015). Federal land managers and researchers predominantly rely on multi-temporal Landsat TM imagery which relates the normalized burn ratio (NBR) to field estimates of fire severity based on the composite burn index (CBI) (Key and Benson, 1999, 2005; MTBS, 2014). The CBI is a metric which was designed for rapid field assessment of post-fire effects, quantifies mean change across 5 strata, and is measured as an index between 0 (unburned) and 3 (high severity) (Morgan et al., 2014; Wulder et al., 2009). The NBR is calculated from Landsat TM/ETM+ bands 4 and 7 which are sensitive to green vegetation and moisture content, respectively (Escuin et al., 2008; Meng and Meentemeyer, 2011). Correlations between the differenced NBR (dNBR) and CBI are then used to derive thresholds of fire severity across broad landscapes and assess fire effects on soils, fuels, vegetation, wildlife habitat, and tree mortality (Miller and Yool, 2002; Verbyla et al., 2008; Wimberly et al., 2009). An alternative estimator called the relative differenced NBR (RdNBR) was designed to account for variations in pre-fire forest structural conditions by weighting the dNBR indices to pre-fire NBR values Miller and Thode (2007). In contrast to dNBR, which is an absolute change metric, RdNBR is expressed relative to pre-fire conditions. We use RdNBR for our comparisons throughout the remainder of our study because evidence continues to suggest that pre-fire forest characteristics influence post-fire effects (Bolton et al., 2015; Casas et al., 2016; Kane et al., 2013; Miller et al., 2009; Montealegre et al., 2014).

Evidence has shown that these methods have inherent limitations. For example, changes in "greenness" and "blackness" over a given area can be influenced by any vegetative layer, such as grasses or shrubs, complicating the relationship between observed spectral response and ecological effects (Kane et al., 2015; Skowronski et al., 2007; Whittier and Gray, 2016; Wulder et al., 2007). Likewise, pre-fire forested stands with high amounts of canopy cover experiencing low severity fires will optically occlude any remotely sensed spectral change from above. Additionally, forest stands with very low canopy cover experiencing low severity burns (low tree mortality) will be confounded by the removal of pre-fire understory vegetation visible from above. While research suggests that RdNBR may account for some of these shortcomings by including variations in pre-fire forest characteristics (Miller et al., 2009; Miller and Thode, 2007), both dNBR and RdNBR are still subject to 2-dimensionality which constrains their ability to obtain highly precise estimates of fire effects (Bolton et al., 2015; Wulder et al., 2009).

Light Detection and Ranging (LiDAR) offers unique benefits unobtainable by passive remote sensing technology and improvements in the ecological assessment of post-fire effects is highly desired (Bolton et al., 2015; Clark et al., 2010; Kane et al., 2015, 2013; Littell et al., 2010; Montealegre et al., 2014; Seidl et al., 2014; Skowronski et al., 2007, 2011; Wulder et al., 2007). LiDAR uses an airborne laser scanner (ALS) to measure canopy vegetation in three dimensions using discrete-return or full-waveform sensors (Sumnall et al., 2016). It is capable of producing high-resolution digital elevation models and can directly measure vegetation cover, height, and structure (Coops et al., 2007; Næsset, 2007; Persson et al., 2002). Likewise, LiDAR can easily produce landscape-scale maps of forest composition and volume which are used by resource managers to assess wildfire risk and fuels, develop wall-to-wall forest inventories, evaluate wildlife habitat, and more (Bouvier et al., 2015; Bright et al., 2014; Brosofske et al., 2014; Clark et al., 2010; García et al., 2010; Guerra-Hernández et al., 2016; Hall et al., 2005; Means et al., 1999; Skowronski et al., 2011; Woods et al., 2011; Wulder et al., 2012). Furthermore, the spatial distribution of forest canopy fuels or patterns of fire severity could be related to pre-fire stand structures, such as the movement of wildfire from one forest type into another. This would aid in identifying high risk areas, spatially optimizing fuel treatments across stand types and ownership boundaries, and protecting specific wildlife habitats. Additionally, research suggests that the spatial arrangement and composition of legacy species (those surviving after disturbance) drives ecosystem recovery (Lenihan et al., 2008; Lindenmayer et al., 2012; Littell et al., 2010; Seidl et al., 2014). Therefore, being able to provide landscape-scale spatial information on the distribution, location, and composition of post-fire legacy species is highly valuable and applicable.

In the first part of our study, we examined the feasibility of using multi-temporal LiDAR to estimate landscape-scale fire severity using change estimation. LiDAR derived metrics have been shown to generally improve model fit and the estimation of forest attributes relative to historical methods, so we believe LiDAR data can be used for change detection to estimate tree mortality. Our objective was to see if we can improve upon existing methodologies by providing additional information in 3-dimensions.

In the second part of our study, we examined the use of multi-temporal LiDAR as a stand-alone remote sensing platform to quantify basal area before fire, basal area mortality, and basal area after fire. Our study was consciously targeted at improving our understanding of fire effects by providing alternative perspectives of post-fire conditions. We address the need for clearly defined measurements of fire severity and directly quantify fire effects using field observations.

Our study area is composed of three large fires located within the Klamath Mountain Ecoregion in southwestern Oregon. The fires were ignited by lightning on July 26th, 2013 and were declared 100% contained on September 3, 2013. The Douglas Complex encompasses 20,689 ha over a mixed ownership landscape and includes the Dad's Creek and Rabbit Mountain fires. The Big Windy fire covers 11,464 ha of Bureau of Land Management administered lands only. All three areas burned with mixed-severity.

We obtained pre-fire LiDAR data between March 6th and August 16th, 2012. Post-fire LiDAR was collected between September 26th and October 23rd, 2013. Data was collected by Watershed Sciences, Inc. (now known as Quantum Spatial), for the Oregon Department of Geology and Mineral Industries (DOGAMI). The intensity values were normalized during processing by Watershed Science's prior to delivery.

1.2 Literature Review

1.2.1 Future Climate Projections & Concerns

Current climate projections and forestland conditions have prompted much concern within scientific literature over the past decade. Many studies consistently advocate for improvements in the resolution of landscape scale post disturbance assessments, such as wildfire, to develop comprehensive and informed future planning strategies (Allen et al., 2010; Lenihan et al., 2008; Littell et al., 2010; Liu et al., 2013; Mallek et al., 2013; Marlon et al., 2012; Westerling et al., 2011, 2006). In addition, forested landscapes have been extensively altered by past management activities, often increasing fuel continuity over broad landscapes by homogenizing forest structures (Hessburg et al., 2007; Naficy et al., 2010). Likewise, human populations continue to grow and expand into the wildland urban interface, increasing the risk of loss to our valuable social, economic, and ecological resources (Attiwill and Binkley, 2013; Calkin et al., 2005; Dale, 2009; Duren et al., 2012; GAO, 2009; Hammer et al., 2007).

Disturbance events such as wildfires also provide many positive benefits to ecosystems worldwide (Franklin et al., 1987, 2002). Wildfires consume dead and living vegetation, facilitate nutrient cycling, release carbon, and create new open growing space (Wright and Bailey, 1982). Evidence shows that fire severity and subsequent effects, vary due to top-down climate controls and bottom up fuels and topography controls, which alters ecosystem composition and structure at scales varying from micro-sites to landscapes (Agee, 1991; Bowman et al., 2009; Perry et al., 2011). While forest ecosystems are highly dynamic and many tree species have adapted to wildfire events (Brown and Smith, 2000; Dunn and Bailey, 2016), land managers are concerned with ecosystem resilience because of altered disturbance regimes and a rapidly changing climate (Gutschick and BassiriRad, 2003; Littell et al., 2010; Liu et al., 2013; Mallek et al., 2013; Marlon et al., 2012).

1.2.2 Remotely Sensed Fire Effects & Limitations

Great improvements have been made when quantifying landscape fire effects. Remote sensing technology has allowed us to quickly quantify fire effects over very broad scales by differencing spectral information before and after fire (Key and Benson, 1999, 2005). These methods have worked well in quantifying changes in green vegetative canopies (Escuin et al., 2008; Hudak et al., 2007; Meng and Meentemeyer, 2011), however, research continues to highlight specific shortcomings. For example, the 2-dimensionality of the data source will often be confounding due to any vegetative canopy (ground or non-ground) influencing spectral information (Bolton et al., 2015; Whittier and Gray, 2016; Wulder et al., 2009). Research continues to bring this forward as a primary drawback from these methodologies. An alternative was proposed which uses a relative differenced metric which was intended to account for variations in pre-fire conditions. However, both estimates of change are still coming from 2-dimensional data which limits their ability to obtain the most accurate information available (Escuin et al., 2008; Kane et al., 2015, 2013; Miller et al., 2009; Miller and Thode, 2007; Montealegre et al., 2014; Reilly et al., view; Wimberly et al., 2009).

How we define fire severity is also another limitation which is often discussed within the current scientific literature (Keeley, 2009). We currently assess post-fire landscape conditions using field observations which estimate fire severity across multiple strata (Bolton et al., 2015; Key and Benson, 1999, 2005; Miller et al., 2009; Wulder et al., 2009). These methods often make direct interpretation difficult when scientists wish to relate fire severity estimates to specific objectives (Safford et al., 2008). For example, fire effects are measured as a proportion which reflects the average magnitude of fire effects across multiple categories (soils, vegetation, and trees), often lacking additional information (Morgan et al., 2014).

Quantifying fire effects using change estimation and ordinary least squares (OLS) regression can be problematic. We often quantify fire severity as a proportion. As such, the range of responses is bound between 0 and 1. Alternative methods for modeling proportions include arcsine transformation or beta regression (Cribari-Neto and Zeileis, 2010; Ferrari and Cribari-Neto, 2004; Warton and Hui, 2011). Additionally, a simple transformation can be applied to the response variable to account for observations equal to 0 or 1 (Smithson and Verkuilen, 2006). Recent studies have shown beta regression to be useful for estimating forest attributes, such as canopy cover or proportion of biomass by tree component (Eskelson et al., 2011; Korhonen et al., 2007; Poudel and Temesgen, 2016). In contrast, arcsine transformation has been shown to be out-dated and less useful.

1.2.3 Quantifying Landscape Forest Attributes with LiDAR

LiDAR technology has been used to accurately map forest attributes for the last 10 years. It uses an airborne laser scanner (ALS) to measure canopy vegetation in three dimensions by directly quantifying forest attributes such as basal area, tree density, and stand height using discrete-return or full-waveform sensors (Sumnall et al., 2016). Many modeling and prediction approaches have been used such as ordinary least squares (OLS), artificial neural networks and machine learning technology, nearest neighbors, random forest permutations, classification and regression trees (CART), and multivariate adaptive regression splines (MARS) (Brosofske et al., 2014; Coops et al., 2007; Goerndt et al., 2010; Guerra-Hernández et al., 2016; Hall et al., 2005; Hudak et al., 2006; Næsset, 2007; Persson et al., 2002; Popescu and Wynne, 2004; Woods et al., 2011; Wulder et al., 2012). Canopy fuels have also been quantified across landscapes (Clark et al., 2010; Skowronski et al., 2007, 2011). While many of these studies have relied on metrics related to forest cover and structure, others are now showing that intensity values are also highly significant regarding upper canopy biomass (García et al., 2010; Means et al., 1999). In contrast, multi-temporal LiDAR data is much more rare (Kane et al., 2015). Most scientific research is forced into relying on multi-temporal Landsat data rather than LiDAR. Studies then augment the Landsat information with either pre-fire or post-fire LiDAR data to obtain more precise landscape estimates (Bright et al., 2014; Erdody and Moskal, 2010; Hudak et al., 2002; Lefsky et al., 1999; McCombs et al., 2003; Wulder et al., 2007). While some research has been completed and published using multi-temporal LiDAR, there is still much more we can explore.

1.2.4 Fire Ecology & Management Implications

Our understanding of landscape-scale fire effects in relation to pre-fire canopy fuel distributions is limited (Kane et al., 2015, 2013). Much of our current knowledge relies on fire scars and limited information (McBride, 1983). While tree level effects, such as variations in fire resistance or resilience by species and location have been well documented (Agee, 1991; Franklin and DeBell, 1988; Franklin et al., 1987, 2002; Ryan and Frandsen, 1991; Vines, 1968), we lack reliable, consistent information related to pre-fire conditions and fire effects (Ager et al., 2007; Betts et al., 2010; Casas et al., 2016; Clark et al., 2011; Fule et al., 2004; Graham et al., 2004; Lindenmayer et al., 2012; Schoennagel et al., 2004; Seidl et al., 2014; Spies et al., 2010; Thompson and Spies, 2009, 2010; Turner et al., 2003; Vogeler et al., 2014, 2016).

One measure of resilience in forested systems is the ability for trees to naturally regenerate following disturbance. Research suggests that the spatial arrangement and composition of legacy trees drives ecosystem development after disturbance (Gutschick and BassiriRad, 2003; Turner et al., 1998). Therefore, being able to provide landscape scale spatial information on the distribution, location, and density of post-fire legacy species is highly valuable and applicable. Finally, as our understanding and technology improves, estimates and interpretations will become more precise, and our ability to improve pro-active land management could become a reality (Agee and Skinner, 2005; Ager et al., 2010, 2013; Finney et al., 2008; Franklin et al., 2013; Franklin and Johnson, 2012; Johnson et al., 2011).

Literature Cited

Agee, J. K. (1991). Fire history of Douglas-fir forests in the Pacific Northwest. In: Wildlife and Vegetation of Unmanaged Douglas-fir Forests. U.S. Department of Agriculture, Forest Service, Pacific Northwest Research Station, Portland, OR, pp. 25–33.

Agee, J. K. and C. N. Skinner (2005). Basic principles of forest fuel reduction treatments. *Forest ecology and management 211*(1), 83–96.

Ager, A. A., M. A. Finney, B. K. Kerns, and H. Maffei (2007). Modeling wildfire risk to northern spotted owl (strix occidentalis caurina) habitat in central oregon, USA. *Forest Ecology and Management 246*(1), 45–56.

Ager, A. A., N. M. Vaillant, and M. A. Finney (2010). A comparison of landscape fuel treatment strategies to mitigate wildland fire risk in the urban interface and preserve old forest structure. *Forest Ecology and Management 259*(8), 1556–1570.

Ager, A. A., N. M. Vaillant, and A. McMahan (2013). Restoration of fire in managed forests: a model to prioritize landscapes and analyze tradeoffs. *Ecosphere 4*(2), 1–19.

Allen, C. D., A. K. Macalady, H. Chenchouni, D. Bachelet, N. McDowell, M. Vennetier, T. Kitzberger, A. Rigling, D. D. Breshears, E. T. Hogg, et al. (2010). A global overview of drought and heat-induced tree mortality reveals emerging climate change risks for forests. *Forest ecology and management 259*(4), 660–684.

Attiwill, P. and D. Binkley (2013). Exploring the mega-fire reality: a forest ecology and managementconference. *Forest Ecology and Management* (294), 1–3.

Betts, M., J. C. Hagar, J. W. Rivers, J. Alexander, K. McGarigal, and B. McComb (2010). Thresholds in forest bird occurrence as a function of the amount of early-seral broadleaf forest at landscape scales. *Ecological Applications 20*(8), 2116–2130.

Bolton, D. K., N. C. Coops, and M. A. Wulder (2015). Characterizing residual structure and forest recovery following high-severity fire in the western boreal of Canada using landsat time-series and airborne lidar data. *Remote Sensing of Environment 163*, 48–60.

Bouvier, M., S. Durrieu, R. A. Fournier, and J.-P. Renaud (2015). Generalizing predictive models of forest inventory attributes using an area-based approach with airborne lidar data. *Remote Sensing of Environment 156*, 322–334.

Bowman, D. M., J. K. Balch, P. Artaxo, W. J. Bond, J. M. Carlson, M. A. Cochrane, C. M. DAntonio, R. S. DeFries, J. C. Doyle, S. P. Harrison, et al. (2009). Fire in the earth system. *science 324*(5926), 481–484.

Bright, B. C., A. T. Hudak, R. E. Kennedy, and A. J. Meddens (2014). Landsat time series and lidar as predictors of live and dead basal area across five bark beetle-affected forests. *IEEE Journal of Selected Topics in Applied Earth Observations and Remote Sensing 7*(8), 3440–3452.

Brosofske, K. D., R. E. Froese, M. J. Falkowski, and A. Banskota (2014). A review of methods for mapping and prediction of inventory attributes for operational forest management. *Forest Science 60*(4), 733–756.

Brown, J. K. and J. K. Smith (2000). Wildland fire in ecosystems: effects of fire on flora. U.S. Department of Agriculture, Forest Service, Gen. Tech. Rep. RMRS-GTR-42-vol. 2. Ogden, UT, 2000. 257 p.

Calkin, D. E., K. M. Gebert, J. G. Jones, and R. P. Neilson (2005). Forest service large fire area burned and suppression expenditure trends, 1970–2002. *Journal of Forestry 103*(4), 179–183.

Casas, Á., M. García, R. B. Siegel, A. Koltunov, C. Ramírez, and S. Ustin (2016). Burned forest characterization at single-tree level with airborne laser scanning for assessing wildlife habitat. *Remote Sensing of Environment 175*, 231–241.

Clark, D. A., R. G. Anthony, and L. S. Andrews (2011). Survival rates of northern spotted owls in post-fire landscapes of southwest oregon. *Journal of Raptor Research 45*(1), 38–47.

Clark, K. L., N. Skowronski, M. Gallagher, N. Carlo, M. Farrell, and M. R. Maghirang (2010). Assessment of canopy fuel loading across a heterogeneous landscape using lidar. Joint Fire Sciences Program, Project 10-1-02-14, Final Report, U.S. Department of Agriculture, Forest Service, New Lisbon, NJ & Morgantown, WV, 2010.

Coops, N. C., T. Hilker, M. A. Wulder, B. St-Onge, G. Newnham, A. Siggins, and J. T. Trofymow (2007). Estimating canopy structure of douglas-fir forest stands from discrete-return lidar. *Trees 21*(3), 295–310.

Cribari-Neto, F. and A. Zeileis (2010). Beta regression in R. *Journal of Statistical Software 34*(2), 1–24. http://www.jstatsoft.org/v34/i02/.

Dale, L. (2009). The true cost of wildfire in the western US. *Western Forestry Leadership Coalition*. Available at: http://wflccenter.org/news_pdf/324_pdf.pdf, Accessed: February 18, 2015.

Dunn, C. J. and J. D. Bailey (2016). Tree mortality and structural change following mixed-severity fire in Pseudotsuga forests of Oregons western cascades, USA. *Forest Ecology and Management 365*, 107–118.

Duren, O. C., P. S. Muir, and P. E. Hosten (2012). Vegetation change from the Euro-American settlement era to the present in relation to environment and disturbance in southwest Oregon. *Northwest Science 86*(4), 310–328.

Erdody, T. L. and L. M. Moskal (2010). Fusion of lidar and imagery for estimating forest canopy fuels. *Remote Sensing of Environment 114*(4), 725–737.

Escuin, S., R. Navarro, and P. Fernandez (2008). Fire severity assessment by using nbr (normalized burn ratio) and ndvi (normalized difference vegetation index) derived from landsat TM/ETM images. *International Journal of Remote Sensing 29*(4), 1053–1073.

Eskelson, B. N., L. Madsen, J. C. Hagar, and H. Temesgen (2011). Estimating riparian understory vegetation cover with beta regression and copula models. *Forest Science 57*(3), 212–221.

Ferrari, S. and F. Cribari-Neto (2004). Beta regression for modelling rates and proportions. *Journal of Applied Statistics 31*(7), 799–815.

Finney, M. A., R. C. Seli, C. W. McHugh, A. A. Ager, B. Bahro, and J. K. Agee (2008). Simulation of long-term landscape-level fuel treatment effects on large wildfires. *International Journal of Wildland Fire 16*(6), 712–727.

Franklin, J., K. Johnson, D. Churchill, K. Hagmann, D. Johnson, and J. Johnston (2013). Restoration of dry forests in eastern oregon: a field guide. *The Nature Conservancy, Portland, OR*, 202 p.

Franklin, J. F. and D. S. DeBell (1988). Thirty-six years of tree population change in an old-growth pseudotsuga-tsuga forest. *Canadian Journal of Forest Research 18*(5), 633–639.

Franklin, J. F. and K. N. Johnson (2012). A restoration framework for federal forests in the pacific northwest. *Journal of Forestry 110*(8), 429–439.

Franklin, J. F., H. Shugart, and M. E. Harmon (1987). Tree death as an ecological process. *BioScience 37*(8), 550–556.

Franklin, J. F., T. A. Spies, R. Van Pelt, A. B. Carey, D. A. Thornburgh, D. R. Berg, D. B. Lindenmayer, M. E. Harmon, W. S. Keeton, D. C. Shaw, et al. (2002).

Disturbances and structural development of natural forest ecosystems with silvicultural implications, using douglas-fir forests as an example. *Forest Ecology and Management 155*(1), 399–423.

Fule, P. Z., A. E. Cocke, T. A. Heinlein, and W. W. Covington (2004). Effects of an intense prescribed forest fire: is it ecological restoration? *Restoration Ecology 12*(2), 220–230.

GAO (2009). Wildland fire management: Federal agencies have taken important steps forward, but additional, strategic action is needed to capitalize on those steps. *Report to Congressional Addressees GAO-09-877*.

García, M., D. Riaño, E. Chuvieco, and F. M. Danson (2010). Estimating biomass carbon stocks for a mediterranean forest in central Spain using lidar height and intensity data. *Remote Sensing of Environment 114*(4), 816–830.

Goerndt, M. E., V. J. Monleon, and H. Temesgen (2010). Relating forest attributes with area-and tree-based light detection and ranging metrics for western oregon. *Western Journal of Applied Forestry 25*(3), 105–111.

Graham, R. T., S. McCaffrey, and T. B. Jain (2004). Science basis for changing forest structure to modify wildfire behavior and severity. Gen. Tech. Re. RMRS-GTR-120. Fort Collins, CO: U.S. Department of Agriculture, Forest Service, Rock Mountain Research Station. 43 p.

Guerra-Hernández, J., M. Tomé, and E. González-Ferreiro (2016). Using low density lidar data to map mediterranean forest characteristics by means of an area-based approach and height threshold analysis. *Revista de Teledetección* (46), 103–117.

Gutschick, V. P. and H. BassiriRad (2003). Extreme events as shaping physiology, ecology, and evolution of plants: toward a unified definition and evaluation of their consequences. *New Phytologist 160*(1), 21–42.

Haas, J. R., D. E. Calkin, and M. P. Thompson (2013). A national approach for integrating wildfire simulation modeling into wildland urban interface risk assessments within the united states. *Landscape and Urban Planning 119*, 44–53.

Hall, S., I. Burke, D. Box, M. Kaufmann, and J. M. Stoker (2005). Estimating stand structure using discrete-return lidar: an example from low density, fire prone ponderosa pine forests. *Forest Ecology and Management 208*(1), 189–209.

Hammer, R. B., V. C. Radeloff, J. S. Fried, and S. I. Stewart (2007). Wildland–urban interface housing growth during the 1990s in California, Oregon, and Washington. *International Journal of Wildland Fire 16*(3), 255–265.

Hessburg, P. F., R. B. Salter, and K. M. James (2007). Re-examining fire severity relations in pre-management era mixed conifer forests: inferences from landscape patterns of forest structure. *Landscape Ecology 22*(1), 5–24.

Hudak, A., P. Morgan, M. Bobbitt, A. Smith, S. Lewis, L. Lentile, P. Robichaud, J. Clark, and R. McKinley (2007). The relationship of multispectral satellite imagery to immediate fire effects. fire ecology 3 (1): 64-90. *Fire Ecology Special Issue Vol 3*, 66.

Hudak, A. T., N. L. Crookston, J. S. Evans, M. J. Falkowski, A. M. Smith, P. E. Gessler, and P. Morgan (2006). Regression modeling and mapping of coniferous forest basal area and tree density from discrete-return lidar and multispectral satellite data. *Canadian Journal of Remote Sensing 32*(2), 126–138.

Hudak, A. T., M. A. Lefsky, W. B. Cohen, and M. Berterretche (2002). Integration of lidar and landsat ETM+ data for estimating and mapping forest canopy height. *Remote sensing of Environment 82*(2), 397–416.

Johnson, M. C., M. C. Kennedy, and D. L. Peterson (2011). Simulating fuel treatment effects in dry forests of the western united states: testing the principles of a fire-safe forest. *Canadian Journal of Forest Research 41*(5), 1018–1030.

Jolly, W. M., M. A. Cochrane, P. H. Freeborn, Z. A. Holden, T. J. Brown, G. J. Williamson, and D. M. Bowman (2015). Climate-induced variations in global wildfire danger from 1979 to 2013. *Nature communications 6*.

Kane, V. R., C. A. Cansler, N. A. Povak, J. T. Kane, R. J. McGaughey, J. A. Lutz, D. J. Churchill, and M. P. North (2015). Mixed severity fire effects within the rim fire: relative importance of local climate, fire weather, topography, and forest structure. *Forest Ecology and Management 358*, 62–79.

Kane, V. R., J. A. Lutz, S. L. Roberts, D. F. Smith, R. J. McGaughey, N. A. Povak, and M. L. Brooks (2013). Landscape-scale effects of fire severity on mixed-conifer and red fir forest structure in yosemite national park. *Forest Ecology and Management 287*, 17–31.

Keeley, J. E. (2009). Fire intensity, fire severity and burn severity: a brief review and suggested usage. *International Journal of Wildland Fire 18*(1), 116–126.

Key, C. and N. Benson (1999). Measuring and remote sensing of burn severity. In L. F. Neuenschwander and K. C. Ryan (Eds.), *Proceedings joint fire science conference and workshop*, Volume 2, Boise, ID, 15-17 June 1999. University of Idaho and International Association of Wildland Fire, pp. 284.

Key, C. and N. Benson (2005). Landscape assessment: remote sensing of severity, the normalized burn ratio and ground measure of severity, the composite burn index. *FIREMON: Fire effects monitoring and inventory system Ogden, Utah: USDA Forest Service, Rocky Mountain Res. Station*. USDA Forest Service Gen. Tech. Rep. RMRS-GTR-164-CD, LA-1-55.

Korhonen, L., K. T. Korhonen, P. Stenberg, M. Maltamo, and M. Rautiainen (2007). Local models for forest canopy cover with beta regression. *Silva Fennica 41*(4), 671.

Lefsky, M. A., W. B. Cohen, A. Hudak, S. A. Acker, and J. Ohmann (1999). Integration of lidar, landsat ETM+ and forest inventory data for regional forest mapping. *International Archives of Photogrammetry and Remote Sensing 32*, 119–126.

Lenihan, J. M., D. Bachelet, R. P. Neilson, and R. Drapek (2008). Response of vegetation distribution, ecosystem productivity, and fire to climate change scenarios for California. *Climatic Change 87*(1), 215–230.

Lindenmayer, D. B., W. Blanchard, L. McBurney, D. Blair, S. Banks, G. E. Likens, J. F. Franklin, W. F. Laurance, J. A. Stein, and P. Gibbons (2012). Interacting factors driving a major loss of large trees with cavities in a forest ecosystem. *PLoS One 7*(10), e41864.

Littell, J. S., D. McKenzie, D. L. Peterson, and A. L. Westerling (2009). Climate and wildfire area burned in western US ecoprovinces, 1916–2003. *Ecological Applications 19*(4), 1003–1021.

Littell, J. S., E. E. Oneil, D. McKenzie, J. A. Hicke, J. A. Lutz, R. A. Norheim, and M. M. Elsner (2010). Forest ecosystems, disturbance, and climatic change in washington state, USA. *Climatic change 102*(1-2), 129–158.

Liu, Y., S. L. Goodrick, and J. A. Stanturf (2013). Future US wildfire potential trends projected using a dynamically downscaled climate change scenario. *Forest Ecology and Management 294*, 120–135.

Mallek, C., H. Safford, J. Viers, and J. Miller (2013). Modern departures in fire severity and area vary by forest type, Sierra Nevada and southern Cascades, California, USA. *Ecosphere 4*(12), 1–28.

Marlon, J. R., P. J. Bartlein, D. G. Gavin, C. J. Long, R. S. Anderson, C. E. Briles, K. J. Brown, D. Colombaroli, D. J. Hallett, M. J. Power, et al. (2012). Long-term perspective on wildfires in the western USA. *Proceedings of the National Academy of Sciences 109*(9), E535–E543.

McBride, J. R. (1983). Analysis of tree rings and fire scars to establish fire history. *Tree-Ring Bulletin*. 43:51-67.

McCombs, J. W., S. D. Roberts, and D. L. Evans (2003). Influence of fusing lidar and multispectral imagery on remotely sensed estimates of stand density and mean tree height in a managed loblolly pine plantation. *Forest Science 49*(3), 457–466.

Means, J. E., S. A. Acker, D. J. Harding, J. B. Blair, M. A. Lefsky, W. B. Cohen, M. E. Harmon, and W. A. McKee (1999). Use of large-footprint scanning airborne lidar to estimate forest stand characteristics in the western cascades of oregon. *Remote Sensing of Environment 67*(3), 298–308.

Meng, Q. and R. K. Meentemeyer (2011). Modeling of multi-strata forest fire severity using landsat TM data. *International Journal of Applied Earth Observation and Geoinformation 13*(1), 120–126.

Miller, J. D., E. E. Knapp, C. H. Key, C. N. Skinner, C. J. Isbell, R. M. Creasy, and J. W. Sherlock (2009). Calibration and validation of the relative differenced normalized burn ratio (rdnbr) to three measures of fire severity in the Sierra Nevada and Klamath Mountains, California, USA. *Remote Sensing of Environment 113*(3), 645–656.

Miller, J. D. and A. E. Thode (2007). Quantifying burn severity in a heterogeneous landscape with a relative version of the delta normalized burn ratio (dnbr). *Remote Sensing of Environment 109*(1), 66–80.

Miller, J. D. and S. R. Yool (2002). Mapping forest post-fire canopy consumption in several overstory types using multi-temporal landsat TM and ETM data. *Remote Sensing of Environment 82*(2), 481–496.

Montealegre, A. L., M. T. Lamelas, M. A. Tanase, and J. de la Riva (2014). Forest fire severity assessment using ALS data in a mediterranean environment. *Remote Sensing 6*(5), 4240–4265.

Morgan, P., R. E. Keane, G. K. Dillon, T. B. Jain, A. T. Hudak, E. C. Karau, P. G. Sikkink, Z. A. Holden, and E. K. Strand (2014). Challenges of assessing fire and burn severity using field measures, remote sensing and modeling. *International Journal of Wildland Fire 23*(8), 1045–1060.

MTBS (2014). Monitoring trends in burn severity. *USDA Forest Service*. Accessed: December 2014. Available at: http://www.mtbs.gov.

Næsset, E. (2007). Airborne laser scanning as a method in operational forest inventory: Status of accuracy assessments accomplished in Scandinavia. *Scandinavian Journal of Forest Research 22*(5), 433–442.

Naficy, C., A. Sala, E. G. Keeling, J. Graham, and T. H. DeLuca (2010). Interactive effects of historical logging and fire exclusion on ponderosa pine forest structure in the northern rockies. *Ecological Applications 20*(7), 1851–1864.

Perry, D. A., P. F. Hessburg, C. N. Skinner, T. A. Spies, S. L. Stephens, A. H. Taylor, J. F. Franklin, B. McComb, and G. Riegel (2011). The ecology of mixed severity fire regimes in Washington, Oregon, and Northern California. *Forest Ecology and Management 262*(5), 703–717.

Persson, A., J. Holmgren, and U. Söderman (2002). Detecting and measuring individual trees using an airborne laser scanner. *Photogrammetric Engineering and Remote Sensing 68*(9), 925–932.

Popescu, S. C. and R. H. Wynne (2004). Seeing the trees in the forest. *Photogrammetric Engineering & Remote Sensing 70*(5), 589–604.

Poudel, K. P. and H. Temesgen (2016). Developing biomass equations for western hemlock and red alder trees in western oregon forests. *Forests 7*(4), 88.

Reilly, M. J., C. J. Dunn, G. W. Meigs, T. A. Spies, R. E. Kennedy, J. D. Bailey, and K. Briggs (*in review*). Contemporary patterns of burn severity in forests of the pacific northwest (1985-2010). *Forest Ecology and Management*.

Ryan, K. C. and W. H. Frandsen (1991). Basal injury from smoldering fires in mature pinus ponderosa laws. *International Journal of Wildland Fire 1*(2), 107–118.

Safford, H. D., J. Miller, D. Schmidt, B. Roath, and A. Parsons (2008). BAER soil burn severity maps do not measure fire effects to vegetation: a comment on Odion and Hanson (2006). *Ecosystems 11*(1), 1–11.

Schoennagel, T., T. T. Veblen, and W. H. Romme (2004). The interaction of fire, fuels, and climate across rocky mountain forests. *BioScience 54*(7), 661–676.

Seidl, R., W. Rammer, and T. A. Spies (2014). Disturbance legacies increase the resilience of forest ecosystem structure, composition, and functioning. *Ecological Applications 24*(8), 2063–2077.

Short, K. (2014). A spatial database of wildfires in the United States, 1992-2011. *Earth System Science Data 6*(1), 1–27.

Skowronski, N., K. Clark, R. Nelson, J. Hom, and M. Patterson (2007). Remotely sensed measurements of forest structure and fuel loads in the pinelands of New Jersey. *Remote Sensing of Environment 108*(2), 123–129.

Skowronski, N. S., K. L. Clark, M. Duveneck, and J. Hom (2011). Three-dimensional canopy fuel loading predicted using upward and downward sensing lidar systems. *Remote Sensing of Environment 115*(2), 703–714.

Smithson, M. and J. Verkuilen (2006). A better lemon squeezer? maximum-likelihood regression with beta-distributed dependent variables. *Psychological methods 11*(1), 54.

Spies, T. A., J. D. Miller, J. B. Buchanan, J. F. Lehmkuhl, J. F. Franklin, S. P. Healey, P. F. Hessburg, H. D. Safford, W. B. Cohen, R. S. Kennedy, et al. (2010).

Underestimating risks to the northern spotted owl in fire-prone forests: Response to Hanson et al. *Conservation Biology 24*(1), 330–333.

Sumnall, M. J., R. A. Hill, and S. A. Hinsley (2016). Comparison of small-footprint discrete return and full waveform airborne lidar data for estimating multiple forest variables. *Remote Sensing of Environment 173*, 214–223.

Thompson, J. R. and T. A. Spies (2009). Vegetation and weather explain variation in crown damage within a large mixed-severity wildfire. *Forest Ecology and Management 258*(7), 1684–1694.

Thompson, J. R. and T. A. Spies (2010). Factors associated with crown damage following recurring mixed-severity wildfires and post-fire management in southwestern oregon. *Landscape Ecology 25*(5), 775–789.

Thompson, M. P., J. R. Haas, M. A. Finney, D. E. Calkin, M. S. Hand, M. J. Browne, M. Halek, K. C. Short, and I. C. Grenfell (2015). Development and application of a probabilistic method for wildfire suppression cost modeling. *Forest Policy and Economics 50*, 249–258.

Turner, M. G., W. L. Baker, C. J. Peterson, and R. K. Peet (1998). Factors influencing succession: lessons from large, infrequent natural disturbances. *Ecosystems 1*(6), 511–523.

Turner, M. G., W. H. Romme, and D. B. Tinker (2003). Surprises and lessons from the 1988 Yellowstone fires. *Frontiers in Ecology and the Environment 1*(7), 351–358.

Verbyla, D. L., E. S. Kasischke, and E. E. Hoy (2008). Seasonal and topographic effects on estimating fire severity from landsat TM/ETM+ data. *International Journal of Wildland Fire 17*(4), 527–534.

Vines, R. (1968). Heat transfer through bark, and the resistance of trees to fire. *Australian Journal of Botany 16*(3), 499–514.

Vogeler, J. C., A. T. Hudak, L. A. Vierling, J. Evans, P. Green, and K. T. Vierling (2014). Terrain and vegetation structural influences on local avian species richness in two mixed-conifer forests. *Remote Sensing of Environment 147*, 13–22.

Vogeler, J. C., Z. Yang, and W. B. Cohen (2016). Mapping post-fire habitat characteristics through the fusion of remote sensing tools. *Remote Sensing of Environment 173*, 294–303.

Warton, D. I. and F. K. C. Hui (2011). The arcsine is asinine: the analysis of proportions in ecology. *Ecology 92*(1), 3–10. http://dx.doi.org/10.1890/10-0340.1.

Westerling, A., B. Bryant, H. Preisler, T. Holmes, H. Hidalgo, T. Das, and S. Shrestha (2011). Climate change and growth scenarios for California wildfire. *Climatic Change 109*(1), 445–463.

Westerling, A. L., H. G. Hidalgo, D. R. Cayan, and T. W. Swetnam (2006). Warming and earlier spring increase western US forest wildfire activity. *Science 313*(5789), 940–943.

Whittier, T. R. and A. N. Gray (2016). Tree mortality based fire severity classification for forest inventories: A pacific northwest national forests example. *Forest Ecology and Management 359*, 199–209.

Wimberly, M. C., M. A. Cochrane, A. D. Baer, and K. Pabst (2009). Assessing fuel treatment effectiveness using satellite imagery and spatial statistics. *Ecological Applications 19*(6), 1377–1384.

Woods, M., D. Pitt, M. Penner, K. Lim, D. Nesbitt, D. Etheridge, and P. Treitz (2011). Operational implementation of a lidar inventory in boreal Ontario. *The Forestry Chronicle 87*(4), 512–528.

Wright, H. A. and A. W. Bailey (1982). *Fire ecology: United States and southern Canada.* John Wiley & Sons. pp 15–22.

Wulder, M., J. White, F. Alvarez, T. Han, J. Rogan, and B. Hawkes (2009). Characterizing boreal forest wildfire with multi-temporal landsat and lidar data. *Remote Sensing of Environment 113*(7), 1540–1555.

Wulder, M. A., T. Han, J. C. White, T. Sweda, and H. Tsuzuki (2007). Integrating profiling lidar with landsat data for regional boreal forest canopy attribute estimation and change characterization. *Remote Sensing of Environment 110*(1), 123–137.

Wulder, M. A., J. C. White, R. F. Nelson, E. Næsset, H. O. Ørka, N. C. Coops, T. Hilker, C. W. Bater, and T. Gobakken (2012). Lidar sampling for large-area forest characterization: A review. *Remote Sensing of Environment 121*, 196–209.

Multi-temporal LiDAR Improves Landsacpe-scale Estimates of Fire Severity

2 Chapter Two

2.1 Abstract

Improving our ability to assess landscape-scale fire effects has become increasingly important to land managers and research scientists for a multitude of reasons. In this study we examined the feasibility of using multi-temporal LiDAR and change estimation to quantify landscape-scale fire severity. We examined metrics related to changes in the x, y, and z-dimensions along with foliar reflectance, with the understanding that fire effects are highly variable and influenced by forest structural characteristics. We also examine combining RdNBR with LiDAR derived metrics to quantify fire severity to find the best method for capturing proportion of fire-induced basal area mortality. We define fire severity as the proportion of fire-induced basal area mortality and model landscape conditions using beta regression. LiDAR models performed the best with 3 covariates (RMSPE: 0.1293). Combined models also substantially improved current estimates, but required 4 covariates related to pre-fire forest structure and change estimation (RdNBR only - 0.20, Combined - 0.1347). Our results confirm that the ability to detect change in 3-dimensions helps ameliorate some of the inaccuracies associated with passive, satellite-based remote sensing platforms.

2.2 Introduction

The wildland urban interface continues to expand as human populations grow, increasing the risk that fire will impact economic and social assets (Haas et al., 2013;

Hammer et al., 2007). Aggressive fire suppression and historical forest management increased fuel loading and homogenized forest structures over broad landscapes (Duren et al., 2012; Hessburg et al., 2007; Naficy et al., 2010). In addition, global climate projections are predicting longer fire seasons, increased drought conditions, and more frequent extreme fire weather events (Liu et al., 2013; Westerling et al., 2006). Many studies suggest that these conditions vastly increase the likelihood that we will experience greater loss to highly-valued ecological, economic, and social resources to wildfires in the years to come (Calkin et al., 2005; Jolly et al., 2015; Littell et al., 2009, 2010; Mallek et al., 2013; Marlon et al., 2012).

Approximately 1-2% of fires escaping initial attack account for >95% of annual area burned making remote sensing technology key to quantifying their impacts (Short, 2014; Thompson et al., 2015). Federal land managers and researchers predominantly rely on multi-temporal Landsat TM imagery which relates the normalized burn ratio (NBR) to field estimates of fire severity based on the composite burn index (CBI) (Key and Benson, 1999, 2005; MTBS, 2014). The CBI is a metric which was designed for rapid field assessment of post-fire effects, quantifies mean change across 5 strata, and is measured as an index between 0 (unburned) and 3 (high severity) (Morgan et al., 2014; Wulder et al., 2009). The NBR is calculated from Landsat TM/ETM+ bands 4 and 7 which are sensitive to green vegetation and moisture content, respectively (Escuin et al., 2008; Meng and Meentemeyer, 2011). Correlations between the differenced NBR (dNBR) and CBI are then used to derive thresholds of fire severity across broad landscapes and assess fire effects on soils, fuels, vegetation, wildlife habitat, and tree mortality (Miller and Yool, 2002; Verbyla et al., 2008; Wimberly et al., 2009). An alternative estimator was designed by Miller and Thode (2007) to account for variations in pre-fire forest structural conditions by weighting the dNBR indices to pre-fire NBR values. In contrast to dNBR, which is an absolute change metric, the relative differenced normalized burn ratio (RdNBR) is expressed relative to pre-fire conditions.

While continuous in spatial coverage over a relatively long time period, Landsat satellite imagery has inherent limitations for use in specific research and management objectives (Lentile et al., 2006; Morgan et al., 2014). For example, RdNBR values are influenced by any visible vegetative layer from above, including grasses, shrubs and trees, complicating the relationship between observed spectral response and ecological effects (Kane et al., 2015; Skowronski et al., 2007; Whittier and Gray, 2016; Wulder et al., 2007). Pre-fire forested stands with high amounts of canopy cover experiencing low severity fires will optically occlude any remotely sensed spectral change from above. Additionally, forest stands with very low canopy cover experiencing low severity burns (low tree mortality) will be confounded by the removal of pre-fire understory vegetation visible from above. While Landsat imagery has been shown to be useful when quantifying changes in “greenness” and “blackness” over a landscape (Escuin et al., 2008; Hudak et al., 2007; Meng and Meentemeyer, 2011), the 2-dimensional nature of the data source constrains our ability to obtain highly precise estimates of fire effects (Bolton et al., 2015; Lentile et al., 2006; Morgan et al., 2014; Wulder et al., 2009).

Alternative remote sensing platforms are available that have the potential to quantify fire effects with greater precision (Bolton et al., 2015; Clark et al., 2010; Kane et al., 2015, 2013; Montealegre et al., 2014; Skowronski et al., 2007, 2011; Wulder et al., 2007). Light Detection and Ranging (LiDAR) uses an airborne laser scanner (ALS) to measure canopy vegetation in three dimensions using discrete-return or full-waveform sensors (Sumnall et al., 2016). Contrary to passive remote sensing platforms, LiDAR is capable of producing high-resolution digital elevation models and can directly measure vegetation cover, height, and structure (Coops et al., 2007; Næsset, 2007; Persson et al., 2002). Recent applications of LiDAR demonstrate its ability to generate landscape level maps of forest attributes, such as canopy fuel weight, canopy bulk density, upper canopy biomass, carbon stocks, and basal area (Bouvier et al., 2015; Bright et al., 2014; Brosofske et al., 2014; Clark et al., 2010; García et al., 2010; Guerra-Hernández et al., 2016; Hall et al., 2005; Means et al., 1999; Skowronski et al., 2011; Woods et al., 2011; Wulder et al., 2012). Additionally, research has shown that LiDAR can improve current remotely sensed data by providing additional information in 3-dimensions using an integrated approach (Erdody and Moskal, 2010; Hudak et al., 2002; Lefsky et al., 1999; McCombs et al., 2003; Popescu and Wynne, 2004). Therefore, we hypothesize that multi-temporal LiDAR could offer an assessment of disturbance effects through change detection based on these and other forest attributes.

In this study we examine the feasibility of using discrete-return multi-temporal LiDAR and change estimation to quantify fire severity. We define fire severity as the proportion of fire-induced basal area mortality (Keeley, 2009; Lentile et al., 2006; Morgan et al., 2014). Our objective is determine whether we can improve the precision of current remotely sensed fire severity estimates. We examine selected models using solely multi-temporal LiDAR. In addition, we apply a combined approach and model basal area mortality using both, RdNBR and LiDAR metrics. Our goal is to find the best method for quantifying proportion of fire-induced basal area mortality.

Question 1: *Can multi-temporal LiDAR quantify fire severity (basal area mortality), through change detection?*

Question 2: *How do fire severity estimates from multi-temporal LiDAR compare with estimates from Landsat derived metrics?*

Question 3: *Can we combine remote sensing data from both (LiDAR and RdNBR) to improve estimates?*

2.3 Methods

2.3.1 Study Area

Our study area focused on three large fires within the Klamath Mountain Ecoregion of southwestern Oregon (Omernik and Griffith, 2014). The fires were ignited by lightning on July 26th, 2013 and were declared 100% contained on September 3, 2013 (InciWeb, 2013). The Douglas Complex encompasses 20,689 ha over a mixed ownership landscape and includes the Dad's Creek and Rabbit Mountain fires. The Big Windy fire covers 11,464 ha of Bureau of Land Management administered lands only (Figure 2.1). All three areas burned with mixed-severity, driven by the dry Mediterranean climate, segmented terrain, and topographical attributes (Agee, 1991; Halofsky et al., 2011; Skinner et al., 2006; Taylor and Skinner, 1998).

The Klamath Mountain Ecoregion has highly diverse flora due to frequent mixed-severity fires (Agee, 1991; Halofsky et al., 2011; Perry et al., 2011; Thompson and Spies, 2010). Forested plant communities are dominated by oak woodlands and mixed-evergreen forests, although some mixed-conifer forests exist at higher elevations (Franklin and DeBell, 1988). Dominant tree species include Douglas-fir (*Pseudotsuga menziesii (Mirb.) Franco*), Pacific madrone (*Arbutus menziesii Pursh*), canyon live oak (*Quercus chrysolepis Liebm.*), Oregon white oak (*Quercus garryana Douglas ex Hook.*), California black oak (*Quercus kelloggii Newberry*), golden chinkapin (*Castanopsis chrysophylla*), tanoak (*Lithocarpus densiflourus*), ponderosa pine (*Pinus ponderosa Lawson & C. Lawson*), and white fir (*Abies concolor (lowina)*. Less abundant upland tree species include incense cedar (*Calocedrus decurrens (Torr.)Florin*), sugar pine (*Pinus lambertiana*), Jeffery pine (*Pinus jefferyi*), big-leaf maple (*Acer macrophyllym*), pacific dogwood (*Cornus nuttallii*), apple (*Malus spp.*, and knobcone pine (*Pinus attenuata*). Chaparral shrub species are common in the understory of most of these vegetation zones and dominate vegetative cover on portions of the landscape (Duren et al., 2012).

2.3.2 LiDAR Datasets

We used multi-temporal LiDAR to quantify fire severity across the burned landscape. Pre-fire LiDAR data (LiDAR Consortium's Rogue River project area ≈ 551,074 ha) was obtained between March 6th and August 16th, 2012. Post-fire LiDAR was collected between September 26th and October 23rd, 2013 ($\approx$ 49,915 ha) and lies within the LiDAR Consortium's Rogue River project area. Data was collected by Watershed Sciences, Inc. (purchased by Quantum Spatial), for the Oregon Department of Geology and Mineral Industries (DOGAMI), at 8 pulses per square meter resolution. The survey altitude across all flights ranged between 900 meters to 1300 meters. Overall, the majority of sensor specifications remained constant between flights with the exception of pulse rate (Tables 2.1 and 2.2). The intensity values were normalized during processing by Watershed Science's prior to delivery.

Three categories of LiDAR variables were examined for use in change detection; 1) vertical structure - changes in the z dimension, 2) horizontal structure - changes in x and y, and 3) foliar reflectance - changes in intensity returned (García et al., 2010). All metrics were evaluated as absolute differences from pre-fire (2012) to post-fire (2013) data sets and processed using FUSION (McGaughey, 2014). We assessed alignment and quality of both LiDAR datasets by comparing stem mapped trees obtained from field data to LiDAR derived tree locations using canopy models and the CanopyMaxima function within FUSION. All of the above layers, including the point cloud, were analyzed in ArcMap for each field plot. A list of metrics evaluated in this study is provided in Table 2.3.

Stratified height bins have been shown to provide significant improvements in LiDAR based estimates of total, live, dead, and proportion of dead basal area (Bright et al., 2014). Therefore, we utilized height bins to examine change within the vertical profile of forest canopies to estimate proportion of fire-induced basal area mortality. We ultimately selected 3 height bins, 0-2 (m), 2-10 (m), above 10 meters (bins: 1, 2, 3 respectively), based on preliminary analysis of several vertical strata options. Other bins examined include 2 m intervals and geometric breaks of 0-2, 2-5, 5-10, 10-20, 20-40 m. Two meter height breaks provided significant results, however, models contained 12-20 covariates and were found to be impractical for Oregon forests. Similarly, geometric breaks were found to be useful, but contained models with 6-12 covariates.

We examined Canopy Reflection Sum (CRS) as a potential change metric for quantifying differences in upper vegetative canopies from wildfire. CRS was developed using the full-waveform SLICER system to quantify canopy closure and was shown to be the most accurate estimator of foliar biomass in Oregon coniferous forests (Means et al., 1999). CRS was further defined for discrete-return systems (Hall et al., 2005) as

$$CRS(m^{-2}) = \frac{\sum_{i=1}^{N} I_i}{A} \tag{2.1}$$

where N is the number of observations, A is the area being sampled, and I_i is the intensity value of the i^{th} observation. Studies often express this metric in relative or proportional terms, in units of X per unit area (García et al., 2010; Hall et al., 2005). Our variation of the above metric is defined as

$$CRSp_i = \frac{CRS_i}{CRS_T} \tag{2.2}$$

where CRS_i is the CRS for the observed height bin, CRS_T is the total CRS, and $CRSp_i$ is expressed as a proportion of the total. We chose to express CRS as a proportion due to our multi-temporal data set and change estimation. The proportional nature of the estimator should provide a metric which is readily comparable across different LiDAR sensors. This can be seen upon its derivation

$$CRSp_i = \frac{CRS_i}{CRS_T} = \frac{\frac{N_i * \bar{I}_i}{A}}{\frac{N * \bar{I}}{A}} = \frac{N_i}{N} * \frac{\bar{I}_i}{\bar{I}} = RP_i * \frac{\bar{I}_i}{\bar{I}} \tag{2.3}$$

where CRSp$_i$ is expressed as a product of two ratios. The first is proportion of returns within the observed height bin (CRS_i). The second is proportion of intensity within the observed height bin (CRS_T). Both are unit-less quantities which account for fluctuations in pulse density (N) and average intensity returned ($\bar{I}$). Additionally, N_i

is the number of returns, $\bar{I}_i$ is the average intensity returned, and RP_i is the return proportion within bin_i. This provides an estimator which is influenced by changes in pixel density and reflectance properties. These properties are highly desirable when the objective is to quantify post-fire effects.

2.3.3 Calibration Plots

A series of calibration plots were installed two years post-fire. Plots were allocated using stratified random sampling based on fire severity and tree heights to capture a wide distribution of post-fire conditions. Fire severity was estimated using RdNBR maps obtained from the Monitoring Trends in Burn Severity (MTBS) database (MTBS, 2014). The landscape was divided into five fire severity classes (high, moderate-high, moderate-low, low, unburned) using thresholds obtained from previous research which modeled basal area mortality by calibrating RdNBR to 304 FIA plots (Reilly et al., *in review*) (Figure 2.2). The 30x30 m RdNBR raster layer was re-sampled to a 90x90 m (3x3 pixels) layer to increase the probability that our plot represented the target severity class. LiDAR derived pre-fire 95%'ile heights were used to approximate mean height across the burned area and further divide forested areas into 2 height classes (> 30 m, < 30 m). We had a combined total of 10 unique strata representing the range of conditions on the landscape. Plots centers were located as close to pixel (Landsat) center as possible, on federal land only, with a minimum spacing requirement of 400 m. We recorded plot locations using a Trimble Geo 7X hand-held GNSS receiver with a minimum of 100 recorded locations per plot. Plot coordinates were then post-processed within Trimble Pathfinder Office™.

We designed our field plots to be comprehensive and useful for a wide range of studies. The total area sampled per plot was 900 m^2 (large plot) to match the size of a Landsat pixel for scaling purposes. We used nested, circular, fixed radius plots to measure all tree and snag species, understory vegetation composition, regeneration, coarse woody debris (1000 hr), and fine fuels (1, 10, 100 hr). Line transects were used for fine fuel measurements and a 2 meter radius circular plot was used for vegetation cover, composition, and regeneration (seedlings by 10 cm height class). Azimuth and distance measurements were taken for all trees and snags (> 10 cm dbh, snags above 2 m tall) within the large plot, along with coarse woody debris (>15cm large end, > 1 m long), trees between 2.54 - 10 cm dbh, and all living shrub species in the smaller subplot (5.4 m radius). Azimuth and distance measurements for coarse wood were taken at small and large ends. We identified top condition for all trees and snags (whole, broken, forked, fallen) and recorded total tree heights for a subsample of all trees within plots including a height measurement for any tree identified as a snag, broken, or fallen. Canopy base height was recorded for any tree with foliage, regardless of whether it was green or red. Additionally, we recorded measurements of percent cover for abiotic attributes such as rock, litter, and bare ground. All plot centers were permanently monumented for future re-measurements.

We reconstructed pre-fire basal area after collecting field data between June 15 and September 24, 2015, 2 years after fire. Pre-fire snags were separated from fire-induced mortality using optical estimates of fire scaring, charring, scorch, and levels of decay (by class: 1-5). All trees above 2.54 cm dbh were included within basal area observations. Mortality rates were calculated by dividing fire-killed by pre-fire living basal area. We provide additional information in Appendix C, which includes a summary of topographical attributes, observed basal area, RdNBR values, plot measurements, coordinates for plot centers, and an illustration of our plot layout.

2.3.4 Statistical Analysis

Variable selection and regression analysis were performed in R using Leaps and Bounds, GLMulti, and GAMboosLSS packages (R Core Team, 2016). Leaps uses an efficient branch and bound algorithm to perform an exhaustive search for the best subsets of predictor variables using linear regression (Lumley, 2009). GLMulti finds the best model(s) among all possible models via a ranking function using a specified information criterion such as AIC or BIC (Hofner et al., 2016, 2015; Mayr et al., 2012). Models are chosen using either an exhaustive search or through a genetic algorithm. GAMboostLSS uses a boosting technique to iterative rotate between distribution parameters while updating one using current fits as offsets (Calcagno, 2013). Pearson correlations were used to evaluate for collinearity between predictor variables and the relationship to basal area mortality. We limited Leaps to a maximum of 5 covariates. GLMulti and GAMboostLSS were not restricted.

Each variable selection procedure provided its own unique benefits and drawbacks. Leaps allowed us to quickly examine statistically significant linear combinations across very large data sets. However, leaps is restricted to linear regression only. GLMulti allowed us to use selection methods which are not restricted by linear regression and test interactions between covariates efficiently. GLMulti also provides the top 5 candidate models which often supported our results from Leaps. While this approach provided us with an alternative perspective and significant results, we found that it lacked the ability to incorporate beta regression. In contrast, GAMboostLSS allowed us to use the BetaLSS() function which performs model selection with beta regression directly. GLMulti and GAMboostLSS also required more technical expertise than Leaps, with GAMboostLSS requiring the most.

We estimated basal area mortality using beta regression and the "logit" link function. Relative to arcsine transformation (Warton and Hui, 2011), beta regression provides parameters which are more easily interpreted, handles asymmetries well, and are naturally heteroskedastic (Cribari-Neto and Zeileis, 2010; Ferrari and Cribari-Neto, 2004). While its use has been sparse within scientific literature, evidence indicates that beta regression is well suited for quantifying forest attributes such as canopy or vegetation cover and proportion of biomass by component (Eskelson et al., 2011; Korhonen et al., 2007; Poudel and Temesgen, 2016). We also applied the following transformation (Smithson and Verkuilen, 2006) to observed basal area mortality (y)

$$\frac{y(n-1)+\frac{1}{2}}{n},$$

with n being the sample size, due to observations of 0 or 1 lying outside the range of a beta distributed variable (Cribari-Neto and Zeileis, 2010).

Evidence continues to suggest that pre-fire forest characteristics influence post-fire effects, therefore we only use RdNBR for our comparisons throughout the remainder of our study (Bolton et al., 2015; Casas et al., 2016; Kane et al., 2013; Miller et al., 2009; Montealegre et al., 2014).

We present the top models which include 1–5 parameters using LiDAR and Combined metrics found during our analysis. Intensity values were not used during the variable selection process for combined models under the assumption that RdNBR provides adequate spectral information. Basal area mortality was also modeled using only RdNBR, for comparison purposes (Reilly et al., *in review*). Model performance was assessed by evaluating bias, root mean square error (RMSE), AIC, BIC, and root mean square prediction error (RMSPE), along with Wald and Likelihood ratio tests for nested models (Cribari-Neto and Zeileis, 2010; Zeileis and Hothorn, 2002). We also examined the use of weighted beta regression using the same comparisons. Variance inflation factors were used to verify that multicollinearity issues were not apparent within any of the chosen models. Finally, we cross validated each model using leave-one-out procedures (Kohavi et al., 1995) before mapping fire severity estimates over the entire study area using the Raster package in R (Hijmans, 2016).

2.4 Results

We sampled a total of 2,435 trees and snags greater than 10 cm dbh, with 1,454 remaining alive two-years post-fire, 958 killed by fire, and 77 snags (dead before fire and still standing), on 51 plots across the full severity gradient within our study area. Approximately 60% (1,464) were coniferous with hardwoods representing the remaining 40% (971). Douglas-fir represented 89% of the coniferous species composition, with a mixture of ponderosa pine, sugar pine, western white pine, and Jeffery pine representing 8%, and > 1% – white fir. In contrast, hardwood species composition was more diverse and primarily composed of Pacific Madrone at 34%, golden chinkapin and canyon live oak at 23%, tanoak at 15%, and the remaining observations being a mixture of big-leaf maple, pacific dogwood, Oregon white oak, California black oak, and 1 apple tree. Many of our observations still retained an intact crown 2-years after fire (2,190 ≈ 90%), with the majority of remaining observations exhibiting broken tops (218 ≈ 9%), and 27 (1%) were recorded as fallen after fire.

Over 60% of the post-processed plot locations maintained sub-meter accuracy with roughly 25% over 1 m, and the remaining observations above 2 meters. Only 1 out of 51 plots exhibited any need for re-alignment. After further examination, it was determined that, at minimum, 2 large trees within this plot had fallen between LiDAR data acquisitions and our field measurements, therefore no adjustment was made. Plots were spread evenly between the three fire areas under varying conditions with our response variable (BA mortality) averaging 0.41, and a standard deviation of 0.36 (Table 2.4).

Many of our multi-temporal LiDAR metrics were highly correlated requiring us to manually reduce the number of potential predictor variables during model selection using GLMulti and GamboostLSS (Figure 2.3). Weighted beta regressions did not provide significant improvements to prediction bias, RMSE, or RMSPE. Therefore they have been omitted from further results. Interactions between covariates were not significant within our selected models. We also found that our most correlated predictors to basal area mortality were $RdNBR$ (0.84), $d\bar{I}_2$ (0.80), $dCRSp_1$ (-0.79), and dRP_1 (-0.75).

Summary statistics for our LiDAR models can be found in Table 2.5. Our best model is shown below:

$$Y = \beta_0 + \beta_1\ d\bar{I}_2 + \beta_2\ dCRSp_3 + \beta_3\ dHT_{max} + \epsilon_i \tag{2.4}$$

Where Y is the fire-induced basal area mortality rate, $d\bar{I}_2$ is the change in the mean intensity value between 2 and 10 meters, $dCRSp_3$ is the change in the proportion of CRS above 10 meters, and dHT_{max} is a change in max height. The approximate root mean square prediction error (RMSPE) is 0.1293 (leave-one-out), with an average bias of -0.01, and the lowest BIC value. Coefficients were found to be stable across all models and most were significant at $\alpha = 0.001$ (Table 2.6).

Our best performing combined model(s) (Table 2.7) contained 4–5 covariates which included a combination of pre-fire structural metrics and change detection. For example, our combined model

$$y = \beta_0 + \beta_1 RdNBR + \beta_2 dRP_1 + \beta_3 HT_{CV_{T0}} + \beta_4 RP_{1_{T0}} \tag{2.5}$$

contained change in return proportion near ground (dRP_1), pre-fire coefficient of variation within height values ($\mathrm{HT}_{CV_{T0}}$), and return proportion near ground before fire ($\mathrm{RP}_{1_{T0}}$). We know that pre-fire return proportions near ground are negatively correlated to upper canopy cover. Likewise, reductions in proportion returned near ground is inversely related to canopy consumption or removal of cover. Whereas, pre-fire coefficient of variation within height values provides a measure of stand variability similar to Rumple (Kane et al., 2010). All model coefficients were found to be stable and most were significant at $\alpha = 0.001$ (Table 2.8).

Our results suggest that multi-temporal LiDAR can estimate basal area mortality with greater accuracy than satellite-based methods. We can see that young, low basal area stands are interspersed within the data and significant improvements have been made with regards to prediction error and bias (Figure 2.4 & 2.5). We provide landscape maps of our best performing model by method, including RdNBR only for comparison in Figure 2.6. We also compared LiDAR based estimates of basal area mortality to RdNBR based thresholds of fire severity using a confusion matrix shown in Table 2.9. We provide a final map of multi-temporal LiDAR derived basal area mortality (Figures 2.7).

2.5 Discussion

The development of dNBR, with subsequent improvements using RdNBR, revolutionized researchers and managers capability to assess fire effects across broad landscapes. These landscape assessments allowed researchers to quantify land surface change and forest disturbance (Cohen et al., 2010; Kennedy et al., 2010), tree defoliation and tree mortality (Bright et al., 2014; Meigs et al., 2011), active fire characteristics and post-fire effects (Escuin et al., 2008; Key and Benson, 1999, 2005; Lentile et al., 2006; Meng and Meentemeyer, 2011; Miller et al., 2009; Miller and Thode, 2007; Turner et al., 2003; Verbyla et al., 2008; Whittier and Gray, 2016), forest attributes and canopy fuels (Erdody and Moskal, 2010; Hudak et al., 2006, 2002; Lefsky et al., 1999; Miller and Yool, 2002; Skowronski et al., 2007, 2011; Thompson and Spies, 2009, 2010; Wulder et al., 2007), and improve habitat suitability models for a variety of rare and endangered avian species (Betts et al., 2010; Spies et al., 2010; Vogeler et al., 2014, 2016). However, RdNBR was also significantly correlated with basal area mortality following mixed-severity fire in southwestern Oregon, but has limitations associated with any two-dimensional imagery.

Satellite-based estimates of fire severity have been found to be lacking (Morgan et al., 2014). Our ability to interpret fire effects is limited by our understanding of what is being measured or quantified (Lentile et al., 2006). For example, passive satellite-based platforms lack the ability to directly measure forest attributes such as tree heights, density, or basal area. In addition, the calibration of remotely sensed estimates of fire effects using the CBI greatly limits our ability to interpret proportional responses.

Change detection using multi-temporal LiDAR improved estimates of fire induced basal area mortality because it provides spectral and 3-dimensional, structural information. Evidence has shown that upper canopy density, cover, stand heights, and variation within each is highly correlated to stand level basal area and volume (Coops et al., 2007; Næsset, 2007). Most recently, metrics related to light penetration and canopy relief ratio have been shown to be very useful in quantifying canopy components and variation over large landscapes (Bouvier et al., 2015; Bright et al., 2014; Guerra-Hernández et al., 2016; Montealegre et al., 2014). Our results indicate that similar metrics are highly correlated to basal area mortality when used with change estimation.

Discrete height bins offered a number of advantages by partitioning vegetative layers and observing them separately. This allowed us to reduce over saturation caused by big data, account for confounding or inverse relationships, check for evidence of reductions in upper canopy densities (canopy consumption), and observe change beneath occluded canopies (Bolton et al., 2015; Bright et al., 2014; Montealegre et al., 2014). Additionally, our ability to interpret vertical movement of fire from ground surfaces into tree canopies greatly improved by providing information related to the consumption of sub-canopy vegetation and tree canopies.

We initially hypothesized that the change in ground returns would greatly reduce errors in prediction because wildfires consume vegetation exposing more ground post-fire. Therefore, we expected to observe increased point densities near ground with increasing fire severity. However, we did not anticipate the role LiDAR intensity values would play into our predictive models. Spectral information is clearly the strongest relationship when modeling post-fire disturbance for any remote sensing platform, with RdNBR and absolute change in mean intensity value between 2–10 m (Figure 2.8) being quite comparable. The addition of other metrics further improved model accuracy, with the change in proportion of canopy reflection sum above 10 m

(Figure 2.9) being the 2nd highest with regards to model selection frequency.

We found that our best two variable model: $y = \beta_0 + \beta_1 d\bar{I}_2 + \beta_2 dCRSp_3 + \epsilon$, was slightly under predicting high severity conditions and omitting information near ground (no observations below 2 meters). Upon inclusion of a third covariate (dHT_{max}), prediction error improved significantly, specifically within the high severity group. We now believe that the change in max height was actually capturing high severity conditions within the youngest stands as this is the most probable scenario where we would observe the largest change in max height values indicating greater severity. Other covariates were also found to be highly useful additions, such as the difference in Rumple (*dRumple*) and coefficient of variation of height values ($dHTcv$). Both covariates are structural metrics where a low value represents a more uniform forest structure and high values indicate greater structural variability. Thus, large changes within either of these would indicate a shift from homogenized to variable forest canopy structures. We concluded that while absolute change in mean intensity value between 2–10 m($d\bar{I}_2$) was explaining the majority of variation, $dCRSp_3$ provided more information for stands taller than 10 m, and dHT_{max} captured higher severity conditions in the youngest forests.

Combining LiDAR change detection with RdNBR also improves estimates of basal area mortality. Similar to LiDAR models, the difference in Rumple was found to be highly significant, however, variable and model selection methods tended to prefer $dHTcv$ over *dRumple*. Pre-fire heights were also significant (not shown in any of these models). Change in proportion of ground returns (Figure 2.10) was the most reliable addition with the highest selection frequency.

We were unable to significantly improve the accuracy of combined models upon inclusion of a third variable until we considered pre-fire forest structure. This likely suggests that knowledge of forest structural attributes before fire provides more precise estimates of fire effects. Biologically this makes sense, as we know that certain trees species tend to be more resistant to fire-induced mortality (Franklin et al., 1987; Ryan and Frandsen, 1991; Vines, 1968).

Lastly, our regression results for predicting basal area mortality from RdNBR were similar to previous findings (Reilly et al., *in review*). We found that RdNBR values below 283 represent low severity (< 25% BA mortality) and above 665, high severity (> 75% BA mortality), when modeling basal area mortality as a function of RdNBR. The largest difference between these two studies is the sample size; 51 vs 304. We found that severity thresholds obtained by modeling basal area mortality as a function of RdNBR provided slightly different values of 232 and 784, respectively. Similar results were described when testing correlations between CBI and LiDAR data flown in Spain (Montealegre et al., 2014). Additionally, r-squared values are highly similar between all 3 studies (0.69, 0.68, 0.68).

2.5.1 Limitations

LiDAR metrics are also subject to optical occlusion and "noise" which provide unique challenges for estimating forest attributes (Habib et al., 2009; Yan and Shaker, 2016). Figures 2.9 and 2.10 provide examples from our own data where we see an inverse relationship to fire severity from observations below 2 meters. This is due to two reasons: 1) reductions in canopy cover post-fire which increases the number of ground returns, and 2) the difference in specularity between LiDAR returns on or near ground versus a vegetative canopy (solid vs broken surface).

Discrete height bins also have limitations. While we used bins of 0-2 m, 2-10 m, and above 10 m, other forest types and geographic regions may require different vertical slices to account for the average stand type, multi-story canopy conditions, suppressed tree species, or ladder fuels. For example, if your forest landscape does not contain trees above 10 m tall, then the use of a height bin above 10 m is not useful.

Timing of data acquisition and field observations must also be taken into account. While we sampled 2-years post-fire, satellite based approaches often sample shortly after disturbance including field calibration. These methodologies will likely provide different results when examining fire effects because of delayed mortality. We are confident that our field measurements of fire-induced basal area mortality are accurate due to the majority of delayed mortality taking place within the first couple years. In contrast, satellite-based approaches may lack precision due to these factors.

The most significant limitation for studies such as these is simply the availability of information. LiDAR data acquisitions cost money, while passive remote sensors such as Landsat, are free. However, research continues to support the use of active remote sensing technology as the next step towards improving our ability to quantify and interpret landscape scale disturbance, ecological effects, and spatial distributions. We believe the benefits of obtaining LiDAR data greatly out-weigh the cost and recent statewide studies suggest \$4 in benefits for every \$1 spent when acquiring LiDAR data (Dewberry, 2016; Hallum and Parent, 2014; Young, 2014). This is largely due to a plethora of potential applications across agency, owner, and objectives.

2.6 Conclusion

Multi-temporal LiDAR technology offers a new frontier in remotely sensed estimates of fire effects. Our results confirm that the ability to detect change in 3-dimensions helps ameliorate some of the inaccuracies associated with passive remote sensing platforms. We examined metrics related to changes in vertical and horizontal structure along with change in foliar reflectance. We modeled basal area mortality using beta regression. LiDAR models performed the best with 3 covariates performed the best. Combined models also improved upon current estimates made by RdNBR only, but required an additional variable. Therefore, we concluded that multi-temporal LiDAR can estimate basal area mortality rate with greater accuracy than RdNBR or a combined approach.

The benefits of acquiring LiDAR data vastly outweigh the cost (Dewberry, 2016; Hallum and Parent, 2014; Young, 2014). Our ability to understand these highly complex interactions is only limited by the information we use to assess the landscape. As LiDAR data become more available, opportunities like these will be studied and our ability quantify, assess, and understand landscape fire effects will continue to improve. Such information will allow us to modify pro-active management practices by helping us identify high risk areas and spatially optimize fuel treatments across ownership boundaries (Fule et al., 2004; Graham et al., 2004; Johnson et al., 2011; Spies et al., 2006). It is essential that we protect our valuable resources in the context of increasing global temperatures and wildfire events (Littell et al., 2010; Marlon et al., 2012).

Literature Cited

Agee, J. K. (1991). Fire history of Douglas-fir forests in the Pacific Northwest. In: Wildlife and Vegetation of Unmanaged Douglas-fir Forests. U.S. Department of Agriculture, Forest Service, Pacific Northwest Research Station, Portland, OR, pp. 25–33.

Betts, M., J. C. Hagar, J. W. Rivers, J. Alexander, K. McGarigal, and B. McComb (2010). Thresholds in forest bird occurrence as a function of the amount of early-seral broadleaf forest at landscape scales. *Ecological Applications 20*(8), 2116–2130.

Bolton, D. K., N. C. Coops, and M. A. Wulder (2015). Characterizing residual structure and forest recovery following high-severity fire in the western boreal of Canada using landsat time-series and airborne lidar data. *Remote Sensing of Environment 163*, 48–60.

Bouvier, M., S. Durrieu, R. A. Fournier, and J.-P. Renaud (2015). Generalizing predictive models of forest inventory attributes using an area-based approach with airborne lidar data. *Remote Sensing of Environment 156*, 322–334.

Bright, B. C., A. T. Hudak, R. E. Kennedy, and A. J. Meddens (2014). Landsat time series and lidar as predictors of live and dead basal area across five bark beetle-affected forests. *IEEE Journal of Selected Topics in Applied Earth Observations and Remote Sensing 7*(8), 3440–3452.

Brosofske, K. D., R. E. Froese, M. J. Falkowski, and A. Banskota (2014). A review of methods for mapping and prediction of inventory attributes for operational forest management. *Forest Science 60*(4), 733–756.

Calcagno, V. (2013). *glmulti: Model selection and multimodel inference made easy.* R package version 1.0.7 https://CRAN.R-project.org/package=glmulti.

Calkin, D. E., K. M. Gebert, J. G. Jones, and R. P. Neilson (2005). Forest service large fire area burned and suppression expenditure trends, 1970–2002. *Journal of Forestry 103*(4), 179–183.

Casas, Á., M. García, R. B. Siegel, A. Koltunov, C. Ramírez, and S. Ustin (2016). Burned forest characterization at single-tree level with airborne laser scanning for assessing wildlife habitat. *Remote Sensing of Environment 175*, 231–241.

Clark, K. L., N. Skowronski, M. Gallagher, N. Carlo, M. Farrell, and M. R. Maghirang (2010). Assessment of canopy fuel loading across a heterogeneous landscape using lidar. Joint Fire Sciences Program, Project 10-1-02-14, Final Report, U.S. Department of Agriculture, Forest Service, New Lisbon, NJ & Morgantown, WV, 2010.

Cohen, W. B., Z. Yang, and R. Kennedy (2010). Detecting trends in forest disturbance and recovery using yearly landsat time series: 2. timesynctools for calibration and validation. *Remote Sensing of Environment 114*(12), 2911–2924.

Coops, N. C., T. Hilker, M. A. Wulder, B. St-Onge, G. Newnham, A. Siggins, and J. T. Trofymow (2007). Estimating canopy structure of douglas-fir forest stands from discrete-return lidar. *Trees 21*(3), 295–310.

Cribari-Neto, F. and A. Zeileis (2010). Beta regression in R. *Journal of Statistical Software 34*(2), 1–24. http://www.jstatsoft.org/v34/i02/.

Dewberry (2016). National enhanced elevation assessment final report - appendix F: Benefit cost analysis process. *Dewberry*, 671–686. Accessed: March 15th, 2016. Available at: http://www.dewberry.com/docs/default-source/documents/neea_final-report_revised-3-29-12.pdf?sfvrsn=0.

Duren, O. C., P. S. Muir, and P. E. Hosten (2012). Vegetation change from the Euro-American settlement era to the present in relation to environment and disturbance in southwest Oregon. *Northwest Science 86*(4), 310–328.

Erdody, T. L. and L. M. Moskal (2010). Fusion of lidar and imagery for estimating forest canopy fuels. *Remote Sensing of Environment 114*(4), 725–737.

Escuin, S., R. Navarro, and P. Fernandez (2008). Fire severity assessment by using nbr (normalized burn ratio) and ndvi (normalized difference vegetation index) derived from landsat TM/ETM images. *International Journal of Remote Sensing 29*(4), 1053–1073.

Eskelson, B. N., L. Madsen, J. C. Hagar, and H. Temesgen (2011). Estimating riparian understory vegetation cover with beta regression and copula models. *Forest Science 57*(3), 212–221.

Ferrari, S. and F. Cribari-Neto (2004). Beta regression for modelling rates and proportions. *Journal of Applied Statistics 31*(7), 799–815.

Franklin, J. F. and D. S. DeBell (1988). Thirty-six years of tree population change in an old-growth pseudotsuga-tsuga forest. *Canadian Journal of Forest Research 18*(5), 633–639.

Franklin, J. F., H. Shugart, and M. E. Harmon (1987). Tree death as an ecological process. *BioScience 37*(8), 550–556.

Fule, P. Z., A. E. Cocke, T. A. Heinlein, and W. W. Covington (2004). Effects of an intense prescribed forest fire: is it ecological restoration? *Restoration Ecology 12*(2), 220–230.

García, M., D. Riaño, E. Chuvieco, and F. M. Danson (2010). Estimating biomass carbon stocks for a mediterranean forest in central Spain using lidar height and intensity data. *Remote Sensing of Environment 114*(4), 816–830.

Graham, R. T., S. McCaffrey, and T. B. Jain (2004). Science basis for changing forest structure to modify wildfire behavior and severity. Gen. Tech. Re. RMRS-GTR-120.

Fort Collins, CO: U.S. Department of Agriculture, Forest Service, Rock Mountain Research Station. 43 p.

Guerra-Hernández, J., M. Tomé, and E. González-Ferreiro (2016). Using low density lidar data to map mediterranean forest characteristics by means of an area-based approach and height threshold analysis. *Revista de Teledetección* (46), 103–117.

Haas, J. R., D. E. Calkin, and M. P. Thompson (2013). A national approach for integrating wildfire simulation modeling into wildland urban interface risk assessments within the united states. *Landscape and Urban Planning 119*, 44–53.

Habib, A. F., Y.-C. Chang, and D. C. Lee (2009). Occlusion-based methodology for the classification of lidar data. *Photogrammetric Engineering & Remote Sensing 75*(6), 703–712.

Hall, S., I. Burke, D. Box, M. Kaufmann, and J. M. Stoker (2005). Estimating stand structure using discrete-return lidar: an example from low density, fire prone ponderosa pine forests. *Forest Ecology and Management 208*(1), 189–209.

Hallum, D. and S. Parent (2014). Developing a business case for statewide light detection and ranging data collection. *Nebraska Department of Natural Resources. Accessed: May 11, 2016*. Accessed: May 10, 2016. Available at: http://watercenter.unl.edu/PRS/PRS2009/Posters/Hallum%20Doug.pdf.

Halofsky, J., D. Donato, D. Hibbs, J. Campbell, M. D. Cannon, J. Fontaine, J. Thompson, R. Anthony, B. Bormann, L. Kayes, et al. (2011). Mixed-severity fire regimes: lessons and hypotheses from the Klamath-Siskiyou ecoregion. *Ecosphere 2*(4), 1–19.

Hammer, R. B., V. C. Radeloff, J. S. Fried, and S. I. Stewart (2007). Wildland–urban interface housing growth during the 1990s in California, Oregon, and Washington. *International Journal of Wildland Fire 16*(3), 255–265.

Hessburg, P. F., R. B. Salter, and K. M. James (2007). Re-examining fire severity relations in pre-management era mixed conifer forests: inferences from landscape patterns of forest structure. *Landscape Ecology 22*(1), 5–24.

Hijmans, R. J. (2016). *raster: Geographic Data Analysis and Modeling.* R package version 2.5-8, https://CRAN.R-project.org/package=raster.

Hofner, B., A. Mayr, N. Fenske, and M. Schmid (2016). *gamboostLSS: Boosting Methods for GAMLSS Models.* R package version 1.2-1 http://CRAN.R-project.org/package=gamboostLSS.

Hofner, B., A. Mayr, and M. Schmid (2015). gamboostLSS: An R package for model building and variable selection in the GAMLSS framework. *Journal of Statistical Software*. Accepted.

Hudak, A., P. Morgan, M. Bobbitt, A. Smith, S. Lewis, L. Lentile, P. Robichaud, J. Clark, and R. McKinley (2007). The relationship of multispectral satellite imagery to immediate fire effects. fire ecology 3 (1): 64-90. *Fire Ecology Special Issue Vol 3*, 66.

Hudak, A. T., N. L. Crookston, J. S. Evans, M. J. Falkowski, A. M. Smith, P. E. Gessler, and P. Morgan (2006). Regression modeling and mapping of coniferous forest basal area and tree density from discrete-return lidar and multispectral satellite data. *Canadian Journal of Remote Sensing 32*(2), 126–138.

Hudak, A. T., M. A. Lefsky, W. B. Cohen, and M. Berterretche (2002). Integration of lidar and landsat ETM+ data for estimating and mapping forest canopy height. *Remote sensing of Environment 82*(2), 397–416.

InciWeb, I. I. S. (2013). Douglas Complex Incident Information. *USDA Forest Service.* Accessed on February 13, 2014. Available at: http://inciweb.nwcg.gov/incident/3559/.

Johnson, M. C., M. C. Kennedy, and D. L. Peterson (2011). Simulating fuel treatment effects in dry forests of the western united states: testing the principles of a fire-safe forest. *Canadian Journal of Forest Research 41*(5), 1018–1030.

Jolly, W. M., M. A. Cochrane, P. H. Freeborn, Z. A. Holden, T. J. Brown, G. J. Williamson, and D. M. Bowman (2015). Climate-induced variations in global wildfire danger from 1979 to 2013. *Nature communications 6*.

Kane, V. R., C. A. Cansler, N. A. Povak, J. T. Kane, R. J. McGaughey, J. A. Lutz, D. J. Churchill, and M. P. North (2015). Mixed severity fire effects within the rim fire: relative importance of local climate, fire weather, topography, and forest structure. *Forest Ecology and Management 358*, 62–79.

Kane, V. R., J. A. Lutz, S. L. Roberts, D. F. Smith, R. J. McGaughey, N. A. Povak, and M. L. Brooks (2013). Landscape-scale effects of fire severity on mixed-conifer and red fir forest structure in yosemite national park. *Forest Ecology and Management 287*, 17–31.

Kane, V. R., R. J. McGaughey, J. D. Bakker, R. F. Gersonde, J. A. Lutz, and J. F. Franklin (2010). Comparisons between field-and lidar-based measures of stand structural complexity. *Canadian Journal of Forest Research 40*(4), 761–773.

Keeley, J. E. (2009). Fire intensity, fire severity and burn severity: a brief review and suggested usage. *International Journal of Wildland Fire 18*(1), 116–126.

Kennedy, R. E., Z. Yang, and W. B. Cohen (2010). Detecting trends in forest disturbance and recovery using yearly landsat time series: 1. LandTrendrTemporal segmentation algorithms. *Remote Sensing of Environment 114*(12), 2897–2910.

Key, C. and N. Benson (1999). Measuring and remote sensing of burn severity. In L. F. Neuenschwander and K. C. Ryan (Eds.), *Proceedings joint fire science conference and workshop*, Volume 2, Boise, ID, 15-17 June 1999. University of Idaho and International Association of Wildland Fire, pp. 284.

Key, C. and N. Benson (2005). Landscape assessment: remote sensing of severity, the normalized burn ratio and ground measure of severity, the composite burn index. *FIREMON: Fire effects monitoring and inventory system Ogden, Utah: USDA Forest Service, Rocky Mountain Res. Station*. USDA Forest Service Gen. Tech. Rep. RMRS-GTR-164-CD, LA-1-55.

Kohavi, R. et al. (1995). A study of cross-validation and bootstrap for accuracy estimation and model selection. In *International Joint Conference on Artificial Intelligence*, Volume 14, pp. 1137–1145.

Korhonen, L., K. T. Korhonen, P. Stenberg, M. Maltamo, and M. Rautiainen (2007). Local models for forest canopy cover with beta regression. *Silva Fennica 41*(4), 671.

Lefsky, M. A., W. B. Cohen, A. Hudak, S. A. Acker, and J. Ohmann (1999). Integration of lidar, landsat ETM+ and forest inventory data for regional forest mapping. *International Archives of Photogrammetry and Remote Sensing 32*, 119–126.

Lentile, L. B., Z. A. Holden, A. M. Smith, M. J. Falkowski, A. T. Hudak, P. Morgan, S. A. Lewis, P. E. Gessler, and N. C. Benson (2006). Remote sensing techniques to assess active fire characteristics and post-fire effects. *International Journal of Wildland Fire 15*(3), 319–345.

Littell, J. S., D. McKenzie, D. L. Peterson, and A. L. Westerling (2009). Climate and wildfire area burned in western US ecoprovinces, 1916–2003. *Ecological Applications 19*(4), 1003–1021.

Littell, J. S., E. E. Oneil, D. McKenzie, J. A. Hicke, J. A. Lutz, R. A. Norheim, and M. M. Elsner (2010). Forest ecosystems, disturbance, and climatic change in washington state, USA. *Climatic change 102*(1-2), 129–158.

Liu, Y., S. L. Goodrick, and J. A. Stanturf (2013). Future US wildfire potential trends projected using a dynamically downscaled climate change scenario. *Forest Ecology and Management 294*, 120–135.

Lumley, T. (2009). *leaps: regression subset selection.* R package version 2.9 https://CRAN.R-project.org/package=leaps.

Mallek, C., H. Safford, J. Viers, and J. Miller (2013). Modern departures in fire severity and area vary by forest type, Sierra Nevada and southern Cascades, California, USA. *Ecosphere 4*(12), 1–28.

Marlon, J. R., P. J. Bartlein, D. G. Gavin, C. J. Long, R. S. Anderson, C. E. Briles, K. J. Brown, D. Colombaroli, D. J. Hallett, M. J. Power, et al. (2012). Long-term perspective on wildfires in the western USA. *Proceedings of the National Academy of Sciences 109*(9), E535–E543.

Mayr, A., N. Fenske, B. Hofner, T. Kneib, and M. Schmid (2012). Generalized additive models for location, scale and shape for high-dimensional data - a flexible approach based on boosting. *Journal of the Royal Statistical Society, Series C - Applied Statistics 61*(3), 403–427.

McCombs, J. W., S. D. Roberts, and D. L. Evans (2003). Influence of fusing lidar and multispectral imagery on remotely sensed estimates of stand density and mean tree height in a managed loblolly pine plantation. *Forest Science 49*(3), 457–466.

McGaughey, R. J. (2014). Fusion: Providing fast, efficient, and flexible access to lidar, ifsar and terrain datasets. *Pacific Northwest Research Station, USDA Forest Service*. Accessed: Sept. 28, 2014. Available at: http://forsys.cfr.washington.edu/fusion/fusionlatest.html.

Means, J. E., S. A. Acker, D. J. Harding, J. B. Blair, M. A. Lefsky, W. B. Cohen, M. E. Harmon, and W. A. McKee (1999). Use of large-footprint scanning airborne lidar to estimate forest stand characteristics in the western cascades of oregon. *Remote Sensing of Environment 67*(3), 298–308.

Meigs, G. W., R. E. Kennedy, and W. B. Cohen (2011). A landsat time series approach to characterize bark beetle and defoliator impacts on tree mortality and surface fuels in conifer forests. *Remote Sensing of Environment 115*(12), 3707–3718.

Meng, Q. and R. K. Meentemeyer (2011). Modeling of multi-strata forest fire severity using landsat TM data. *International Journal of Applied Earth Observation and Geoinformation 13*(1), 120–126.

Miller, J. D., E. E. Knapp, C. H. Key, C. N. Skinner, C. J. Isbell, R. M. Creasy, and J. W. Sherlock (2009). Calibration and validation of the relative differenced normalized burn ratio (rdnbr) to three measures of fire severity in the Sierra Nevada and Klamath Mountains, California, USA. *Remote Sensing of Environment 113*(3), 645–656.

Miller, J. D. and A. E. Thode (2007). Quantifying burn severity in a heterogeneous landscape with a relative version of the delta normalized burn ratio (dnbr). *Remote Sensing of Environment 109*(1), 66–80.

Miller, J. D. and S. R. Yool (2002). Mapping forest post-fire canopy consumption in several overstory types using multi-temporal landsat TM and ETM data. *Remote Sensing of Environment 82*(2), 481–496.

Montealegre, A. L., M. T. Lamelas, M. A. Tanase, and J. de la Riva (2014). Forest fire severity assessment using ALS data in a mediterranean environment. *Remote Sensing 6*(5), 4240–4265.

Morgan, P., R. E. Keane, G. K. Dillon, T. B. Jain, A. T. Hudak, E. C. Karau, P. G. Sikkink, Z. A. Holden, and E. K. Strand (2014). Challenges of assessing fire and burn severity using field measures, remote sensing and modeling. *International Journal of Wildland Fire 23*(8), 1045–1060.

MTBS (2014). Monitoring trends in burn severity. *USDA Forest Service*. Accessed: December 2014. Available at: http://www.mtbs.gov.

Næsset, E. (2007). Airborne laser scanning as a method in operational forest inventory: Status of accuracy assessments accomplished in Scandinavia. *Scandinavian Journal of Forest Research 22*(5), 433–442.

Naficy, C., A. Sala, E. G. Keeling, J. Graham, and T. H. DeLuca (2010). Interactive effects of historical logging and fire exclusion on ponderosa pine forest structure in the northern rockies. *Ecological Applications 20*(7), 1851–1864.

Omernik, J. M. and G. E. Griffith (2014). Ecoregions of the conterminous United States: evolution of a hierarchical spatial framework. *Environmental management 54*(6), 1249–1266.

Perry, D. A., P. F. Hessburg, C. N. Skinner, T. A. Spies, S. L. Stephens, A. H. Taylor, J. F. Franklin, B. McComb, and G. Riegel (2011). The ecology of mixed severity fire regimes in Washington, Oregon, and Northern California. *Forest Ecology and Management 262*(5), 703–717.

Persson, A., J. Holmgren, and U. Söderman (2002). Detecting and measuring individual trees using an airborne laser scanner. *Photogrammetric Engineering and Remote Sensing 68*(9), 925–932.

Popescu, S. C. and R. H. Wynne (2004). Seeing the trees in the forest. *Photogrammetric Engineering & Remote Sensing 70*(5), 589–604.

Poudel, K. P. and H. Temesgen (2016). Developing biomass equations for western hemlock and red alder trees in western oregon forests. *Forests 7*(4), 88.

R Core Team (2016). R: A language and environment for statistical computing. *R Foundation for Statistical Computing*. Vienna, Austria. https://www.R-project.org/.

Reilly, M. J., C. J. Dunn, G. W. Meigs, T. A. Spies, R. E. Kennedy, J. D. Bailey, and K. Briggs (*in review*). Contemporary patterns of burn severity in forests of the pacific northwest (1985-2010). *Forest Ecology and Management*.

Ryan, K. C. and W. H. Frandsen (1991). Basal injury from smoldering fires in mature pinus ponderosa laws. *International Journal of Wildland Fire 1*(2), 107–118.

Short, K. (2014). A spatial database of wildfires in the United States, 1992-2011. *Earth System Science Data 6*(1), 1–27.

Skinner, C., A. Taylor, and J. Agee (2006). Klammath mountains bioregion. In N. G. Sugihara, J. W. van Wagtendonk, J. Fites-Kaufmann, K. E. Shaffer, and A. E. Thode, editors, *Fire in California's ecosystems*, pp. 170–194. Berkeley, CA: University of California Press.

Skowronski, N., K. Clark, R. Nelson, J. Hom, and M. Patterson (2007). Remotely sensed measurements of forest structure and fuel loads in the pinelands of New Jersey. *Remote Sensing of Environment 108*(2), 123–129.

Skowronski, N. S., K. L. Clark, M. Duveneck, and J. Hom (2011). Three-dimensional canopy fuel loading predicted using upward and downward sensing lidar systems. *Remote Sensing of Environment 115*(2), 703–714.

Smithson, M. and J. Verkuilen (2006). A better lemon squeezer? maximum-likelihood regression with beta-distributed dependent variables. *Psychological methods 11*(1), 54.

Spies, T. A., M. A. Hemstrom, A. Youngblood, and S. Hummel (2006). Conserving old-growth forest diversity in disturbance-prone landscapes. *Conservation Biology 20*(2), 351–362.

Spies, T. A., J. D. Miller, J. B. Buchanan, J. F. Lehmkuhl, J. F. Franklin, S. P. Healey, P. F. Hessburg, H. D. Safford, W. B. Cohen, R. S. Kennedy, et al. (2010).

Underestimating risks to the northern spotted owl in fire-prone forests: Response to Hanson et al. *Conservation Biology 24*(1), 330–333.

Sumnall, M. J., R. A. Hill, and S. A. Hinsley (2016). Comparison of small-footprint discrete return and full waveform airborne lidar data for estimating multiple forest variables. *Remote Sensing of Environment 173*, 214–223.

Taylor, A. H. and C. N. Skinner (1998). Fire history and landscape dynamics in a late-successional reserve, Klamath Mountains, California, USA. *Forest Ecology and Management 111*(2), 285–301.

Thompson, J. R. and T. A. Spies (2009). Vegetation and weather explain variation in crown damage within a large mixed-severity wildfire. *Forest Ecology and Management 258*(7), 1684–1694.

Thompson, J. R. and T. A. Spies (2010). Factors associated with crown damage following recurring mixed-severity wildfires and post-fire management in southwestern oregon. *Landscape Ecology 25*(5), 775–789.

Thompson, M. P., J. R. Haas, M. A. Finney, D. E. Calkin, M. S. Hand, M. J. Browne, M. Halek, K. C. Short, and I. C. Grenfell (2015). Development and application of a probabilistic method for wildfire suppression cost modeling. *Forest Policy and Economics 50*, 249–258.

Turner, M. G., W. H. Romme, and D. B. Tinker (2003). Surprises and lessons from the 1988 Yellowstone fires. *Frontiers in Ecology and the Environment 1*(7), 351–358.

Verbyla, D. L., E. S. Kasischke, and E. E. Hoy (2008). Seasonal and topographic effects on estimating fire severity from landsat TM/ETM+ data. *International Journal of Wildland Fire 17*(4), 527–534.

Vines, R. (1968). Heat transfer through bark, and the resistance of trees to fire. *Australian Journal of Botany 16*(3), 499–514.

Vogeler, J. C., A. T. Hudak, L. A. Vierling, J. Evans, P. Green, and K. T. Vierling (2014). Terrain and vegetation structural influences on local avian species richness in two mixed-conifer forests. *Remote Sensing of Environment 147*, 13–22.

Vogeler, J. C., Z. Yang, and W. B. Cohen (2016). Mapping post-fire habitat characteristics through the fusion of remote sensing tools. *Remote Sensing of Environment 173*, 294–303.

Warton, D. I. and F. K. C. Hui (2011). The arcsine is asinine: the analysis of proportions in ecology. *Ecology 92*(1), 3–10. http://dx.doi.org/10.1890/10-0340.1.

Westerling, A. L., H. G. Hidalgo, D. R. Cayan, and T. W. Swetnam (2006). Warming and earlier spring increase western US forest wildfire activity. *Science 313*(5789), 940–943.

Whittier, T. R. and A. N. Gray (2016). Tree mortality based fire severity classification for forest inventories: A pacific northwest national forests example. *Forest Ecology and Management 359*, 199–209.

Wimberly, M. C., M. A. Cochrane, A. D. Baer, and K. Pabst (2009). Assessing fuel treatment effectiveness using satellite imagery and spatial statistics. *Ecological Applications 19*(6), 1377–1384.

Woods, M., D. Pitt, M. Penner, K. Lim, D. Nesbitt, D. Etheridge, and P. Treitz (2011). Operational implementation of a lidar inventory in boreal Ontario. *The Forestry Chronicle 87*(4), 512–528.

Wulder, M., J. White, F. Alvarez, T. Han, J. Rogan, and B. Hawkes (2009). Characterizing boreal forest wildfire with multi-temporal landsat and lidar data. *Remote Sensing of Environment 113*(7), 1540–1555.

Wulder, M. A., T. Han, J. C. White, T. Sweda, and H. Tsuzuki (2007). Integrating profiling lidar with landsat data for regional boreal forest canopy attribute estimation and change characterization. *Remote Sensing of Environment 110*(1), 123–137.

Wulder, M. A., J. C. White, R. F. Nelson, E. Næsset, H. O. Ørka, N. C. Coops, T. Hilker, C. W. Bater, and T. Gobakken (2012). Lidar sampling for large-area forest characterization: A review. *Remote Sensing of Environment 121*, 196–209.

Yan, W. Y. and A. Shaker (2016). Reduction of striping noise in overlapping lidar intensity data by radiometric normalization. *International Archives of the Photogrammetry, Remote Sensing & Spatial Information Sciences 41*.

Young, J. (2014). Maine geolibrary: Cost benefit analysis and typical uses of lidar data. *Maine Library of Geographic Information*. Accessed: May 11, 2016. Available at: http://www.maine.gov/geolib/LiDAR.html.

Zeileis, A. and T. Hothorn (2002). Diagnostic checking in regression relationships. *R News 2*(3), 7–10. http://CRAN.R-project.org/doc/Rnews/.

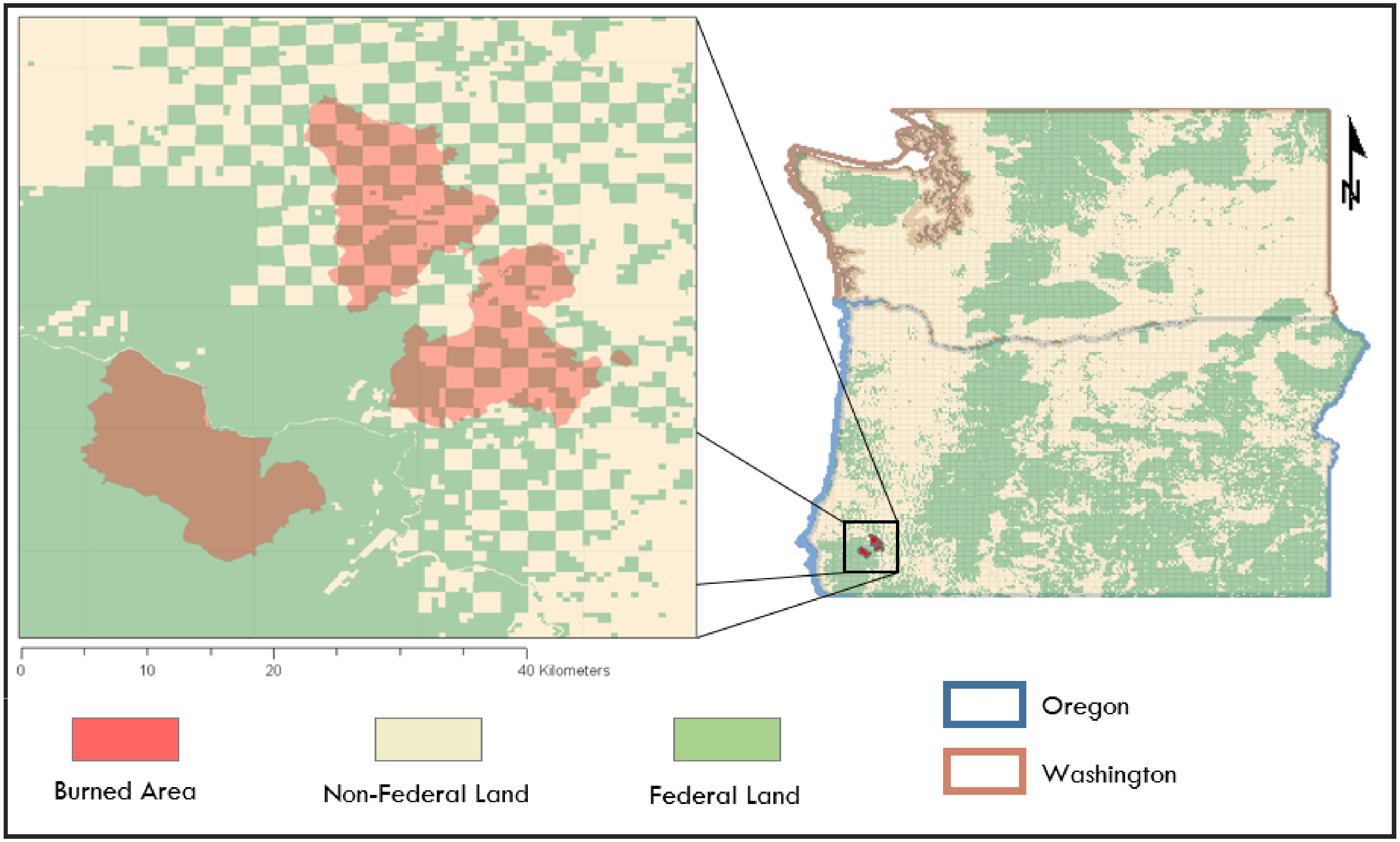

FIGURE 2.1: Study area located in southwestern Oregon, near Riddle and Glendale. Oregon and Washington shown on the right with federal land in green and non-federal land in white. Multi-temporal LiDAR coverage boundary outlined in orange. Shaded regions are the burn areas.

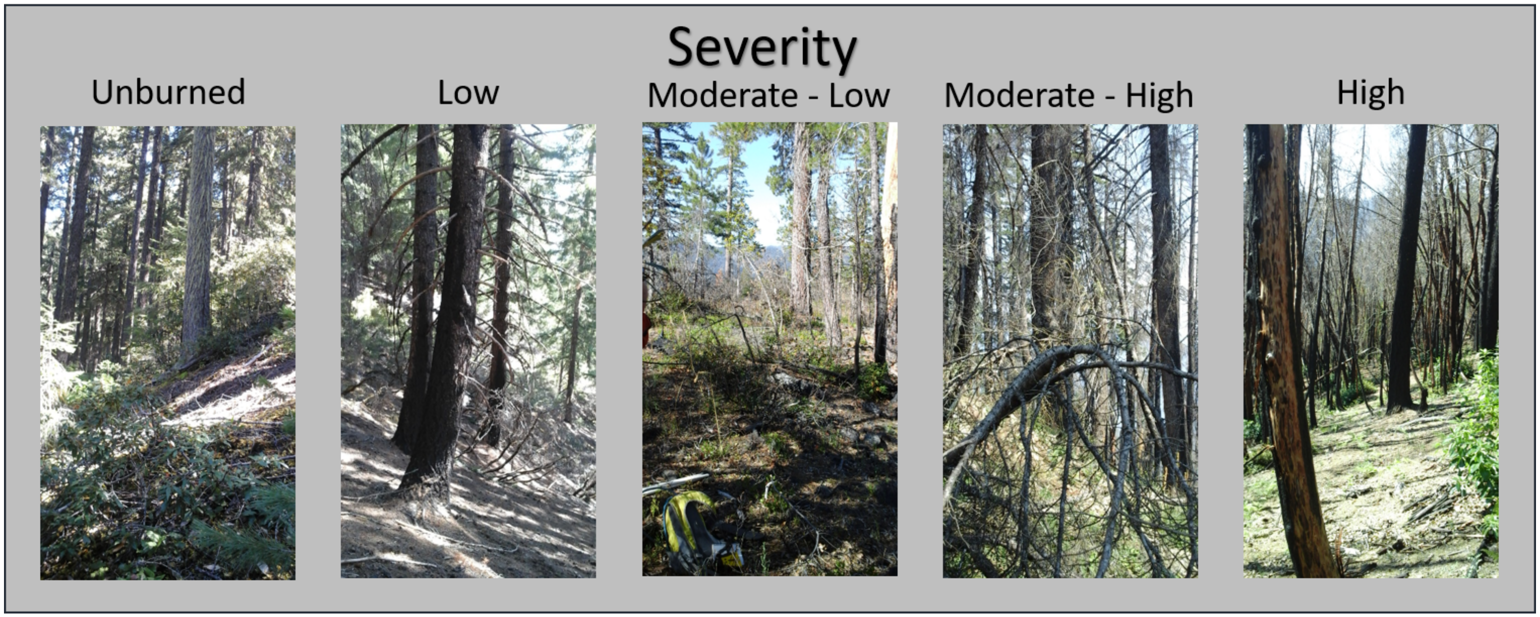

FIGURE 2.2: Photographic illustration of plot stratification and allocation on the ground by severity class. Thresholds used during stratification were: 0-235 (low), 235-406 (moderate-low), 406-648 (moderate-high), 648+ (high). Low, moderate-low, moderate-high, and high represent 0-25, 25-50, 50-75, and 75+ % basal area mortality, respectively. Photos were taken by Michael Hoe in 2015 to document each plot location (2-years after fire).

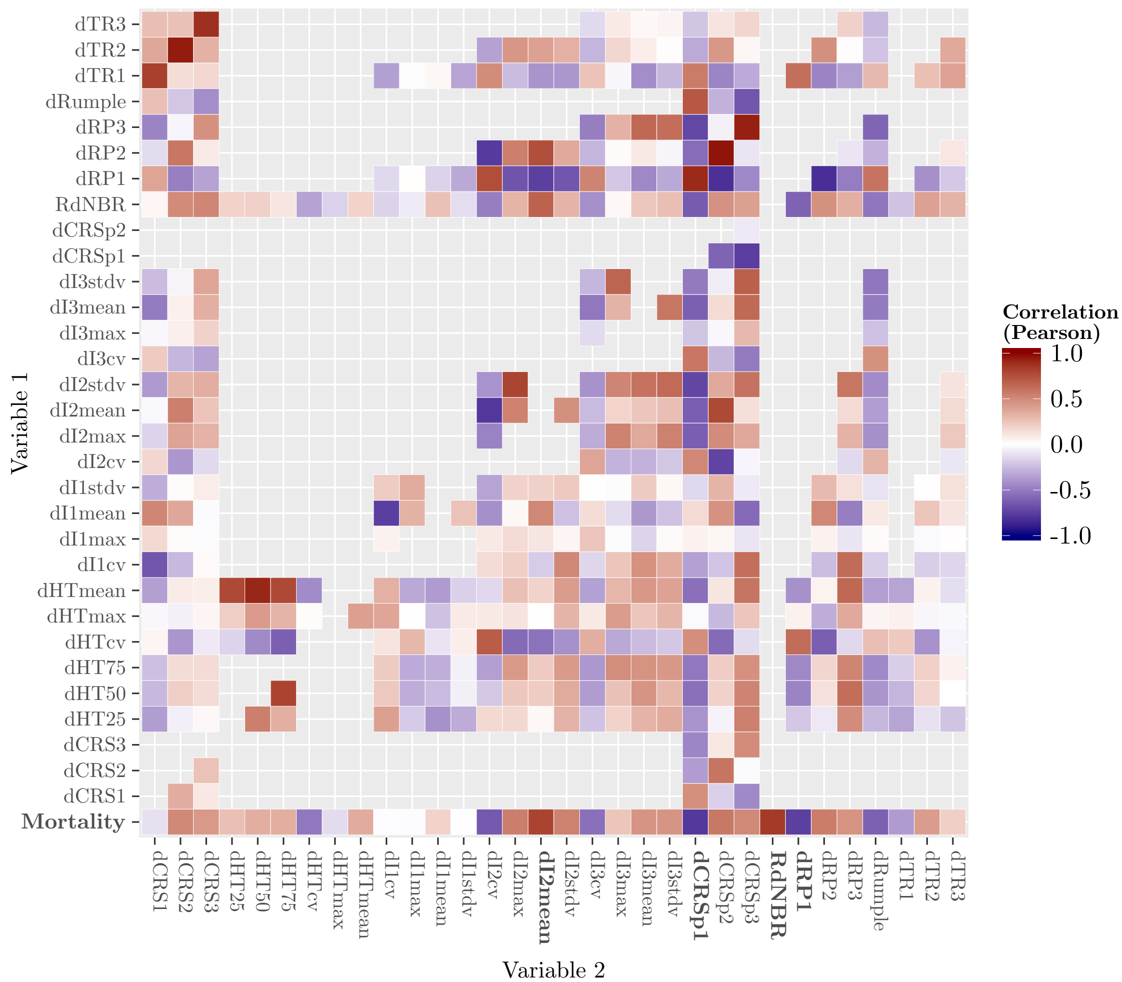

FIGURE 2.3: Pearson correlations across a subset of LiDAR metrics using change estimation. Mortality rates and RdNBR included for reference. Diagonals have been set to zero and duplicates (lower triangle) have been removed for clearer illustration. Observed basal area mortality (response) can be found at the bottom of the y-axis (Variable 1). This subset was used during the use of GLMulti. Top 4 correlated variables are in bold on the x-axis.

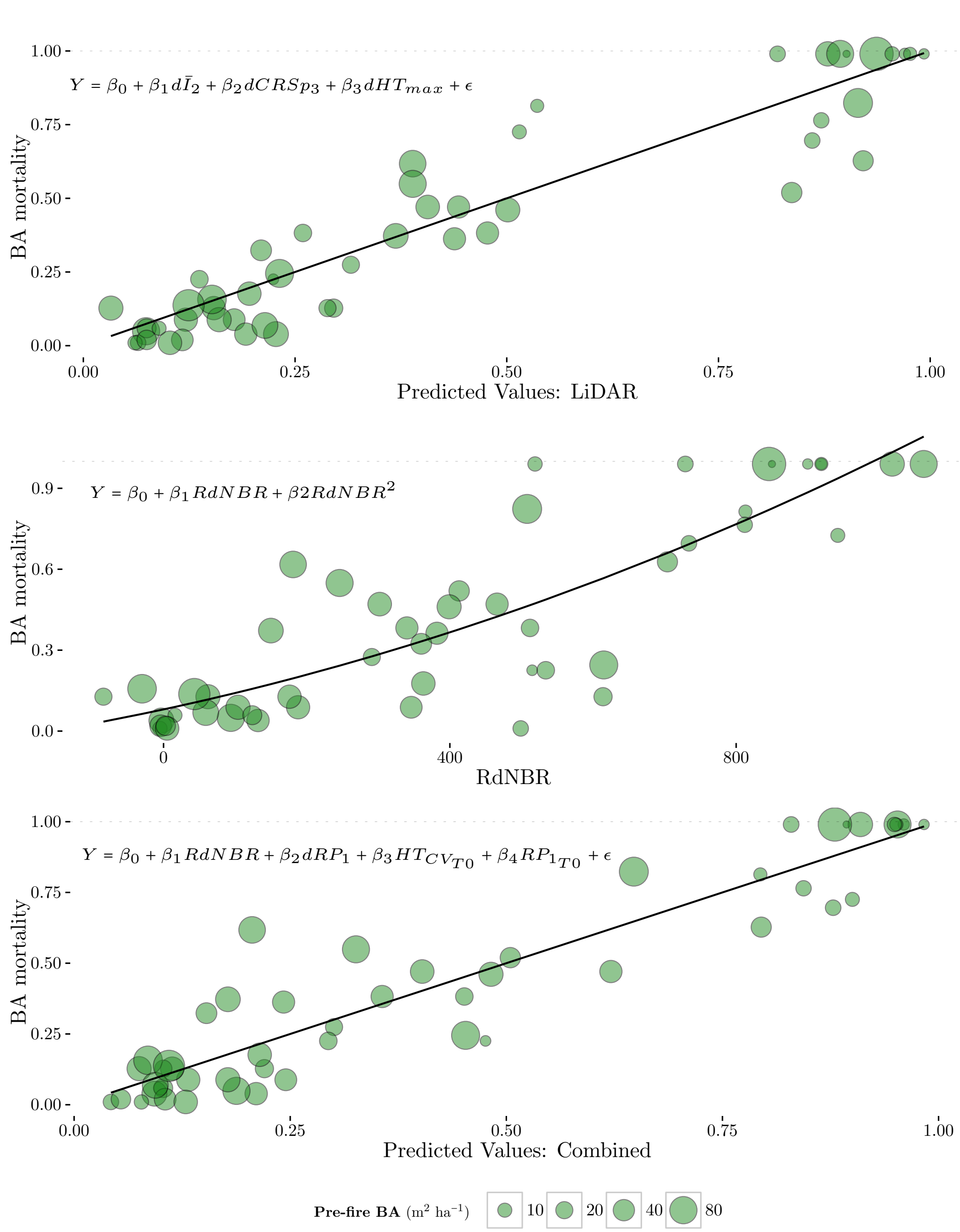

FIGURE 2.4: Comparison of observed versus predicted values for LiDAR (top), RdNBR (middle), and Combined (bottom) models. Circles are sized by pre-fire basal area (m^2 ha^{-1}).

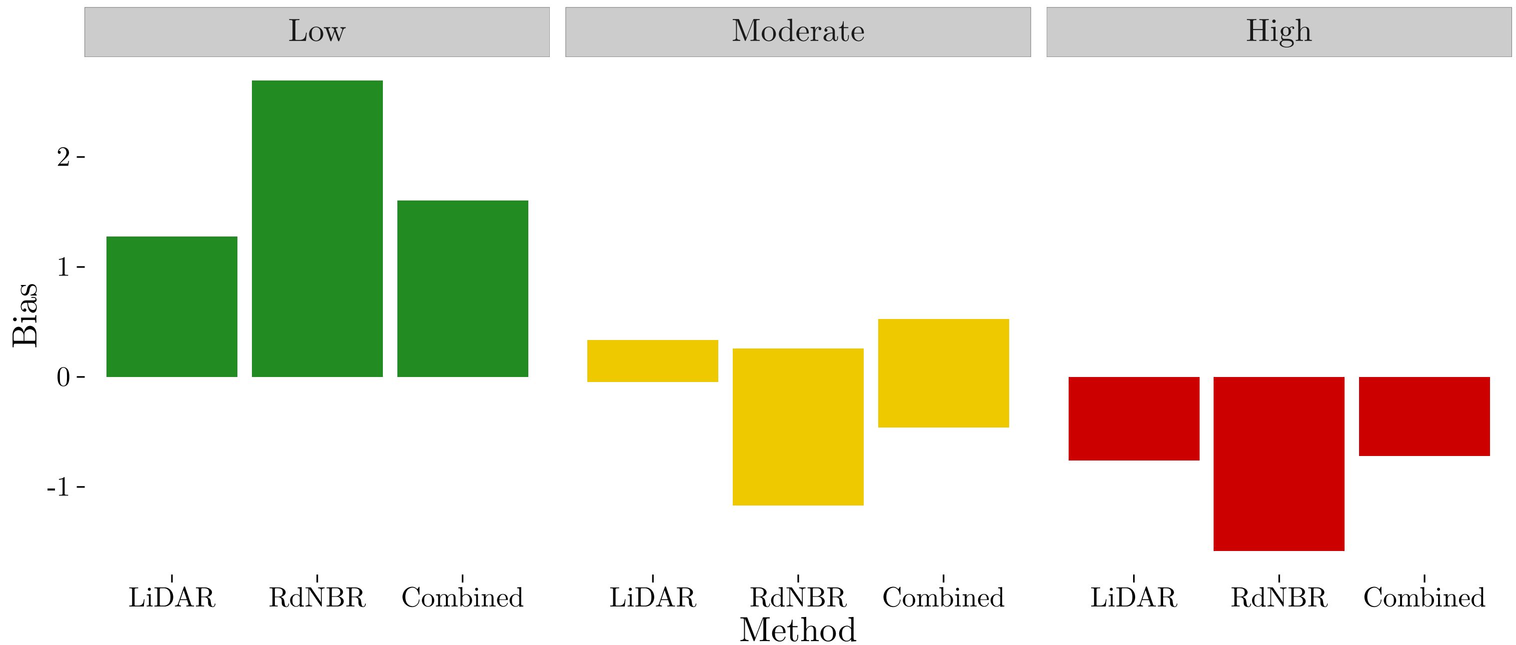

FIGURE 2.5: Comparison of model bias by severity class. Continuous RdNBR values were reclassified using thresholds obtained by modeling RdNBR by observed basal area mortality rate. Model predictions were then back-cast to determine thresholds. LiDAR (left) based predictions produce the least bias for low and moderate severity conditions. High severity conditions appear greatly biased by RdNBR predictions, however, this is largely due to a reduction in the observed threshold for the high severity group during the back-cast, modeling process. We typically see an increase from 648 to 780 or 800's when we model mortality rate as a function of RdNBR. This effect will substantially reduce the bias in the high severity group (RdNBR only) seen here.

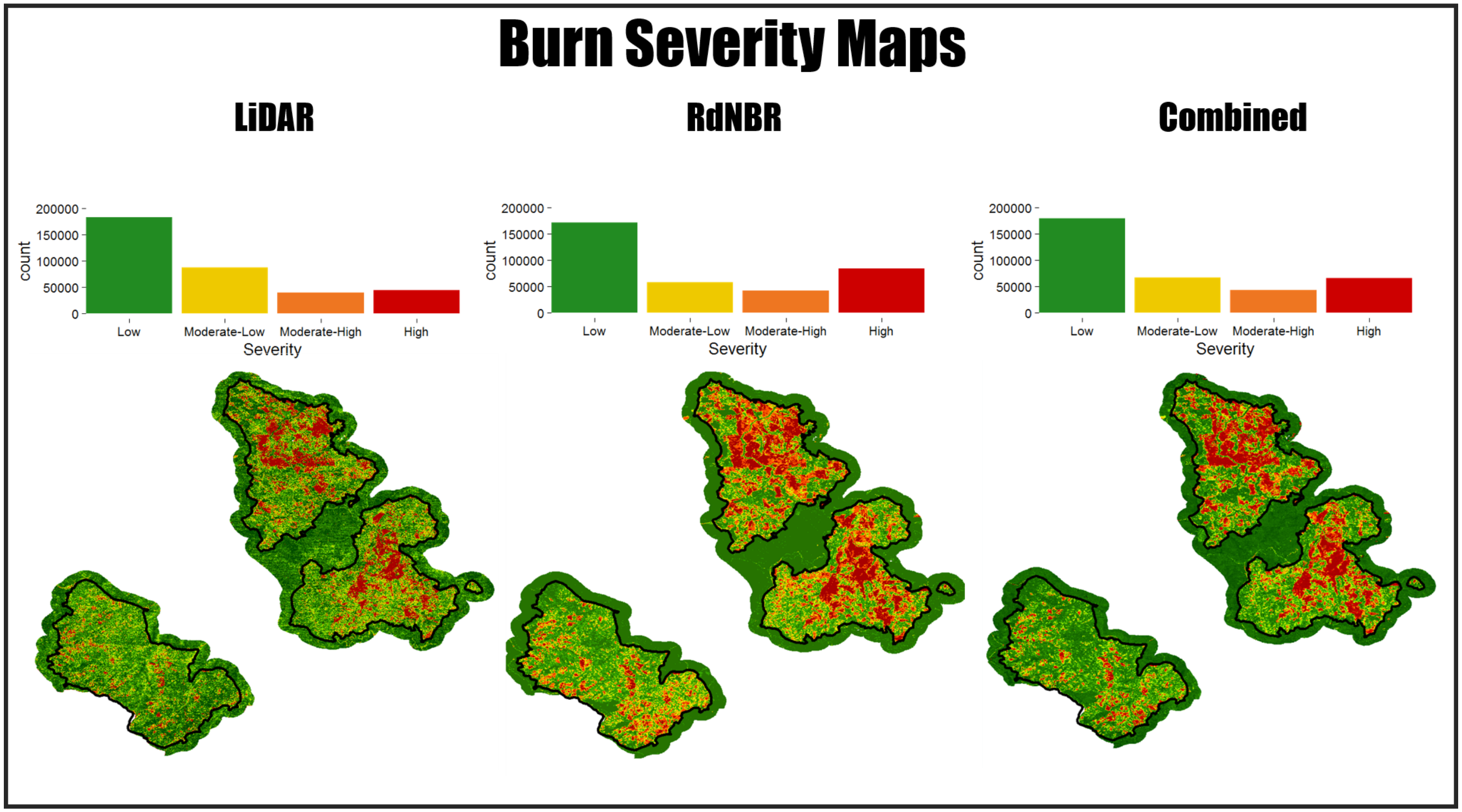

FIGURE 2.6: Landscape classification comparison of basal area mortality estimates. Current maps of the study area were classified using thresholds obtained by modeling RdNBR as a function of observed basal area mortality rate. Low severity (<25%), Moderate-Low (25-50%), Moderate-High (50-75%), High (>75%). The un-burned area was removed prior to the creation of burn severity histograms. Similar to Figure 2.5, high severity thresholds are reduced when modeling RdNBR as a function of observed basal area mortality. The number of pixels within the high severity group for the RdNBR model drops to approximately 55,000 when we use an upper threshold of 784.

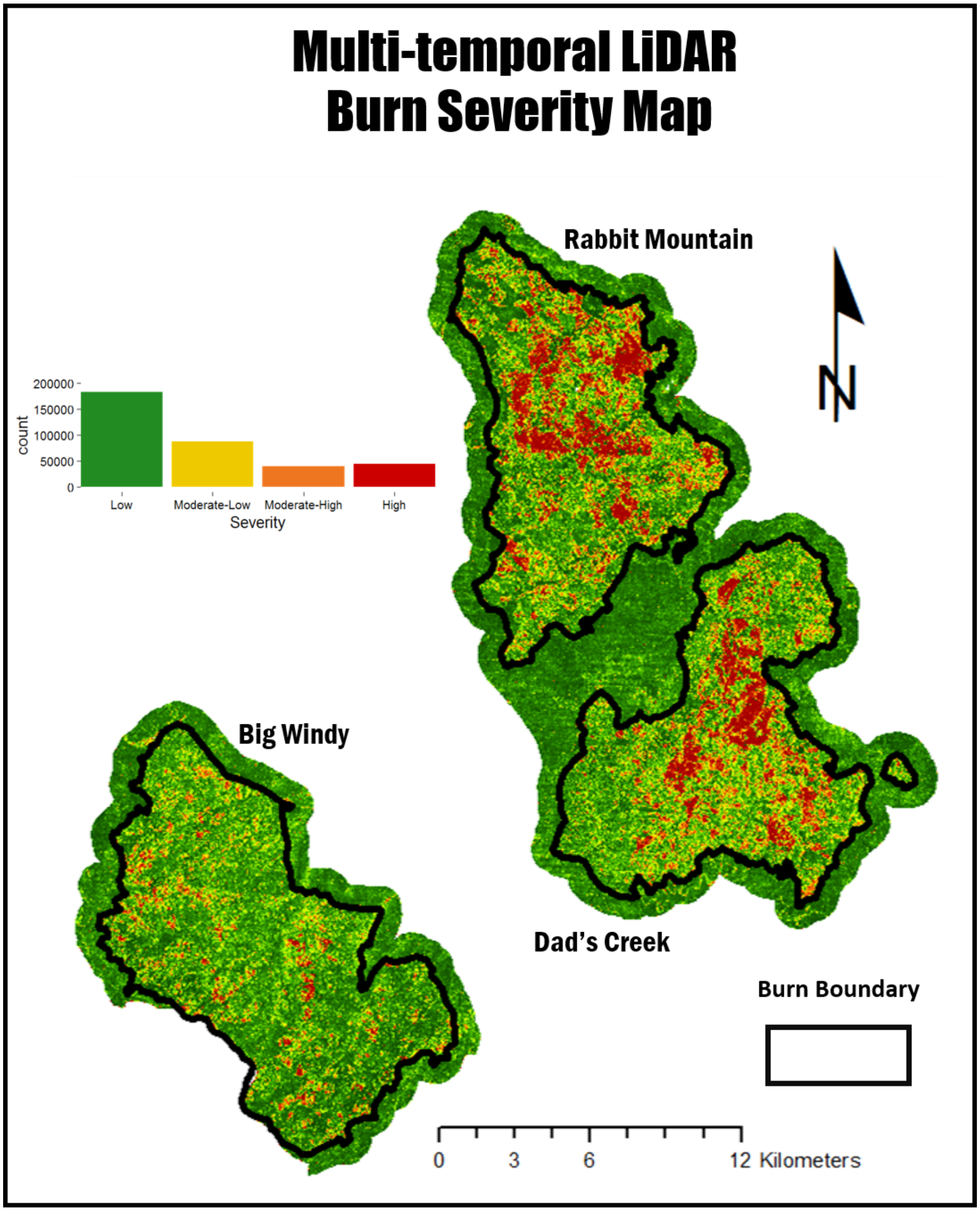

FIGURE 2.7: Basal area mortality map. Modeled using multi-temporal LiDAR metrics obtained in 2012 and 2013. Calibrated using field observations obtained in 2015 (2-years after fire).

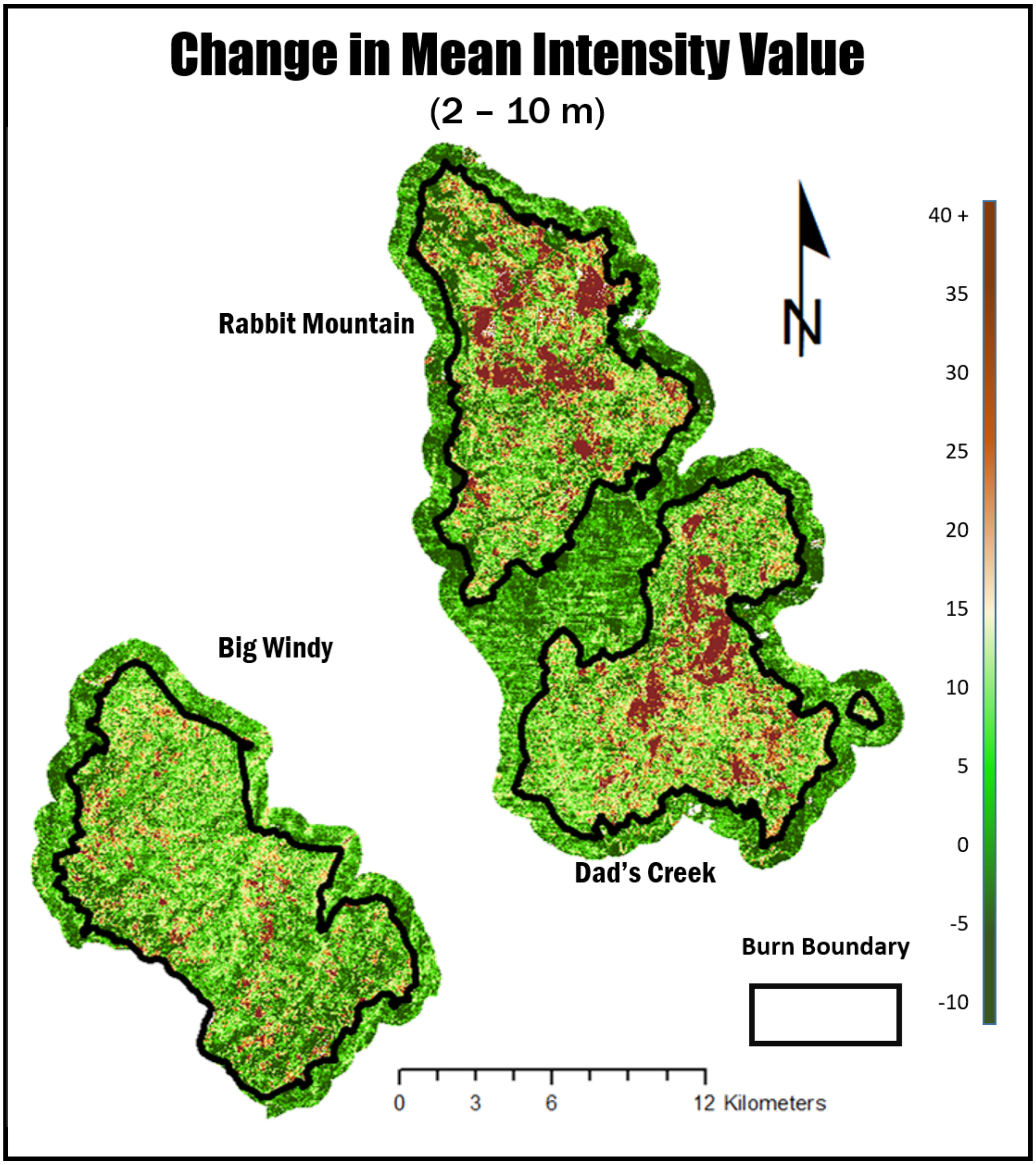

FIGURE 2.8: Landscape map of the absolute difference in mean intensity values between 0 - 2 meters. This change estimator performed the best out of all our examined metrics.

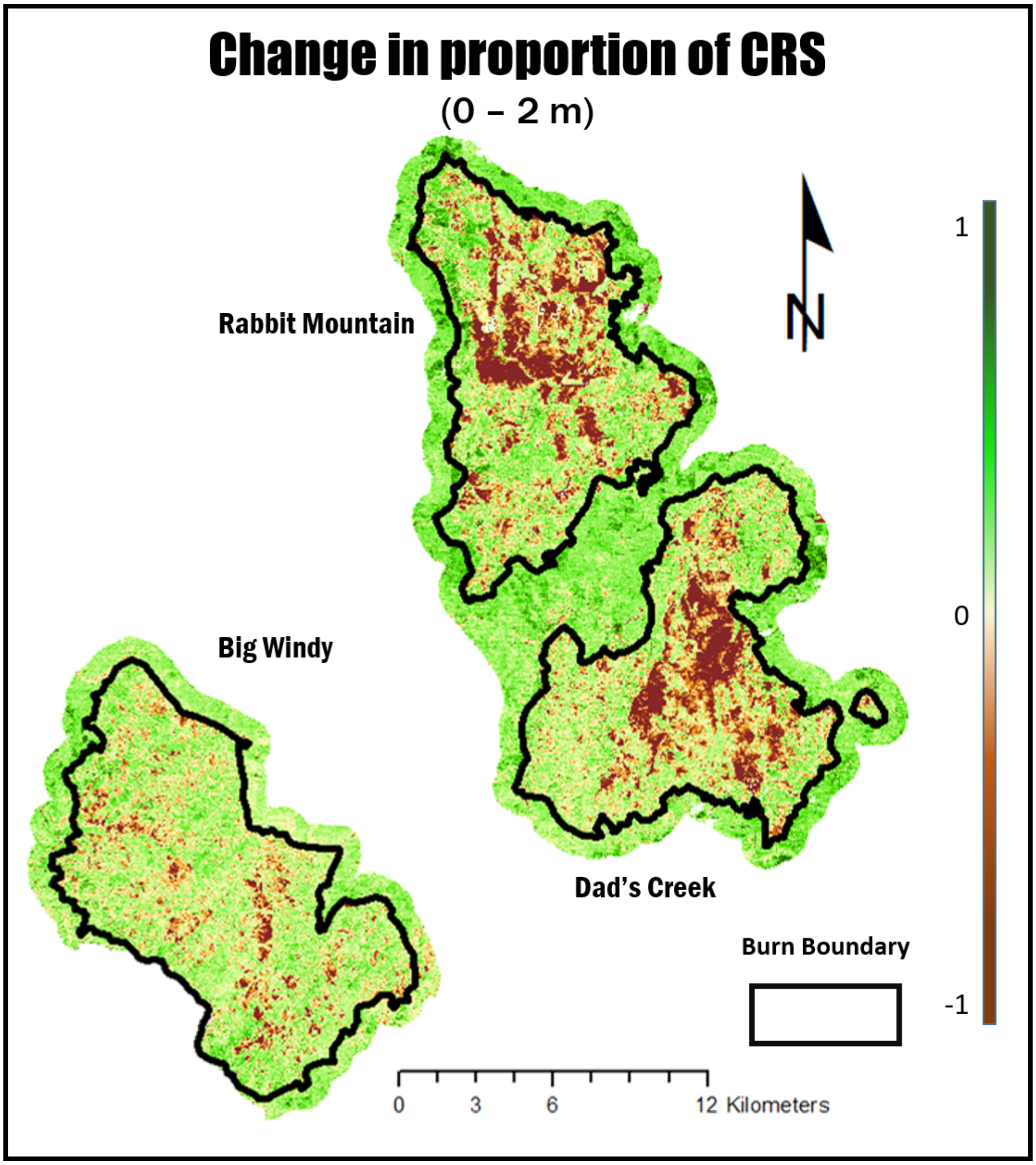

FIGURE 2.9: Landscape map of the absolute difference in the proportion of canopy reflection sum below 2 meters. This change estimator was our second best performing metric, and is inversely related to basal area mortality. It also highly correlated with the change in return proportion below 2 m.

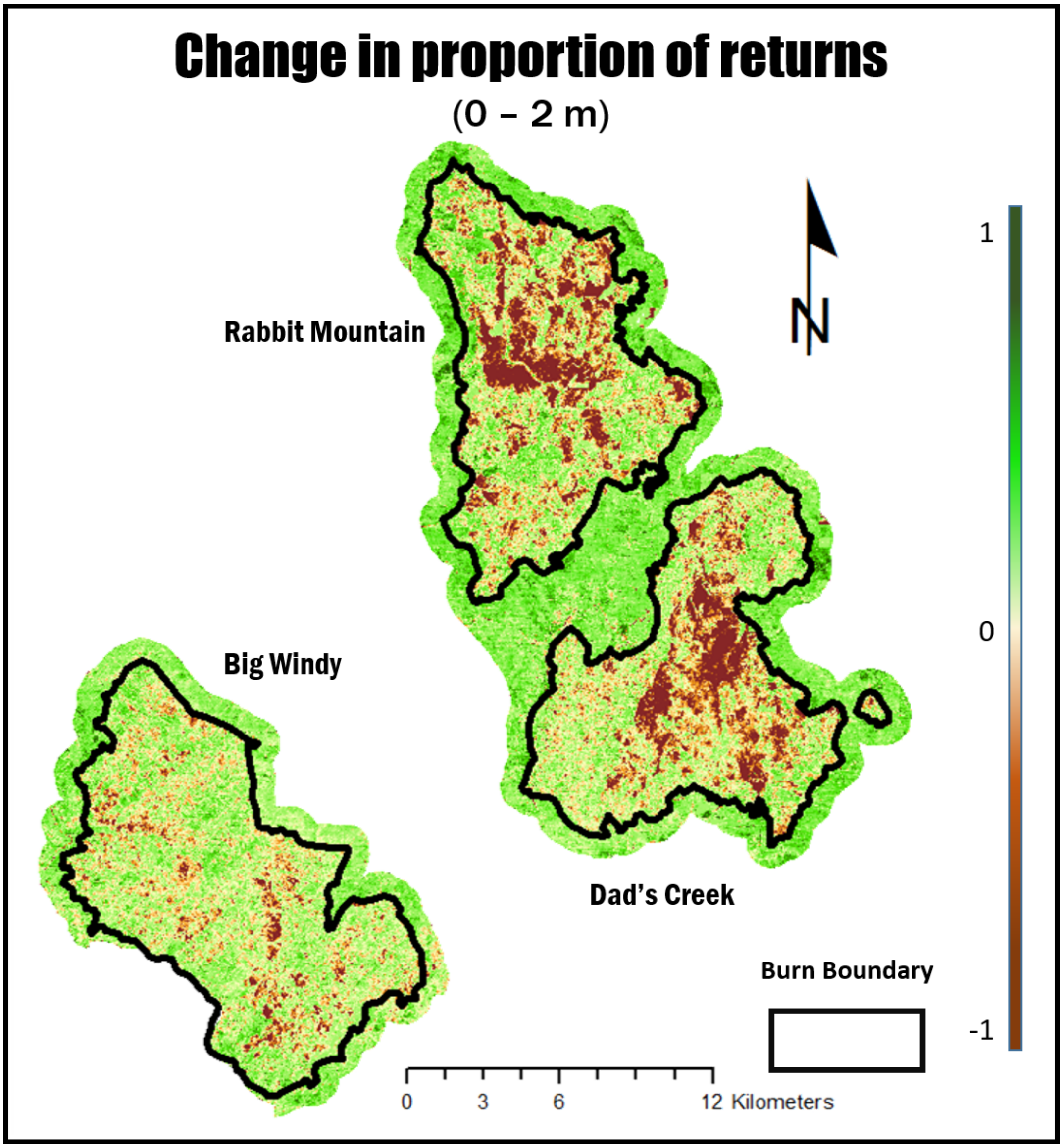

FIGURE 2.10: Landscape map of the absolute difference in proportion of all returns below 2 meters. This estimator was rank third among all tested metrics. It is inversely related to basal area mortality and the reciprocal of canopy cover above 2 m. It is also highly correlated to the absolute difference in the proportion of canopy reflection sum below 2 m.

TABLE 2.1: BLM Fires LiDAR Acquisition Specs (2012). Data obtained between March 6th and August 16th, 2012 by Watershed Sciences, Inc. (known now as Quantum Spatial).

Aircraft	Partenavia P38, Cessna Caravan 208B
Sensor	Leica ALS 50, Leica ALS 60
Survey Altitude (AGL)	900m / 1300m
Targeted Aircraft Speed	NA
Coverage	100% Overlap with 60% Sidelap
Field of View (FOV)	30 (at 900m) / 28 (at 1300m)
Laser Pulse Rate	52.2 hz (at 900m) / 46.7 hz (at 1300m)
Targeted Pulse Density	> 8 pulses per square meter
Aircraft Position	Monitored twice per second (2 Hz)
Aircraft Alititude	Monitored 200 times per second (200 Hz)

TABLE 2.2: BLM Fires LiDAR Acquisition Specs (2013). Data obtained between September 26th and October 23rd, 2013 by Watershed Sciences, Inc. (known now as Quantum Spatial).

Aircraft	Cessna Caravan 208B
Sensor	Leica ALS 50
Survey Altitude (AGL)	900 m
Targeted Aircraft Speed	105 knots
Coverage	100% Overlap with 65% Sidelap
Field of View (FOV)	30
Laser Pulse Rate	96,000 - 105,900 Hz
Targeted Pulse Density	> 8 pulses per square meter
Aircraft Position	Monitored twice per second (2 Hz)
Aircraft Alititude	Monitored 200 times per second (200 Hz)

TABLE 2.3: LiDAR variables examined during analysis. Variables listed represent raw metrics for pre- and post-fire conditions. Estimates of change were derived by taking the absolute difference (example: dRP_1) between pre- and post-fire conditions; similar to RdNBR and dNBR. Three height bins were used: 1 (0-2m), 2 (2-10m), and 3 (above 10m).

Variable	**Definition**
HT_{max}	Maximum height
$\overline{HT}$	Mean height
HT_{CV}	Coefficient of variation of height
$HT_{.95}$	95th percentile height
$HT_{.75}$	75th percentile height
$HT_{.50}$	50th percentile height
$HT_{.25}$	25th percentile height
$Rumple$	Canopy surface (m^2) / ground surface (m^2)
TR	Total Returns
TR_i	Total Returns per height bin$_i$
RP_i	Return proportion per height bin$_i$
I_{max}	Maximum intensity value
I_{max_i}	Maximum intensity value in height bin$_i$
$\bar{I}$	Mean intensity value
$\bar{I}_i$	Mean intensity per height bin$_i$
I_{CV}	Coefficient of variation of the intensity values
$I_{i_{CV}}$	Coefficient of variation of the intensity values in height bin$_i$
I_σ	Standard deviation of the intensity values
I_{i_σ}	Standard deviation of the intensity values in height bin$_i$
$I_{.95}$	95^{th} percentile intensity value
$I_{.75}$	75^{th} percentile intensity value
$I_{.50}$	50^{th} percentile intensity value
$I_{.25}$	25^{th} percentile intensity value
CRS_T	Total canopy reflection sum per unit area
CRS_i	Canopy reflection sum per height bin$_i$
$CRSp_i$	proportion of CRS per height bin$_i$ (range: 0 - 1)

TABLE 2.4: General summary of plot allocation, stratification, and observed mortality. Stratification, plot allocation, and general data summary. Includes information on the number of plots by location, severity, or height class (upper). Additional attributes are provided in the lower table. H - high, MH - Moderate-High, ML - Moderate-Low, L - Low, Un - Unburned, Short - < 30m, Tall - > 30m. Elevations and aspects were derived from the delivered digital terrain models. Height class was obtained using pre-fire LiDAR 95%'ile heights. RdNBR and estimated thresholds from previous studies were used for our severity estimates.

Location	#	**Severity**	#	**Height Class**	#
Big Windy	17	**H**	13	**Short**	29
Dad's Creek	12	**MH**	8	**Tall**	26
Rabbit Mountain	14	**ML**	11		
Outside Burn Area	8	**L**	11		
		Un	8		

Attribute	**Min**	**Max**	**Mean**	**SD**
Aspect (°)	0.39	357.71	167.92	96.78
Slope (°)	4.11	58.32	21.86	9.34
Elevation (m)	297.80	1303.30	758.80	268.48
Pre-fire BA (m^2/ha)	0.41	135.20	43.30	30.87
RdNBR	-84.00	1062.00	405.55	330.11
Mortality (proportion killed)	0.00	1.00	0.41	0.36

TABLE 2.5: Summary statistics for the best performing LiDAR models chosen during regression analysis (top) including cross validated results (bottom). N = 51.

LiDAR Models

Model	**Bias**	**Bias(%)**	**RMSE**	**RMSE(%)**	**AIC**	**BIC**
$y = \beta_0 + \beta_1 d\bar{I}_2 + \epsilon$	-0.0303	-7.40	0.2085	50.94	-56.92	-51.12
$y = \beta_0 + \beta_1 d\bar{I}_2 + \beta_2 dCRSp_3 + \epsilon$	-0.0189	-4.62	0.1474	36.02	-83.58	-75.85
$y = \beta_0 + \beta_1 d\bar{I}_2 + \beta_2 dCRSp_3 + \beta_3 dHT_{max} + \epsilon$	-0.0136	-3.32	0.1207	29.49	-99.71	-90.05
$y = \beta_0 + \beta_1 d\bar{I}_2 + \beta_2 dCRSp_3 + \beta_3 dHT_{max} + \beta_4 dHT_{CV} + \epsilon$	-0.0147	-3.59	0.1161	28.37	-100.06	-88.47
$y = \beta_0 + \beta_1 d\bar{I}_2 + \beta_2 dCRSp_3 + \beta_3 dHT_{max} + \beta_4 dHT_{CV} + \beta_5 dCRS_1 + \epsilon$	-0.0121	-2.96	0.1136	27.76	-102.82	-89.30

Cross Validated (Leave-One-Out)

Model	**Bias**	**Bias(%)**	**RMSPE**	**RMSPE(%)**
$y = \beta_0 + \beta_1 d\bar{I}_2 + \epsilon$	-0.0305	-7.45	0.2145	52.41
$y = \beta_0 + \beta_1 d\bar{I}_2 + \beta_2 dCRSp_3 + \epsilon$	-0.0180	-4.40	0.1548	37.82
$y = \beta_0 + \beta_1 d\bar{I}_2 + \beta_2 dCRSp_3 + \beta_3 dHT_{max} + \epsilon$	-0.0127	-3.10	0.1293	31.59
$y = \beta_0 + \beta_1 d\bar{I}_2 + \beta_2 dCRSp_3 + \beta_3 dHT_{max} + \beta_4 dHT_{CV} + \epsilon$	-0.0097	-2.37	0.1312	32.06
$y = \beta_0 + \beta_1 d\bar{I}_2 + \beta_2 dCRSp_3 + \beta_3 dHT_{max} + \beta_4 dHT_{CV} + \beta_5 dCRS_1 + \epsilon$	-0.0104	-2.54	0.1259	30.76

TABLE 2.6: LiDAR model summaries including coefficient estimates, z-values, and variance inflation factors for the best performing beta regressions found during data analysis.

Variable	Parameter	Estimate	SE	t-value	Pr(>|t|)	VIF
$Intercept$	β_0	-1.1741	0.198	-5.93	3.08E-09	-
$d\bar{I}_2$	β_1	0.0600	0.008	7.65	1.94E-14	-
Φ	Φ	2.6807	0.504	5.32	1.04E-07	-
$Intercept$	β_0	-1.6157	0.178	-9.08	1.13E-19	-
$d\bar{I}_2$	β_1	0.0706	0.007	9.70	2.95E-22	1.018
$dCRSp_3$	β_2	5.3151	0.953	5.58	2.46E-08	1.018
Φ	Φ	5.4980	1.115	4.93	8.24E-07	-
$Intercept$	β_0	-1.9810	0.172	-11.54	8.49E-31	-
$d\bar{I}_2$	β_1	0.0773	0.007	11.43	2.99E-30	1.019
$dCRSp_3$	β_2	6.6482	0.910	7.31	2.74E-13	1.083
dHT_{max}	β_3	-0.1806	0.041	-4.40	1.07E-05	1.063
Φ	Φ	8.5164	1.751	4.86	1.14E-06	-
$Intercept$	β_0	-2.0351	0.173	-11.76	6.20E-32	-
$d\bar{I}_2$	β_1	0.0753	0.007	11.00	3.93E-28	1.071
$dCRSp_3$	β_2	6.0348	1.024	5.89	3.78E-09	1.501
dHT_{max}	β_3	-0.1663	0.042	-3.98	6.96E-05	1.136
$I_{3_{CV}}$	β_4	-1.0340	0.705	-1.47	1.43E-01	1.498
Φ	Φ	8.9281	1.836	4.86	1.15E-06	-
$Intercept$	β_0	-2.1025	0.172	-12.21	2.72E-34	-
$d\bar{I}_2$	β_1	0.0739	0.007	11.05	2.31E-28	1.072
$dCRSp_3$	β_2	7.1620	1.104	6.49	8.58E-11	1.795
dHT_{max}	β_3	-0.1753	0.041	-4.26	2.00E-05	1.147
$I_{3_{CV}}$	β_4	-0.8980	0.701	-1.28	2.00E-01	1.498
CRS_1	β_5	0.0000	0.000	2.16	3.10E-02	1.263
Φ	Φ	9.6624	1.981	4.88	1.07E-06	-

TABLE 2.7: Summary of the best performing combined models chosen during regression analysis (top), including cross-validated results (bottom). Note that models with greater than 2 covariates (not including intercept) contain metrics related to pre-fire forest conditions (T0). N = 51.

Combined Models

Model	**Bias**	**Bias(%)**	**RMSE**	**RMSE(%)**	**AIC**	**BIC**
$y = \beta_0 + \beta_1 RdNBR + \epsilon$	-0.0323	-7.89	0.1984	48.48	-64.55	-58.76
$y = \beta_0 + \beta_1 RdNBR + \beta_2 dRP_1 + \epsilon$	-0.0207	-5.06	0.1562	38.17	-79.92	-72.19
$y = \beta_0 + \beta_1 RdNBR + \beta_2 dRP_1 + \beta_3 dHT_{CV_{T0}} + \epsilon$	-0.0189	-4.62	0.1387	33.89	-90.18	-80.52
$y = \beta_0 + \beta_1 RdNBR + \beta_2 dRP_1 + \beta_3 HT_{CV_{T0}} + \beta_4 RP_{1_{T0}} + \epsilon$	-0.0081	-1.98	0.1231	30.08	-101.25	-89.66
$y = \beta_0 + \beta_1 RdNBR + \beta_2 dRP_1 + \beta_3 HT_{CV_{T0}} + \beta_4 RP_{1_{T0}} + \beta_5 dHT_{.95} + \epsilon$	-0.0083	-2.03	0.1149	28.07	-102.72	-89.20

Cross Validated (Leave-One-Out)

Model	**Bias**	**Bias(%)**	**RMSPE**	**RMSPE(%)**
$y = \beta_0 + \beta_1 RdNBR + \epsilon$	-0.0325	-7.94	0.2044	49.94
$y = \beta_0 + \beta_1 RdNBR + \beta_2 dRP_1 + \epsilon$	-0.0199	-4.86	0.1675	40.93
$y = \beta_0 + \beta_1 RdNBR + \beta_2 dRP_1 + \beta_3 HT_{CV_{T0}} + \epsilon$	-0.0181	-4.42	0.1511	36.92
$y = \beta_0 + \beta_1 RdNBR + \beta_2 dRP_1 + \beta_3 HT_{CV_{T0}} + \beta_4 RP_{1_{T0}} + \epsilon$	-0.0092	-2.25	0.1347	32.91
$y = \beta_0 + \beta_1 RdNBR + \beta_2 dRP_1 + \beta_3 HT_{CV_{T0}} + \beta_4 RP_{1_{T0}} + \beta_5 dHT_{.95} + \epsilon$	-0.0102	-2.49	0.1333	32.57

TABLE 2.8: Combined model summaries including coefficient estimates, z-values, and variance inflation factors for the best performing beta regressions found during data analysis.

Variable	**Parameter**	**Estimate**	**SE**	**Z-value**	**Pr(>|z|)**	**VIF**
$Intercept$	β_0	-1.9063	0.257	-7.41	1.31E-13	-
$RdNBR$	β_1	0.0040	0.001	7.91	2.50E-15	-
Φ	Φ	3.1368	0.608	5.16	2.45E-07	-
$Intercept$	β_0	-2.1619	0.239	-9.05	1.44E-19	-
$RdNBR$	β_1	0.0034	0.001	6.46	1.05E-10	1.566
dRP_1	β_2	-5.1593	1.285	-4.02	5.93E-05	1.566
Φ	Φ	4.8414	0.975	4.96	6.91E-07	-
$Intercept$	β_0	-1.5126	0.333	-4.54	5.71E-06	-
$RdNBR$	β_1	0.0042	0.001	7.96	1.74E-15	1.7
dRP_1	β_2	-4.2369	1.243	-3.41	6.55E-04	1.697
$HT_{CV_{T0}}$	β_3	-1.1478	0.381	-3.01	2.62E-03	1.106
Φ	Φ	6.5252	1.332	4.90	9.70E-07	-
$Intercept$	β_0	-1.3243	0.325	-4.07	4.62E-05	-
$RdNBR$	β_1	0.0035	0.001	6.69	2.27E-11	1.981
dRP_1	β_2	-5.4713	1.222	-4.48	7.59E-06	1.717
$HT_{CV_{T0}}$	β_3	-2.2568	0.500	-4.52	6.26E-06	1.996
$RP_{1_{T0}}$	β_4	2.7760	0.812	3.42	6.31E-04	2.278
Φ	Φ	8.6229	1.762	4.89	9.90E-07	-
$Intercept$	β_0	-1.4618	0.328	-4.46	8.38E-06	-
$RdNBR$	β_1	0.0036	0.001	7.02	2.29E-12	1.986
dRP_1	β_2	-5.0131	1.216	-4.12	3.73E-05	1.777
$HT_{CV_{T0}}$	β_3	-2.2113	0.494	-4.48	7.53E-06	2.016
$RP_{1_{T0}}$	β_4	2.9304	0.799	3.67	2.43E-04	2.3
$dHT_{.95}$	β_5	0.0497	0.025	1.97	4.85E-02	1.132
Φ	Φ	9.3256	1.908	4.89	1.01E-06	-

TABLE 2.9: Confusion matrix of RdNBR derived fire severity estimates versus LiDAR over all 3 fire areas. RdNBR values were classified using thresholds derived from modeling RdNBR as a function of basal area mortality rate. Thresholds used during severity classification were further validated via comparison to observed results from 304 FIA plots.

		LiDAR				
		Low	**Moderate-Low**	**Moderate-High**	**High**	**Total**
RdNBR	**Low**	122,834	39,054	7,901	1,621	171,410
	Moderate-Low	29,649	18,870	7,222	2,507	58,248
	Moderate-High	15,870	13,148	7,673	4,797	41,488
	High	14,235	16,109	16,965	35,904	83,213
	Total	182,588	87,181	39,761	44,829	354,359

Multi-temporal LiDAR Provides New Perspectives of Fire Effects and Post-fire Landscapes

3 Chapter 3

3.1 Abstract

Quantitative assessments of fire effects are key to improving our understanding of ecosystem resilience. While remote sensing technology has allowed us to assess fire landscape effects, we are often limited by the lack of information related to pre-fire forest attributes. As a result, our ability to improve pro-active management practices to protect our forested landscapes is severely inhibited. Furthermore, with longer fire seasons and extended drought conditions, our ability to make a significant difference through pro-active management is dwindling. We used multi-temporal Light Detection and Ranging (LiDAR) as a stand-alone remote sensing platform to 1) model pre-fire basal area using log-linear regression, 2) estimate fire effects using change estimation, and 3) map living post-fire basal area by combining 1) and 2). Our research is consciously targeted at improving our understanding of post-fire ecological effects by providing a well defined landscape assessment of pre- and post-fire conditions. Our results illustrate that multi-temporal LiDAR can be used as a standalone platform to provide more precise and interpretable estimations of fire effects across broad landscapes.

3.2 Introduction

Disturbance events such as wildfires provide many positive benefits to ecosystems worldwide (Franklin et al., 1987, 2002). Wildfires consume dead and living vegetation, facilitate nutrient cycling, release carbon, and create new open growing space (Wright and Bailey, 1982). Evidence shows that fire severity and subsequent effects, vary due to top-down climate controls and bottom up fuels and topography controls, which alters ecosystem composition and structure at scales varying from micro-sites to landscapes (Agee, 1991; Bowman et al., 2009; Perry et al., 2011). While forest ecosystems are highly dynamic and many tree species have adapted to wildfire events (Brown and Smith, 2000; Dunn and Bailey, 2016), land managers are concerned with ecosystem resilience because of altered disturbance regimes and a rapidly changing climate (Gutschick and BassiriRad, 2003; Littell et al., 2010; Liu et al., 2013; Mallek et al., 2013; Marlon et al., 2012). For example, aggressive fire suppression and past management activities increased fuel continuity and homogenized forest structure across broad landscapes (Hessburg et al., 2007; Naficy et al., 2010). At the same time, global climate projections are suggesting more frequent wildfire events due to longer fire seasons and elevated drought conditions (Liu et al., 2013; Stephens et al., 2014; Westerling et al., 2006). Evidence suggests these factors have already contributed to increased fire severity relative to historical conditions, potentially impacting the resilience of tree species across dry forests of the western U.S. (Mallek et al., 2013; Miller and Safford, 2012).

One measure of resilience in forested systems is the ability for trees to naturally regenerate following disturbance. Research suggests that the spatial arrangement and composition of legacy species drives ecosystem development after disturbance (Gutschick and BassiriRad, 2003; Turner et al., 1998). In the context of this study, legacy species refer to trees surviving after fire. Therefore, being able to provide landscape scale spatial information on the distribution, location, and composition of post-fire legacy species is highly valuable and applicable. This information would help identify high risk areas, spatially optimize fuel treatments across stand types and ownership boundaries, and protect specific wildlife habitats.

Quantitative assessments of fire effects are key to improving our understanding of ecosystem resilience (Seidl et al., 2014). Landsat data is commonly used by scientists and managers to quantify fire effects at landscape scales (Bolton et al., 2015; Kennedy et al., 2010; Key and Benson, 1999, 2005; Lentile et al., 2006; Miller et al., 2009). These methods have been shown to be useful when detecting and describing fire severity, however, they have inherent limitations: 1) Landsat imagery is 2-dimensional and lacks information related to vertical forest structure (Morgan et al., 2014; Safford et al., 2008; Wulder et al., 2009); and 2) the interpretation of ecological effects due to severity estimates can be challenging (Keeley, 2009). For example, Landsat imagery is influenced by any visible vegetative layer from above, including grasses, shrubs and trees, complicating the relationship between observed spectral response and ecological effects (Kane et al., 2015; Skowronski et al., 2007; Whittier and Gray, 2016; Wulder et al., 2007). Furthermore, fire severity is recorded as a proportion and includes no additional information related to the abundance or type of remaining resources which influences fire effects across broad landscapes (Bolton et al., 2015; Lentile et al., 2006; Morgan et al., 2014; Wulder et al., 2009).

Multi-temporal Light Detection and Ranging (LiDAR) can be used to quantify map pre-fire forest attributes, estimate fire effects, and map post-fire legacy distributions, as a stand-alone analysis. Light Detection and Ranging (LiDAR) uses an airborne laser scanner (ALS) to measure canopy vegetation in three dimensions using discrete-return or full-waveform sensors (Sumnall et al., 2016). Contrary to passive remote sensing technologies, LiDAR is capable of producing high-resolution digital elevation models and can directly measure vegetation cover, height, structure, and basal area (Bright et al., 2014; Coops et al., 2007; Næsset, 2007; Persson et al., 2002). Recent applications of LiDAR demonstrate its ability to generate landscape level maps of other forest attributes, such as canopy fuel weight (CFW) and canopy bulk density (CBD) (Skowronski et al., 2011), and estimate upper canopy biomass and carbon stocks (García et al., 2010; Hall et al., 2005; Means et al., 1999).

LiDAR offers unique benefits unobtainable by passive remote sensing technology. The ability to quantify and map pre-fire forest attributes in relation to fire effects provides new perspectives on post-fire conditions. For example, the spatial distribution or fire patterns could be related to stand structures pre-fire, such as the movement of wildfire from one forest type into another. Additionally, our ability to quantify and define fire effects should greatly improve. Research has shown that LiDAR based estimations of fire-induced basal area mortality are more accurate than satellite-based methods. Therefore, in this study, we use a single remote sensing technology (discrete-return multi-temporal LiDAR) to quantify pre-fire basal area, basal area mortality, and post-fire basal area. Our objective is to provide a well defined landscape assessment of fire effects. Lastly, we provide an example of severity estimates by ownership and pre-fire basal area class. Our research is consciously targeted at improving our understanding of the ecological effects of contemporary wildfires (Keeley, 2009; Morgan et al., 2014).

3.3 Methods

3.3.1 Study Area

Three large wildfires were ignited by lightning on July 26th, 2013 within the Klamath Mountain Ecoregion in southwestern Oregon (InciWeb, 2013; Omernik and Griffith, 2014). All three areas burned with mixed-severity, driven by the dry Mediterranean climate, segmented terrain, and topographical attributes (Agee, 1991; Halofsky et al., 2011; Skinner et al., 2006; Taylor and Skinner, 1998). The Douglas Complex encompasses 20,689 ha over a mixed ownership landscape and includes the Dad's Creek and Rabbit Mountain fires. The Big Windy fire covers 11,464 ha of federal land only (Figure 3.1).

The Klamath Mountain Ecoregion is characterized by highly diverse flora and is often described as having a mixed-severity fire regime (Agee, 1991; Halofsky et al., 2011; Taylor and Skinner, 1998). The dry Mediterranean climate, segmented terrain, and topographical attributes greatly influenced fire frequency and severity over time (Skinner et al., 2006). Frequent disturbances and repeated exposure create highly diverse patches of legacy species which influence stand succession and wildlife habitat suitability over long time scales (Agee, 1991; Halofsky et al., 2011; Seidl et al., 2014). Dominant tree species include Douglas-fir (*Pseudotsuga menziesii (Mirb.) Franco*), Pacific madrone (*Arbutus menziesii Pursh*), canyon live oak (*Quercus chrysolepis Liebm.*), Oregon white oak (*Quercus garryana Douglas ex Hook.*), California black oak (*Quercus kelloggii Newberry*), golden chinkapin (*Castanopsis chrysophylla*), tanoak (*Lithocarpus densiflourus*), ponderosa pine (*Pinus ponderosa Lawson & C. Lawson*), and white fir (*Abies concolor (lowina)*. Less abundant upland tree species include incense cedar (*Calocedrus decurrens (Torr.)Florin*), sugar pine (*Pinus lambertiana*), Jeffery pine (*Pinus jefferyi*), big-leaf maple (*Acer macrophyllym*), pacific dogwood (*Cornus nuttallii*), apple (*Malus spp.*, and knobcone pine (*Pinus attenuata*). Chaparral shrub species are common in the understory of most of these vegetation zones and dominate vegetative cover on portions of the landscape (Duren et al., 2012).

3.3.2 Calibration Plots

Field data was collected between June 15 and September 24, 2015 (2 years after fire) to create a series of calibration plots. We used stratified random sampling based on fire severity and tree heights (Figure 3.2). In total, we had 10 unique strata representing the range of conditions across the landscape. Fire severity groups were classified using thresholds obtained by modeling basal area mortality using RdNBR and 304 Forest Inventory and Analysis plots (FIA) (Reilly et al., *in review*). LiDAR derived pre-fire 95%'ile heights were used to approximate the average stand height across all 3 fires and partition forested areas into 2 height classes (tall/short). The raw RdNBR raster layer (30x30 m pixels) was re-sampled to a 90x90 m layer to increase the probability that our plot represented the targeted severity class. Plot centers were permanently monumented for future re-measurements and were located as close to pixel (Landsat) center as possible. We further constrained plot locations by requiring plot centers to be a minimum of 400 m apart. Over 100 GPS points were recorded per plot using a Trimble Geo 7X hand-held GNSS receiver and post-processed in Pathfinder Office™.

Our field plots were designed to be comprehensive and useful for a wide range of research objectives. We used nested, circular, fixed radius plots to measure all tree and snag species, understory vegetation composition, regeneration, coarse woody debris (1000 hr), and fine fuels (1, 10, 100 hr). Line transects were used for fine fuel measurements and a 2 meter radius circular plot was used for vegetation cover, composition, and regeneration (seedlings by 10 cm height class). Azimuth and distance measurements were taken for all trees and snags (> 10 cm dbh, snags above 2 m tall) within the large plot, along with coarse woody debris (>15cm large end, > 1 m long), trees between 2.54 - 10 cm dbh, and all living shrub species in the smaller subplot (5.4 m radius). Azimuth and distance measurements for coarse wood were taken at small and large ends. We identified top condition for all trees and snags (whole, broken, forked, fallen) and recorded total tree heights for a subsample of all trees within plots including a height measurement for any tree identified as a snag, broken, or fallen. Canopy base height was recorded for any tree with foliage, regardless of whether it was green or red. Additionally, we recorded measurements of percent cover for abiotic attributes such as rock, litter, and bare ground. The total area sampled per plot was 900 m^2 (large plot) to match the size of a Landsat pixel for scaling purposes.

Pre-fire basal area was reconstructed by identifying and removing pre-fire snags prior to calculating plot level estimates of basal area per hectare. Snags were identified using optical estimates of fire scaring, charring, scorch, and levels of decay (by class: 1-5). All trees above 2.54 cm dbh were included in plot level basal area calculations. Mortality rates were calculated by dividing fire-induced basal area mortality by pre-fire living basal area. Additional information is provided in Appendix C, including a summary of topographical attributes, observed basal area, RdNBR values, plot measurements, coordinates for plot centers, and an illustration of our plot layout.

3.3.3 LiDAR Datasets

We used multi-temporal LiDAR to quantify pre-fire basal area, basal area mortality, and surviving basal area (legacy). Pre-fire LiDAR data (LiDAR Consortium's Rogue River project area ≈ 551,074 ha) was obtained between March 6th and August 16th, 2012 (Table 3.1). Post-fire LiDAR was collected between September 26th and October 23rd, 2013 (≈ 49,915 ha) and lies within the Rogue River LiDAR dataset. Data was collected by Watershed Sciences, Inc (Table 3.2). (purchased by Quantum Spatial), for the Oregon Department of Geology and Mineral Industries (DOGAMI). Intensity values were normalized during processing prior to delivery.

We examined multi-temporal LiDAR metrics related to, structure (z dimension), cover (x and y dimensions), and foliar reflectance (intensity returned) (Table 3.3) (García et al., 2010). Pre-fire basal area was modeled using data from 2012 and calibration plots measured in 2015. Basal area mortality was quantified using data from 2012, 2013, and change estimation. Legacy basal area was directly quantified using field data obtained in 2015. We processed both datasets using FUSION (McGaughey, 2014). Alignment and quality between pre- and post-fire LiDAR data was assessed by comparing stem maps derived from field observations to those derived by LiDAR. We also used plot level canopy models and the LiDAR point cloud to optically assess potential misalignment concerns.

We used stratified height bins to vertically partition vegetative canopies within forest profiles (Bright et al., 2014). We ultimately selected 3 height bins, 0-2 (m), 2-10 (m), above 10 meters (bins: 1, 2, 3 respectively), after examining several options. Other bins examined include 2 m intervals and geometric breaks of 0-2, 2-5, 5-10, 10-20, 20-40 m. Both alternatives were removed from further analysis due to model selection procedures choosing over 12 covariates and our ability to practically apply such methods under realistic scenarios.

3.3.4 Statistical Analysis

Variable selection and regression analysis for our pre-fire basal area models was performed R (R Core Team, 2016). The Leaps package was used to perform an exhaustive search for the best subsets of predictor variables using linear regression and an efficient branch and bound algorithm (Lumley, 2009). We also performed a box-cox transformation using the MASS package due to heteroskedasticity which suggested the use of the natural logarithm transformation (Osborne, 2010). Therefore, we applied a natural logarithm transformation to observed pre-fire basal area (m^2 ha^{-1}) (Hudak et al., 2006; Næsset, 2007; Woods et al., 2011). LiDAR covariates were not transformed and we applied a bias correction factor prior to back-transforming our response (Sprugel, 1983).

Variable selection and subsequent analysis for basal area mortality was also performed in R using Leaps, GLMulti, and GAMboostLSS packages (Hoe et al., See Chapter 2, *in preparation*). All metrics were evaluated as differences from pre-fire (2012) to post-fire (2013) data sets. Beta regression was used to model basal area mortality and a landscape map was created using the Raster package in R (Cribari-Neto and Zeileis, 2010; Ferrari and Cribari-Neto, 2004; Hijmans, 2016; R Core Team, 2016; Smithson and Verkuilen, 2006). Models were derived using LiDAR metrics only and a combined approach using RdNBR and LiDAR together. LiDAR intensity values were not used within the combined models under the assumption that RdNBR provides adequate spectral information.

We evaluated model performance using identical criterion when quantifying pre-fire basal area or basal area mortality (Hoe et al., See Chapter 2, *in preparation*). Likewise, we examined multi-collinearity within both using Pearson correlations. Variance inflation factors were also examined to verify that multi-collinearity was not present within our final models. Bias, root mean square error (RMSE), AIC, BIC, and root mean square prediction error (RMSPE) were used to compare model performance. RMSPE was calculated for all model(s) using leave-one-out cross validation (Kohavi et al., 1995).

Post-fire basal area was quantified by combining landscape-scale estimates of pre-fire basal area and basal area mortality. This allowed us to create a series of landscape maps related to basal area before fire, basal area mortality, and basal area after fire. We also delineate pre- and post-fire living basal area by ownership and basal area class. We isolate Big Windy prior to this comparison due to lower fire severities being attributed to localized weather conditions, inversions, and shading from smoke (Ruediger, 2014).

3.4 Results

Over 60% of the post-processed plot locations maintained sub-meter accuracy with roughly 25% over $1(m)$ accuracy and the remaining observations above 2 meters. We sampled a total of 2,435 trees ($\geq$ 10cm dbh) with 1,454 remaining alive after fire, 958 killed by fire, and 77 snags (dead before fire), on 51 plots across the full severity gradient within our study area. Approximately 60% (1,464 trees) were coniferous with hardwoods representing the remaining 40% (971 trees). 1,302 of our observations were Douglas-fir, which comprise 89% of the coniferous species composition, with a mixture of ponderosa pine, sugar pine, western white pine , and Jeffery pine representing 8%, and 3 observations of white fir. In contrast, hardwood species composition was more diverse and primarily composed of Pacific Madrone at 34%, golden chinkapin and canyon live oak at 23%, tanoak at 15%, and the remaining observations being a mixture of big-leaf maple, pacific dogwood, Oregon white oak, and California black oak.

Our results suggest that intensity values are very useful when quantifying basal area using LiDAR metrics over highly variable landscapes (Table 3.4). While structural covariates were significant, the inclusion of intensity metrics improved model performance consistently (reduction in AIC/BIC $\approx$ 20-40, not shown). We also found that models with fewer covariates tended to truncate the range of fitted values (max value < 80), creating a disparate relationship between the range of our observations and model estimates. We therefore selected a model which contains 4 covariates (HT_{cv}, HT_{25}, I_{stdv}, I_{95}), has the lowest bias , and fit the range of our observations the best (observed values: 0.4 - 135 m^2/ha, fitted: 0.06 - 120 m^2/ha). We provide additional information in Table 3.5 which includes parameter estimates, standard errors, and variance inflation factors for models shown.

We found that multi-temporal LiDAR can quantify basal area mortality over variable landscapes using change estimation (Table 3.6) (Hoe et al., *in preparation*). The most correlated predictors to basal area mortality were $RdNBR$ (0.84), $d\bar{I}_2$ (0.80), $dCRSp_1$ (-0.79), and dRP_1 (-0.75). Results indicate a reduction in bias across all severity classes and a decrease in RMSPE. Each variable selection procedure provided its own benefits and ultimately they all selected the same model.

$$Y = \beta_0 + \beta_1\, d\bar{I}_2 + \beta_2\, dCRSp_3 + \beta_3\, dHT_{max} + \epsilon_i \tag{3.1}$$

Where Y is the fire-induced basal area mortality rate, $d\bar{I}_2$ is the change in the mean intensity value between 2 and 10 meters, $dCRSp_3$ is the change in the proportion of CRS above 10 meters, and dHT_{max} is a change in max height. We concluded that while absolute change in mean intensity value between 2–10 m($d\bar{I}_2$) is explaining the majority of variation, $dCRSp_3$ provides more information for the older stands, and dHT_{max} captures stand replacement conditions in the youngest forests (Hoe et al., *in preparation*).

3.5 Discussion

Active remote sensing technologies such as LiDAR have become increasingly useful in quantifying forest attributes for a wide range of management objectives. For example, landscape scale maps of forest composition and volume are used by resource managers to assess wildfire risk and fuels (Bright et al., 2014; Clark et al., 2010; Erdody and Moskal, 2010; Skowronski et al., 2007, 2011), develop wall-to-wall forest inventories (Bolton et al., 2015; Bouvier et al., 2015; Brosofske et al., 2014; Coops et al., 2007; Goerndt et al., 2010; Guerra-Hernández et al., 2016; Hall et al., 2005; Hudak et al., 2006, 2002; Næsset, 2007; Woods et al., 2011; Wulder et al., 2012), and evaluate wildlife habitat (Betts et al., 2010; Casas et al., 2016; Vogeler et al., 2014, 2016). We quantified pre-fire basal area, basal area mortality, and post-fire basal area using a single remote sensing technology. These methods can improve upon existing data and information by: 1) quantifying pre-fire and post-fire forest conditions under consistent measures; and 2) clearly defining the forest attribute of interest (Bolton et al., 2015; Keeley, 2009; Morgan et al., 2014).

Pre-fire basal area maps provide an improved perspective for managers and research scientists (Figure 3.5). We know that fire severity is driven by topography, weather, and fuels (Agee, 1991; Bowman et al., 2009; Perry et al., 2011). However, we often lack information related to pre-fire forest conditions making it difficult to ascertain relationships between landscape-scale canopy fuel distributions and fire effects. By modeling and mapping pre-fire conditions, we provide necessary information for improving our ability to manage dynamic landscapes and promote more resilient ecosystems.

Multi-temporal LiDAR data has the capability to improve our understanding of how pre-fire forest structures influence fire effects (Figure 3.6) (Hoe et al., *in preparation*). Our results confirm that the ability to detect change in 3-dimensions helps ameliorate some of the inaccuracies associated with passive remote sensing of fire effects. For example, we focus explicitly on fire effects to trees with the understanding that forest trajectories and recovery rates are driven by these dominant biological legacies (Franklin et al., 2002; Lindenmayer et al., 2012; Turner et al., 1998). We isolated LiDAR returns near ground and observed change in upper and sub-canopy components, separately. These advantages allow us to reduce over saturation caused by big data, account for confounding or inverse relationships, check for evidence of reductions in upper canopy densities (canopy consumption), and observe change beneath occluded canopies (Bolton et al., 2015; Bright et al., 2014; Montealegre et al., 2014).

We provide mangers and research scientists with a new perspective of post-fire landscapes by combining pre-fire basal area estimates with basal area mortality using only multi-temporal LiDAR. By directly quantifying basal area before fire we can apply estimates of basal area mortality to obtain landscape-scale maps of post-fire living and dead basal area. We provide 3 examples of how these maps can be utilized to improve our understanding of fire effects across highly variable landscapes.

3.5.1 Application of Legacy Maps

Post-fire landscape maps of living basal area provide scientists and managers with well defined, easily interpreted, and operationally useful information (Figure 3.7). Legacy tree density, distance to seed source, and tree species resilience influence forest recovery, habitat suitability, and re-burn severity conditions (Ager et al., 2007; Halofsky et al., 2011; Seidl et al., 2014; Spies et al., 2010). Early seral sites and high density patches of large legacy trees can be identified (lowest and highest basal area, respectively). Additionally, post-fire habitat continuity could be examined. All of these potential applications improve our ability to manage dynamic forest landscapes on varying temporal scales.

Legacy basal area maps also provide estimates of remaining forest inventory. We can estimate the value and volume of remaining timber resources across the landscape. We can provide managers with highly useful information for rehabilitation, soil stabilization, and forest recovery measures. Ultimately, we can identify spatial and structural relationships which reduce risk of catastrophic loss to our highly-valued natural resources during wildfire events.

Post-fire maps of fire-killed basal area improve our ability to assess ecological impacts from fire across heterogeneous landscapes (Figure 3.8). Dead biological legacies are important for wildlife habitat, carbon and nutrient cycling, and protection from predation (Franklin et al., 1987; Harmon et al., 1986). For example, many rare, specialized avian species benefit from increases in habitat abundance and food availability due to the creation of new snags and patches of early seral conditions (Betts et al., 2010; Casas et al., 2016; Vogeler et al., 2014, 2016). Keystone species, such as the pileated woodpecker (*Dryocopus pileatus*), often feed on insects within the bark fire-killed trees creating cavities which are colonized and re-colonized by subsequent, specialized avian species (Aubry and Raley, 2002). Therefore, information on the abundance, spatial, and temporal continuity of these resources is essential for many wildlife managers.

Similar to post-fire living basal area distributions, dead basal area provides information which could be used to inform rehabilitation efforts. By identifying areas with the greatest abundance of dead basal area, we can optimize treatment strategies to reduce risk, hazard, and/or loss. For example, salvage operations could target areas with the greatest abundance of dead basal area and remove merchantable timber products while reducing the likelihood of bark beetle outbreaks. Likewise, soil stabilization and other rehabilitation efforts could be spatial optimized across the landscape.

The Douglas Complex is unique in that it burned through a checkerboard landscape of mutually exclusive management regimes (O&C lands). Due to the checkerboard landscape, we can assume weather and topography to be constant across ownership. In contrast, the Big Windy fire experienced much lower fire severity due to localized weather conditions such as inversions, higher relative humidity, and shading from smoke (Ruediger, 2014). The spatial orientation of land owners across this landscape provides a great opportunity to examine how land management practices influence fire effects.

LiDAR offers us the opportunity to begin quantifying fire severity across ownership, management regime, and pre-fire forest conditions. For example, in Figure

3.9 we can clearly see that Big Windy experienced less basal area mortality than the Douglas Complex. We can also see that young stands within the Douglas Complex experienced the highest mortality, regardless of owner. This makes sense biologically because young trees with thin bark and low crowns have a low probability of survival. In contrast, trees with thick bark, deep roots, and high crown base heights have a higher probability for survival (Franklin et al., 1987; Ryan and Frandsen, 1991; Vines, 1968). Furthermore, it appears that private land is experiencing greater mortality than federal regardless of basal area group. We believe that this is due to fuel continuity and relative stand density varying by owner. No formal tests were performed, however, this illustrates the capabilities of landscape level multi-temporal LiDAR analyses. We provide additional information in Tables 3.7 & 3.8.

3.5.2 Future opportunities & Limitations

As our LIDAR technology improves, estimates and ecological interpretations of fire effects will become more precise, and our ability to improve pro-active land management practices could become a reality. Research such as this will be invaluable as we begin prepare for a future with longer wildfire seasons, increased drought conditions, and expanding populations Hammer et al. (2007); Liu et al. (2013); Stephens et al. (2014); Westerling et al. (2006). Furthermore, our ability to sustain spatial and temporal habitat continuity while promoting more resilient ecosystems will vastly improve.

One of the major limitations with studies such as these is simply the availability of information. LiDAR data acquisitions cost money, while passive remote sensors such as Landsat, are free. However, research continues to support the use of active remote sensing technology as the next step towards improving our ability to quantify and interpret landscape scale disturbance, ecological effects, and spatial distributions. We believe the benefits of obtaining LiDAR data greatly out-weigh the cost and recent statewide studies suggest \$4 in benefits for every \$1 spent when acquiring LiDAR data (Dewberry, 2016; Hallum and Parent, 2014; Young, 2014). This is largely due to a wide breadth of potential applications across agency, ownership, and management objectives.

3.6 Conclusion

Remote sensing technologies allow us to rapidly assess fire effects over large landscapes, however, their inherent limitations constrain our ability to obtain the most accurate information available. We used multi-temporal LiDAR as a stand-alone analysis of fire effects over a mixed-ownership landscape in southwestern Oregon. We provide highly interpretable assessments of fire effects by defining fire severity as basal area mortality. We model and map pre-fire basal area to provide information related to fuels distributions before fire. We use change estimation between 2 separate LiDAR flights to quantify basal area mortality. Post-fire legacy basal area was obtained by combining estimates of pre-fire basal area and basal area mortality. Finally, we provide multiple examples of how this information can be used in practical terms. While our results illustrate how we can improve landscape assessments using LiDAR as a stand-alone remote sensing technology, many future opportunities remain to be explored. As LiDAR data become more available, opportunities like these will be studied and our ability quantify, assess, and understand landscape fire effects will continue to improve.

Literature Cited

Agee, J. K. (1991). Fire history of Douglas-fir forests in the Pacific Northwest. In: Wildlife and Vegetation of Unmanaged Douglas-fir Forests. U.S. Department of Agriculture, Forest Service, Pacific Northwest Research Station, Portland, OR, pp. 25–33.

Ager, A. A., M. A. Finney, B. K. Kerns, and H. Maffei (2007). Modeling wildfire risk to northern spotted owl (strix occidentalis caurina) habitat in central oregon, USA. *Forest Ecology and Management 246*(1), 45–56.

Aubry, K. B. and C. M. Raley (2002). The pileated woodpecker as a keystone habitat modifier in the pacific northwest. *USDA Forest Service General Technical Report PSW-GTR-181*, 257–274.

Betts, M., J. C. Hagar, J. W. Rivers, J. Alexander, K. McGarigal, and B. McComb (2010). Thresholds in forest bird occurrence as a function of the amount of early-seral broadleaf forest at landscape scales. *Ecological Applications 20*(8), 2116–2130.

Bolton, D. K., N. C. Coops, and M. A. Wulder (2015). Characterizing residual structure and forest recovery following high-severity fire in the western boreal of Canada using landsat time-series and airborne lidar data. *Remote Sensing of Environment 163*, 48–60.

Bouvier, M., S. Durrieu, R. A. Fournier, and J.-P. Renaud (2015). Generalizing predictive models of forest inventory attributes using an area-based approach with airborne lidar data. *Remote Sensing of Environment 156*, 322–334.

Bowman, D. M., J. K. Balch, P. Artaxo, W. J. Bond, J. M. Carlson, M. A. Cochrane, C. M. DAntonio, R. S. DeFries, J. C. Doyle, S. P. Harrison, et al. (2009). Fire in the earth system. *science 324*(5926), 481–484.

Bright, B. C., A. T. Hudak, R. E. Kennedy, and A. J. Meddens (2014). Landsat time series and lidar as predictors of live and dead basal area across five bark beetle-affected forests. *IEEE Journal of Selected Topics in Applied Earth Observations and Remote Sensing 7*(8), 3440–3452.

Brosofske, K. D., R. E. Froese, M. J. Falkowski, and A. Banskota (2014). A review of methods for mapping and prediction of inventory attributes for operational forest management. *Forest Science 60*(4), 733–756.

Brown, J. K. and J. K. Smith (2000). Wildland fire in ecosystems: effects of fire on flora. U.S. Department of Agriculture, Forest Service, Gen. Tech. Rep. RMRS-GTR-42-vol. 2. Ogden, UT, 2000. 257 p.

Casas, Á., M. García, R. B. Siegel, A. Koltunov, C. Ramírez, and S. Ustin (2016). Burned forest characterization at single-tree level with airborne laser scanning for assessing wildlife habitat. *Remote Sensing of Environment 175*, 231–241.

Clark, K. L., N. Skowronski, M. Gallagher, N. Carlo, M. Farrell, and M. R. Maghirang (2010). Assessment of canopy fuel loading across a heterogeneous landscape using lidar. Joint Fire Sciences Program, Project 10-1-02-14, Final Report, U.S. Department of Agriculture, Forest Service, New Lisbon, NJ & Morgantown, WV, 2010.

Coops, N. C., T. Hilker, M. A. Wulder, B. St-Onge, G. Newnham, A. Siggins, and J. T. Trofymow (2007). Estimating canopy structure of douglas-fir forest stands from discrete-return lidar. *Trees 21*(3), 295–310.

Cribari-Neto, F. and A. Zeileis (2010). Beta regression in R. *Journal of Statistical Software 34*(2), 1–24. http://www.jstatsoft.org/v34/i02/.

Dewberry (2016). National enhanced elevation assessment final report - appendix F: Benefit cost analysis process. *Dewberry*, 671–686. Accessed: March 15th,

2016. Available at: http://www.dewberry.com/docs/default-source/documents/neea_final-report_revised-3-29-12.pdf?sfvrsn=0.

Dunn, C. J. and J. D. Bailey (2016). Tree mortality and structural change following mixed-severity fire in Pseudotsuga forests of Oregons western cascades, USA. *Forest Ecology and Management 365*, 107–118.

Duren, O. C., P. S. Muir, and P. E. Hosten (2012). Vegetation change from the Euro-American settlement era to the present in relation to environment and disturbance in southwest Oregon. *Northwest Science 86*(4), 310–328.

Erdody, T. L. and L. M. Moskal (2010). Fusion of lidar and imagery for estimating forest canopy fuels. *Remote Sensing of Environment 114*(4), 725–737.

Ferrari, S. and F. Cribari-Neto (2004). Beta regression for modelling rates and proportions. *Journal of Applied Statistics 31*(7), 799–815.

Franklin, J. F., H. Shugart, and M. E. Harmon (1987). Tree death as an ecological process. *BioScience 37*(8), 550–556.

Franklin, J. F., T. A. Spies, R. Van Pelt, A. B. Carey, D. A. Thornburgh, D. R. Berg, D. B. Lindenmayer, M. E. Harmon, W. S. Keeton, D. C. Shaw, et al. (2002). Disturbances and structural development of natural forest ecosystems with silvicultural implications, using douglas-fir forests as an example. *Forest Ecology and Management 155*(1), 399–423.

García, M., D. Riaño, E. Chuvieco, and F. M. Danson (2010). Estimating biomass carbon stocks for a mediterranean forest in central Spain using lidar height and intensity data. *Remote Sensing of Environment 114*(4), 816–830.

Goerndt, M. E., V. J. Monleon, and H. Temesgen (2010). Relating forest attributes with area-and tree-based light detection and ranging metrics for western oregon. *Western Journal of Applied Forestry 25*(3), 105–111.

Guerra-Hernández, J., M. Tomé, and E. González-Ferreiro (2016). Using low density lidar data to map mediterranean forest characteristics by means of an area-based approach and height threshold analysis. *Revista de Teledetección* (46), 103–117.

Gutschick, V. P. and H. BassiriRad (2003). Extreme events as shaping physiology, ecology, and evolution of plants: toward a unified definition and evaluation of their consequences. *New Phytologist 160*(1), 21–42.

Hall, S., I. Burke, D. Box, M. Kaufmann, and J. M. Stoker (2005). Estimating stand structure using discrete-return lidar: an example from low density, fire prone ponderosa pine forests. *Forest Ecology and Management 208*(1), 189–209.

Hallum, D. and S. Parent (2014). Developing a business case for statewide light detection and ranging data collection. *Nebraska Department of Natural Resources. Accessed: May 11, 2016*. Accessed: May 10, 2016. Available at: http://watercenter.unl.edu/PRS/PRS2009/Posters/Hallum%20Doug.pdf.

Halofsky, J., D. Donato, D. Hibbs, J. Campbell, M. D. Cannon, J. Fontaine, J. Thompson, R. Anthony, B. Bormann, L. Kayes, et al. (2011). Mixed-severity fire regimes: lessons and hypotheses from the Klamath-Siskiyou ecoregion. *Ecosphere 2*(4), 1–19.

Hammer, R. B., V. C. Radeloff, J. S. Fried, and S. I. Stewart (2007). Wildland–urban interface housing growth during the 1990s in California, Oregon, and Washington. *International Journal of Wildland Fire 16*(3), 255–265.

Harmon, M. E., J. F. Franklin, F. J. Swanson, P. Sollins, S. Gregory, J. Lattin, N. Anderson, S. Cline, N. G. Aumen, J. Sedell, et al. (1986). Ecology of coarse woody debris in temperate ecosystems. *Advances in ecological research 15*, 133–302.

Hessburg, P. F., R. B. Salter, and K. M. James (2007). Re-examining fire severity relations in pre-management era mixed conifer forests: inferences from landscape patterns of forest structure. *Landscape Ecology 22*(1), 5–24.

Hijmans, R. J. (2016). *raster: Geographic Data Analysis and Modeling*. R package version 2.5-8, https://CRAN.R-project.org/package=raster.

Hoe, M. S., C. Dunn, and H. Temesgen (*in preparation*). Improving landscape scale fire severity estimates using multi-temporal lidar and change estimation. *To be submitted to the International Journal of Wildland Fire*.

Hudak, A. T., N. L. Crookston, J. S. Evans, M. J. Falkowski, A. M. Smith, P. E. Gessler, and P. Morgan (2006). Regression modeling and mapping of coniferous forest basal area and tree density from discrete-return lidar and multispectral satellite data. *Canadian Journal of Remote Sensing 32*(2), 126–138.

Hudak, A. T., M. A. Lefsky, W. B. Cohen, and M. Berterretche (2002). Integration of lidar and landsat ETM+ data for estimating and mapping forest canopy height. *Remote sensing of Environment 82*(2), 397–416.

InciWeb, I. I. S. (2013). Douglas Complex Incident Information. *USDA Forest Service*. Accessed on February 13, 2014. Available at: http://inciweb.nwcg.gov/incident/3559/.

Kane, V. R., C. A. Cansler, N. A. Povak, J. T. Kane, R. J. McGaughey, J. A. Lutz, D. J. Churchill, and M. P. North (2015). Mixed severity fire effects within the rim fire: relative importance of local climate, fire weather, topography, and forest structure. *Forest Ecology and Management 358*, 62–79.

Keeley, J. E. (2009). Fire intensity, fire severity and burn severity: a brief review and suggested usage. *International Journal of Wildland Fire 18*(1), 116–126.

Kennedy, R. E., Z. Yang, and W. B. Cohen (2010). Detecting trends in forest disturbance and recovery using yearly landsat time series: 1. LandTrendrTemporal segmentation algorithms. *Remote Sensing of Environment 114*(12), 2897–2910.

Key, C. and N. Benson (1999). Measuring and remote sensing of burn severity. In L. F. Neuenschwander and K. C. Ryan (Eds.), *Proceedings joint fire science conference and workshop*, Volume 2, Boise, ID, 15-17 June 1999. University of Idaho and International Association of Wildland Fire, pp. 284.

Key, C. and N. Benson (2005). Landscape assessment: remote sensing of severity, the normalized burn ratio and ground measure of severity, the composite burn index. *FIREMON: Fire effects monitoring and inventory system Ogden, Utah: USDA Forest Service, Rocky Mountain Res. Station*. USDA Forest Service Gen. Tech. Rep. RMRS-GTR-164-CD, LA-1-55.

Kohavi, R. et al. (1995). A study of cross-validation and bootstrap for accuracy estimation and model selection. In *International Joint Conference on Artificial Intelligence*, Volume 14, pp. 1137–1145.

Lentile, L. B., Z. A. Holden, A. M. Smith, M. J. Falkowski, A. T. Hudak, P. Morgan, S. A. Lewis, P. E. Gessler, and N. C. Benson (2006). Remote sensing techniques to assess active fire characteristics and post-fire effects. *International Journal of Wildland Fire 15*(3), 319–345.

Lindenmayer, D. B., W. Blanchard, L. McBurney, D. Blair, S. Banks, G. E. Likens, J. F. Franklin, W. F. Laurance, J. A. Stein, and P. Gibbons (2012). Interacting factors driving a major loss of large trees with cavities in a forest ecosystem. *PLoS One 7*(10), e41864.

Littell, J. S., E. E. Oneil, D. McKenzie, J. A. Hicke, J. A. Lutz, R. A. Norheim, and M. M. Elsner (2010). Forest ecosystems, disturbance, and climatic change in washington state, USA. *Climatic change 102*(1-2), 129–158.

Liu, Y., S. L. Goodrick, and J. A. Stanturf (2013). Future US wildfire potential trends projected using a dynamically downscaled climate change scenario. *Forest Ecology and Management 294*, 120–135.

Lumley, T. (2009). *leaps: regression subset selection.* R package version 2.9 https://CRAN.R-project.org/package=leaps.

Mallek, C., H. Safford, J. Viers, and J. Miller (2013). Modern departures in fire severity and area vary by forest type, Sierra Nevada and southern Cascades, California, USA. *Ecosphere 4*(12), 1–28.

Marlon, J. R., P. J. Bartlein, D. G. Gavin, C. J. Long, R. S. Anderson, C. E. Briles, K. J. Brown, D. Colombaroli, D. J. Hallett, M. J. Power, et al. (2012). Long-term perspective on wildfires in the western USA. *Proceedings of the National Academy of Sciences 109*(9), E535–E543.

McGaughey, R. J. (2014). Fusion: Providing fast, efficient, and flexible access to lidar, ifsar and terrain datasets. *Pacific Northwest Research Station, USDA Forest Service*. Accessed: Sept. 28, 2014. Available at: http://forsys.cfr.washington.edu/fusion/fusionlatest.html.

Means, J. E., S. A. Acker, D. J. Harding, J. B. Blair, M. A. Lefsky, W. B. Cohen, M. E. Harmon, and W. A. McKee (1999). Use of large-footprint scanning airborne lidar to estimate forest stand characteristics in the western cascades of oregon. *Remote Sensing of Environment 67*(3), 298–308.

Miller, J. D., E. E. Knapp, C. H. Key, C. N. Skinner, C. J. Isbell, R. M. Creasy, and J. W. Sherlock (2009). Calibration and validation of the relative differenced normalized burn ratio (rdnbr) to three measures of fire severity in the Sierra Nevada and Klamath Mountains, California, USA. *Remote Sensing of Environment 113*(3), 645–656.

Miller, J. D. and H. Safford (2012). Trends in wildfire severity: 1984 to 2010 in the Sierra Nevada, Modoc Plateau, and southern Cascades, California, USA. *Fire Ecology 8*(3), 41–57.

Montealegre, A. L., M. T. Lamelas, M. A. Tanase, and J. de la Riva (2014). Forest fire severity assessment using ALS data in a mediterranean environment. *Remote Sensing 6*(5), 4240–4265.

Morgan, P., R. E. Keane, G. K. Dillon, T. B. Jain, A. T. Hudak, E. C. Karau, P. G. Sikkink, Z. A. Holden, and E. K. Strand (2014). Challenges of assessing fire and burn severity using field measures, remote sensing and modeling. *International Journal of Wildland Fire 23*(8), 1045–1060.

Næsset, E. (2007). Airborne laser scanning as a method in operational forest inventory: Status of accuracy assessments accomplished in Scandinavia. *Scandinavian Journal of Forest Research 22*(5), 433–442.

Naficy, C., A. Sala, E. G. Keeling, J. Graham, and T. H. DeLuca (2010). Interactive effects of historical logging and fire exclusion on ponderosa pine forest structure in the northern rockies. *Ecological Applications 20*(7), 1851–1864.

Omernik, J. M. and G. E. Griffith (2014). Ecoregions of the conterminous United States: evolution of a hierarchical spatial framework. *Environmental management 54*(6), 1249–1266.

Osborne, J. W. (2010). Improving your data transformations: Applying the box-cox transformation. *Practical Assessment, Research & Evaluation 15*(12), 1–9.

Perry, D. A., P. F. Hessburg, C. N. Skinner, T. A. Spies, S. L. Stephens, A. H. Taylor, J. F. Franklin, B. McComb, and G. Riegel (2011). The ecology of mixed severity fire regimes in Washington, Oregon, and Northern California. *Forest Ecology and Management 262*(5), 703–717.

Persson, A., J. Holmgren, and U. Söderman (2002). Detecting and measuring individual trees using an airborne laser scanner. *Photogrammetric Engineering and Remote Sensing 68*(9), 925–932.

R Core Team (2016). R: A language and environment for statistical computing. *R Foundation for Statistical Computing*. Vienna, Austria. https://www.R-project.org/.

Reilly, M. J., C. J. Dunn, G. W. Meigs, T. A. Spies, R. E. Kennedy, J. D. Bailey, and K. Briggs (*in review*). Contemporary patterns of burn severity in forests of the pacific northwest (1985-2010). *Forest Ecology and Management*.

Ruediger, L. (2014). Big windy fire report: Wildfire on the wild rogue - an analysis of fire effects, fire suppression impacts and management implications. *Klamath Forest Alliance*. Accessed on: August 13, 2016. Available at:http://www.klamathforestalliance.org/documents/Big_Windy_Fire_Report.pdf.

Ryan, K. C. and W. H. Frandsen (1991). Basal injury from smoldering fires in mature pinus ponderosa laws. *International Journal of Wildland Fire 1*(2), 107–118.

Safford, H. D., J. Miller, D. Schmidt, B. Roath, and A. Parsons (2008). BAER soil burn severity maps do not measure fire effects to vegetation: a comment on Odion and Hanson (2006). *Ecosystems 11*(1), 1–11.

Seidl, R., W. Rammer, and T. A. Spies (2014). Disturbance legacies increase the resilience of forest ecosystem structure, composition, and functioning. *Ecological Applications 24*(8), 2063–2077.

Skinner, C., A. Taylor, and J. Agee (2006). Klammath mountains bioregion. In N. G. Sugihara, J. W. van Wagtendonk, J. Fites-Kaufmann, K. E. Shaffer, and A. E. Thode, editors, *Fire in California's ecosystems*, pp. 170–194. Berkeley, CA: University of California Press.

Skowronski, N., K. Clark, R. Nelson, J. Hom, and M. Patterson (2007). Remotely sensed measurements of forest structure and fuel loads in the pinelands of New Jersey. *Remote Sensing of Environment 108*(2), 123–129.

Skowronski, N. S., K. L. Clark, M. Duveneck, and J. Hom (2011). Three-dimensional canopy fuel loading predicted using upward and downward sensing lidar systems. *Remote Sensing of Environment 115*(2), 703–714.

Smithson, M. and J. Verkuilen (2006). A better lemon squeezer? maximum-likelihood regression with beta-distributed dependent variables. *Psychological methods 11*(1), 54.

Spies, T. A., J. D. Miller, J. B. Buchanan, J. F. Lehmkuhl, J. F. Franklin, S. P. Healey, P. F. Hessburg, H. D. Safford, W. B. Cohen, R. S. Kennedy, et al. (2010). Underestimating risks to the northern spotted owl in fire-prone forests: Response to Hanson et al. *Conservation Biology 24*(1), 330–333.

Sprugel, D. (1983). Correcting for bias in log-transformed allometric equations. *Ecology 64*(1), 209–210.

Stephens, S. L., N. Burrows, A. Buyantuyev, R. W. Gray, R. E. Keane, R. Kubian, S. Liu, F. Seijo, L. Shu, K. G. Tolhurst, et al. (2014). Temperate and boreal forest mega-fires: characteristics and challenges. *Frontiers in Ecology and the Environment 12*(2), 115–122.

Sumnall, M. J., R. A. Hill, and S. A. Hinsley (2016). Comparison of small-footprint discrete return and full waveform airborne lidar data for estimating multiple forest variables. *Remote Sensing of Environment 173*, 214–223.

Taylor, A. H. and C. N. Skinner (1998). Fire history and landscape dynamics in a late-successional reserve, Klamath Mountains, California, USA. *Forest Ecology and Management 111*(2), 285–301.

Turner, M. G., W. L. Baker, C. J. Peterson, and R. K. Peet (1998). Factors influencing succession: lessons from large, infrequent natural disturbances. *Ecosystems 1*(6), 511–523.

Vines, R. (1968). Heat transfer through bark, and the resistance of trees to fire. *Australian Journal of Botany 16*(3), 499–514.

Vogeler, J. C., A. T. Hudak, L. A. Vierling, J. Evans, P. Green, and K. T. Vierling (2014). Terrain and vegetation structural influences on local avian species richness in two mixed-conifer forests. *Remote Sensing of Environment 147*, 13–22.

Vogeler, J. C., Z. Yang, and W. B. Cohen (2016). Mapping post-fire habitat characteristics through the fusion of remote sensing tools. *Remote Sensing of Environment 173*, 294–303.

Westerling, A. L., H. G. Hidalgo, D. R. Cayan, and T. W. Swetnam (2006). Warming and earlier spring increase western US forest wildfire activity. *Science 313*(5789), 940–943.

Whittier, T. R. and A. N. Gray (2016). Tree mortality based fire severity classification for forest inventories: A pacific northwest national forests example. *Forest Ecology and Management 359*, 199–209.

Woods, M., D. Pitt, M. Penner, K. Lim, D. Nesbitt, D. Etheridge, and P. Treitz (2011). Operational implementation of a lidar inventory in boreal Ontario. *The Forestry Chronicle 87*(4), 512–528.

Wright, H. A. and A. W. Bailey (1982). *Fire ecology: United States and southern Canada*. John Wiley & Sons. pp 15–22.

Wulder, M., J. White, F. Alvarez, T. Han, J. Rogan, and B. Hawkes (2009). Characterizing boreal forest wildfire with multi-temporal landsat and lidar data. *Remote Sensing of Environment 113*(7), 1540–1555.

Wulder, M. A., T. Han, J. C. White, T. Sweda, and H. Tsuzuki (2007). Integrating profiling lidar with landsat data for regional boreal forest canopy attribute estimation and change characterization. *Remote Sensing of Environment 110*(1), 123–137.

Wulder, M. A., J. C. White, R. F. Nelson, E. Næsset, H. O. Ørka, N. C. Coops, T. Hilker, C. W. Bater, and T. Gobakken (2012). Lidar sampling for large-area forest characterization: A review. *Remote Sensing of Environment 121*, 196–209.

Young, J. (2014). Maine geolibrary: Cost benefit analysis and typical uses of lidar data. *Maine Library of Geographic Information*. Accessed: May 11, 2016. Available at: http://www.maine.gov/geolib/LiDAR.html.

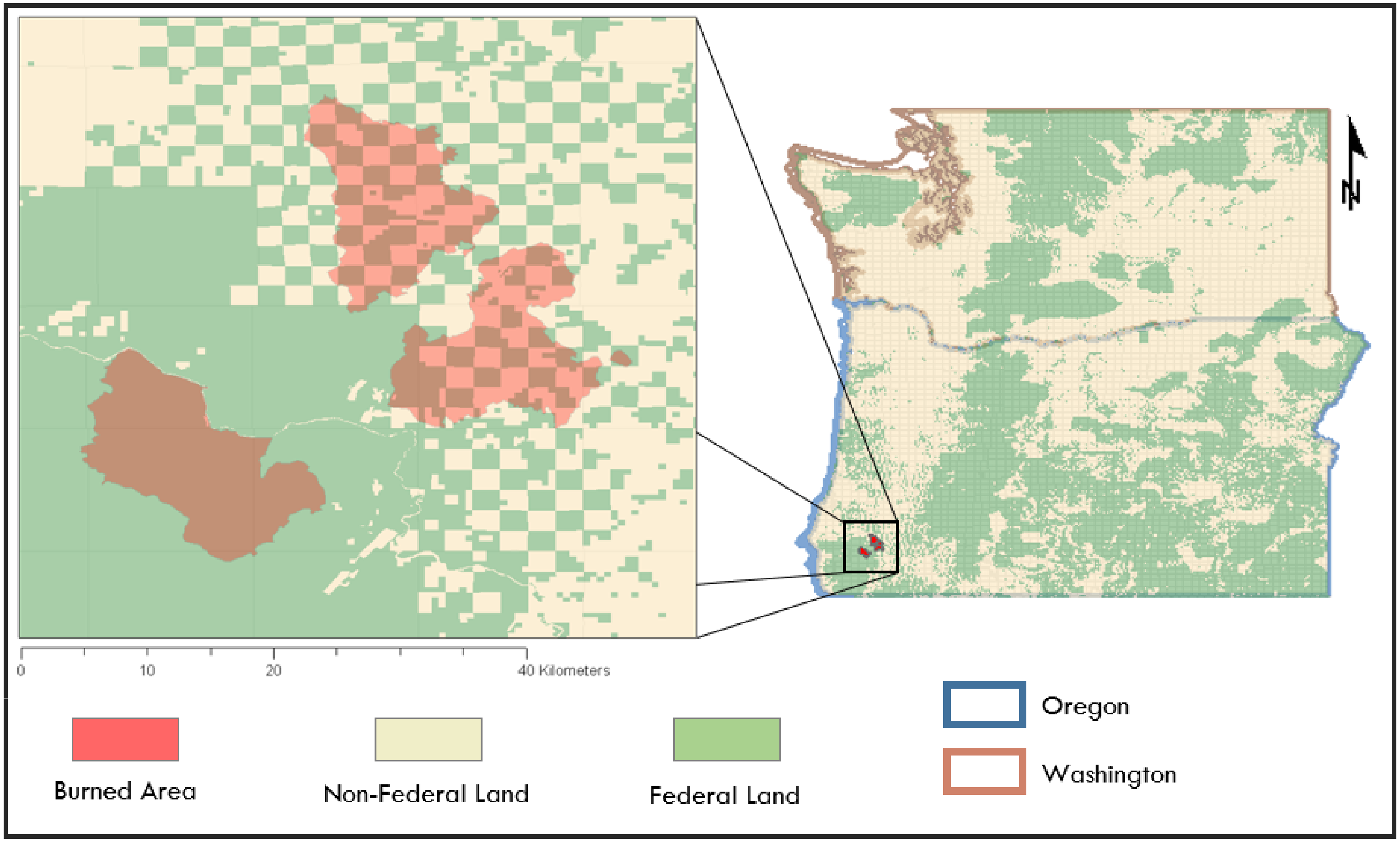

FIGURE 3.1: Study area located in southwestern Oregon, near Riddle and Glendale. Oregon and Washington shown on the right with federal land in green and non-federal land in white. Multi-temporal LiDAR coverage boundary outlined in orange. Shaded regions are the burn areas.

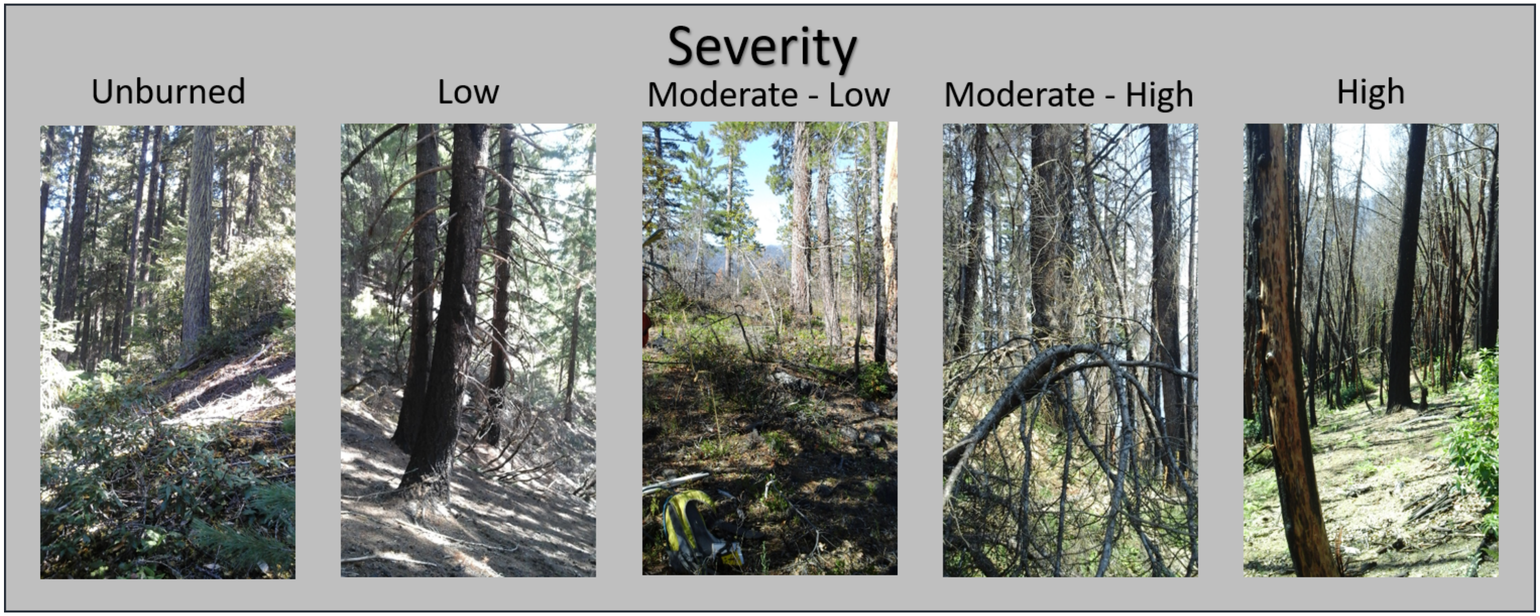

FIGURE 3.2: Photographic illustration of plot stratification and allocation on the ground by severity class. Thresholds used during stratification were: 0-235 (low), 235-406 (moderate-low), 406-648 (moderate-high), 648+ (high). Low, moderate-low, moderate-high, and high represent 0-25, 25-50, 50-75, and 75+ % basal area mortality, respectively. Photos were taken by Michael Hoe in 2015 to document each plot location (2-years after fire).

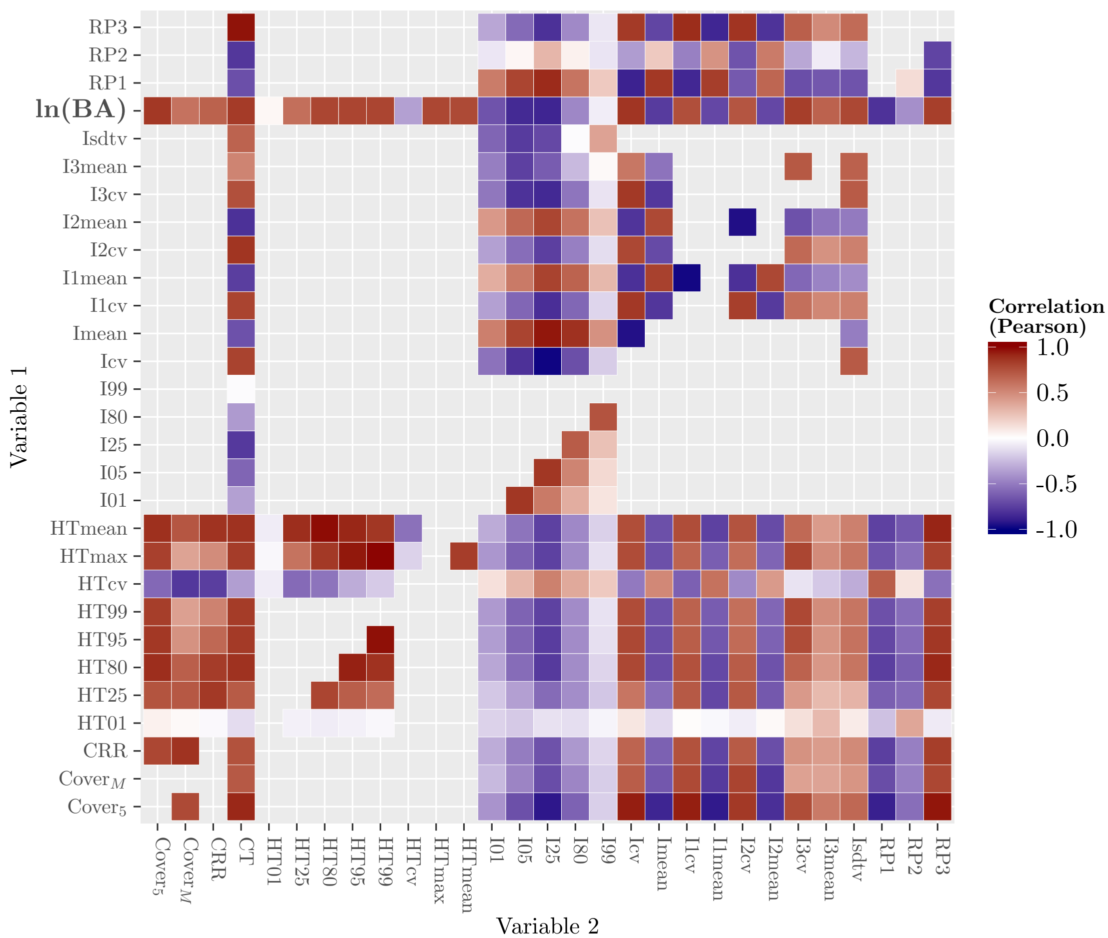

FIGURE 3.3: Pearson correlations across our examined LiDAR metrics including our response variable (ln(BA)). Diagonals have been set to zero and duplicates (lower triangle) have been removed for clearer illustration. ln(BA) can be seen on the y-axis as the 4th variable from the top. Many LiDAR metrics are highly correlated to ln(BA) and each other.

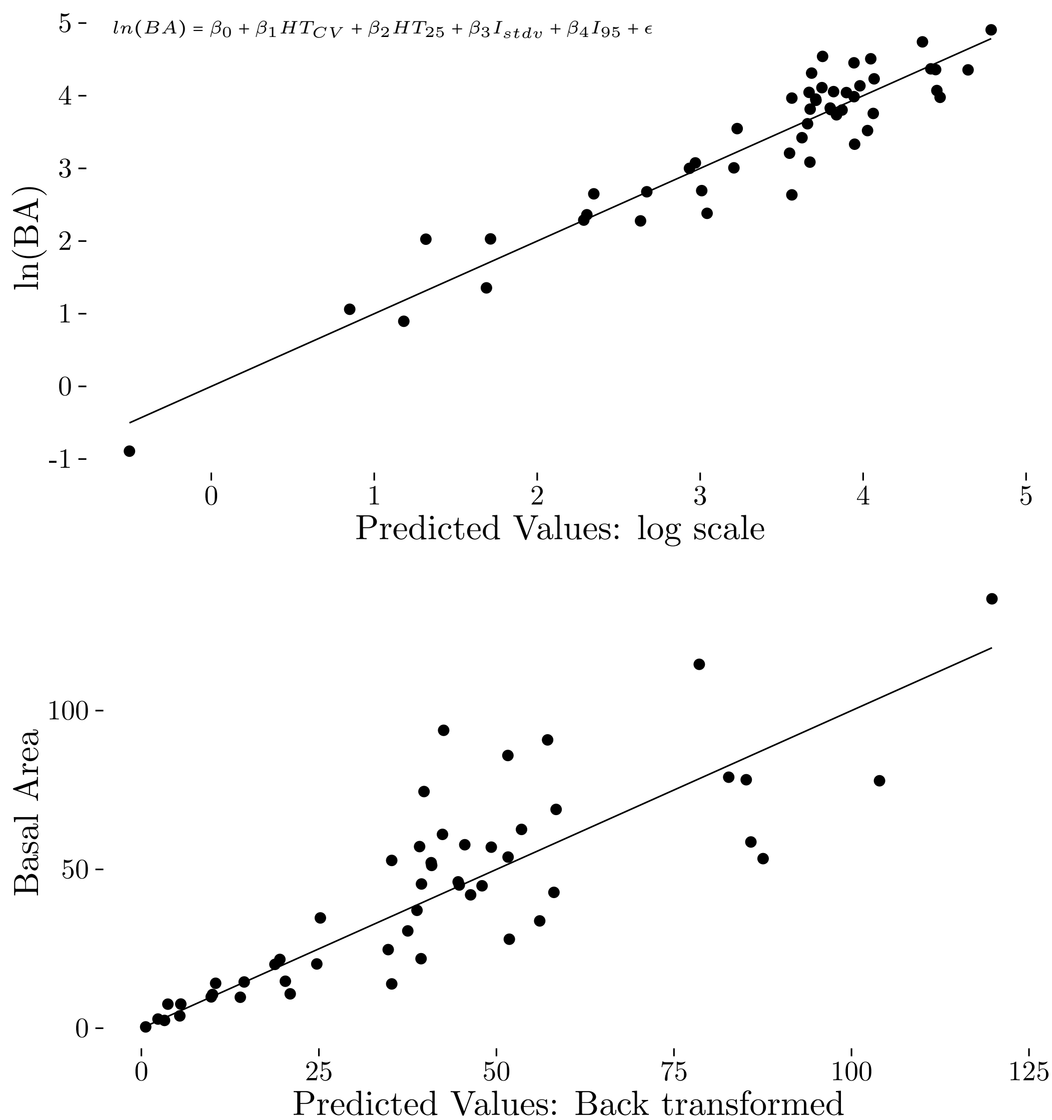

FIGURE 3.4: Observed versus predicted values shown on log scale (top) and back-transformed (bottom). Our response variable is basal area in square meters per hectare. Bias and RMSE are provided in Table 3.4.

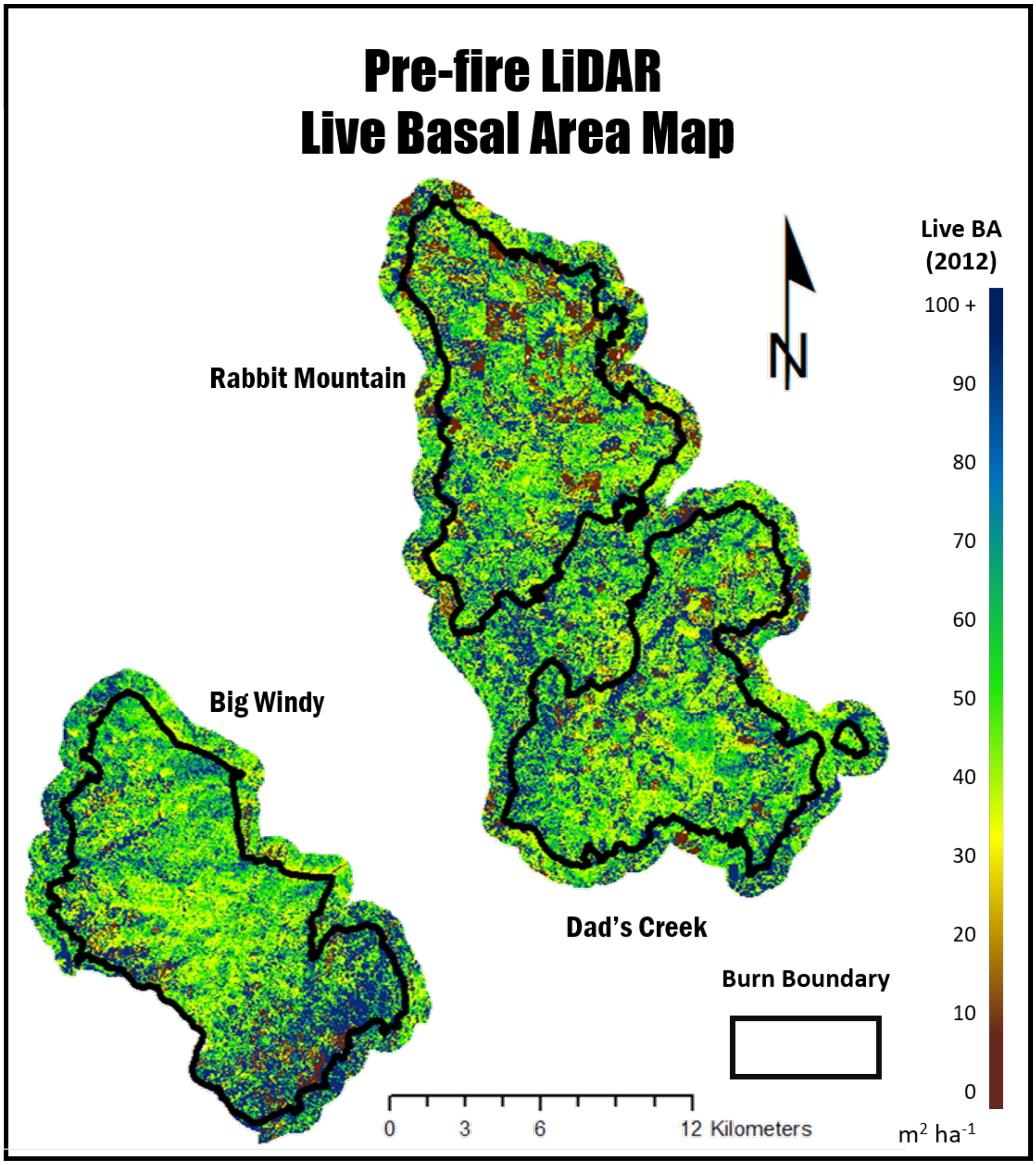

FIGURE 3.5: Landscape map of living basal area (m^2 ha^{-1}) before fire. Modeled using LiDAR metrics obtained in 2012 and calibrated using field observations obtained in 2015 (2-years after fire). Snags (dead before fire) were removed prior to modeling. Note that O&C lands within Rabbit Mountain are clearly visable and certain topographical conditions appear to have higher basal area (moisture availability).

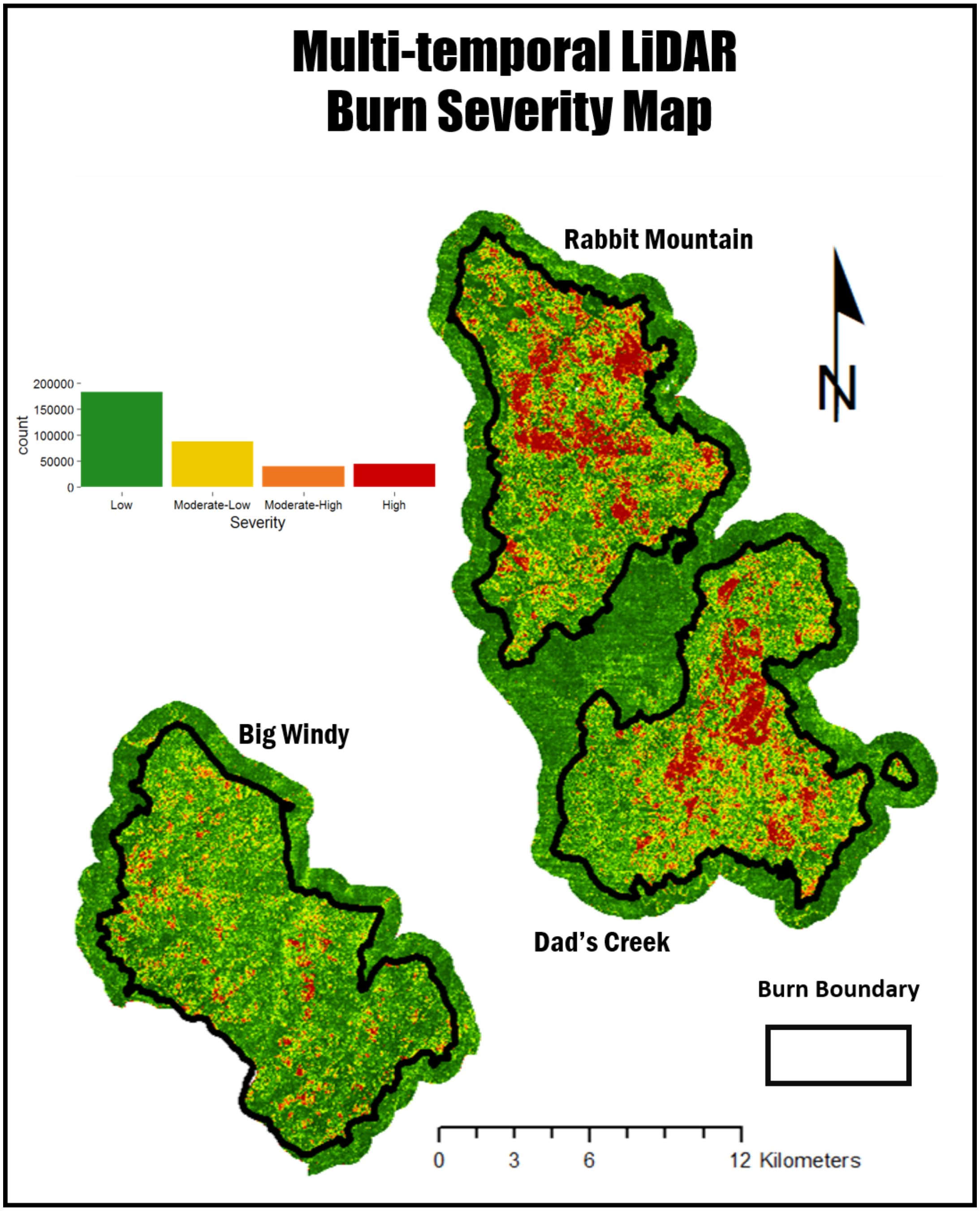

FIGURE 3.6: Landscape map of basal area mortality. Modeled using multi-temporal LiDAR metrics obtained in 2012 and calibrated using field observations obtained in 2015 (2-years after fire).

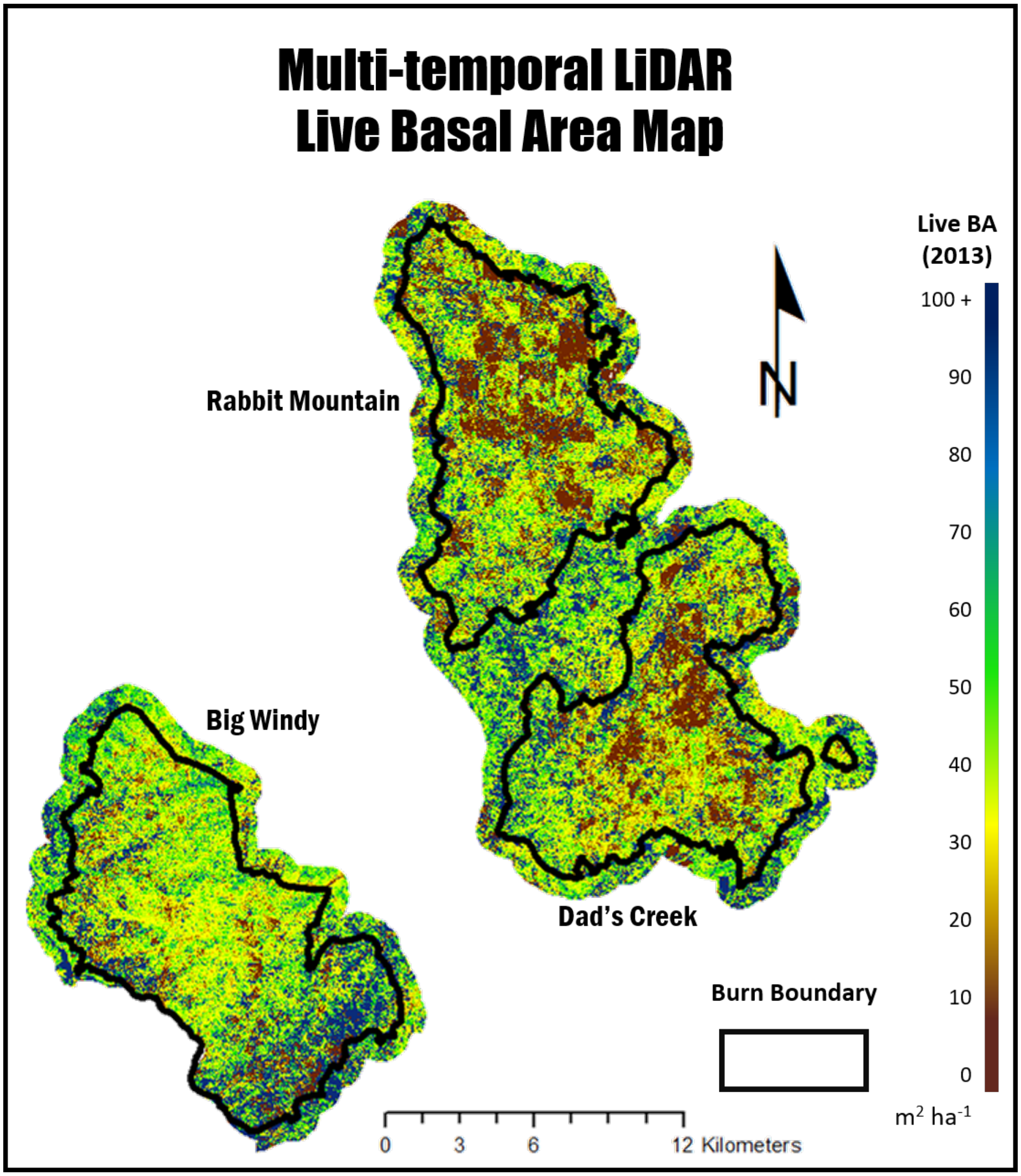

FIGURE 3.7: Landscape map of living basal area (m^2 ha^{-1}) after fire. Calculated by multiplying our living basal area map (2012) by 1 minus basal area mortality rate obtained from multi-temporal LiDAR. Beta regression was used to model mortality rates (30x30 m pixels) across our entire study area.

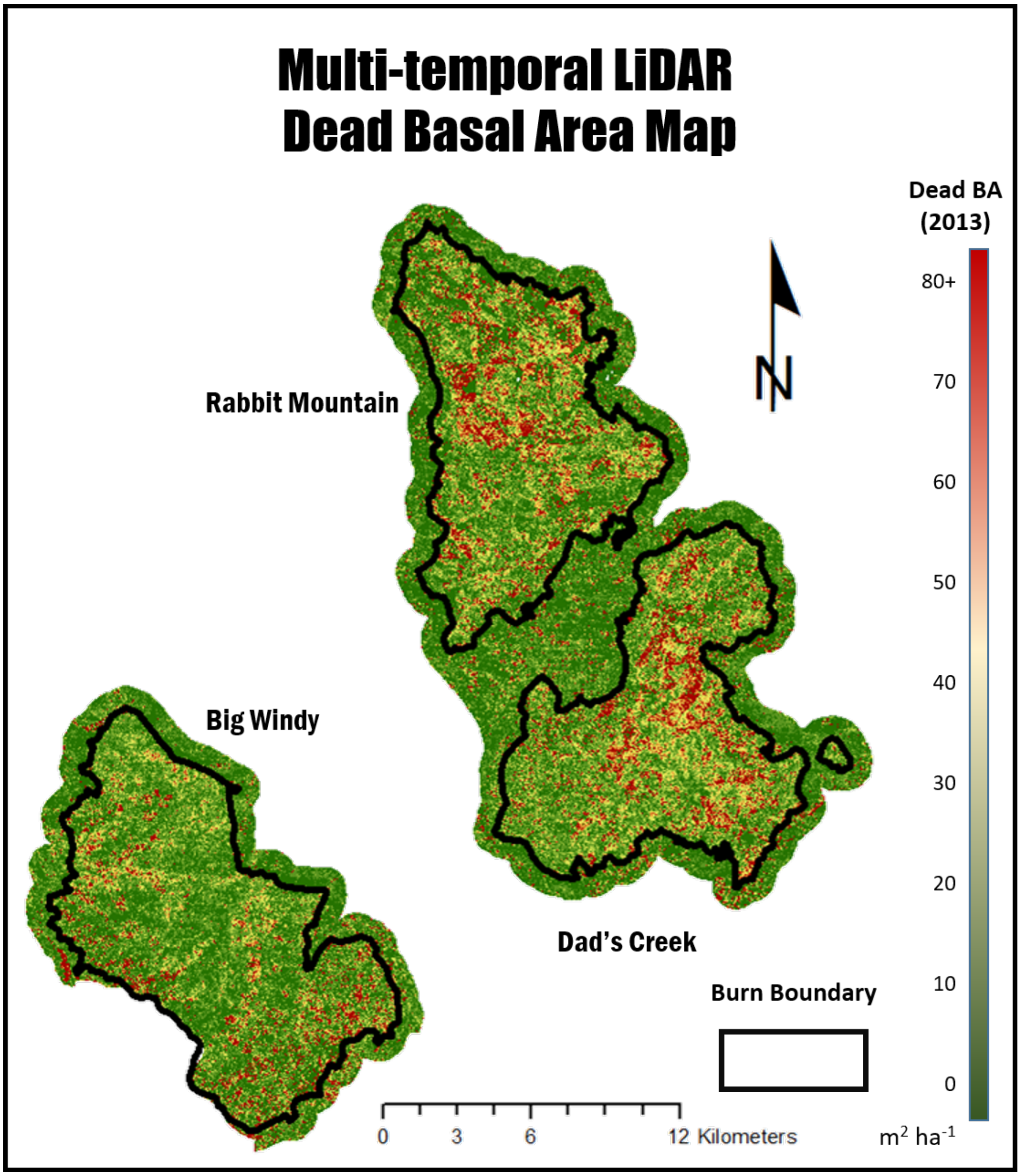

FIGURE 3.8: Landscape map of dead basal area (m^2 ha^{-1}) after fire. Created by combining living basal area map (2012) with basal area mortality estimates obtained from multi-temporal LiDAR and change estimation. Beta regression was used to model mortality rates (30x30 m pixels) across our entire study area.

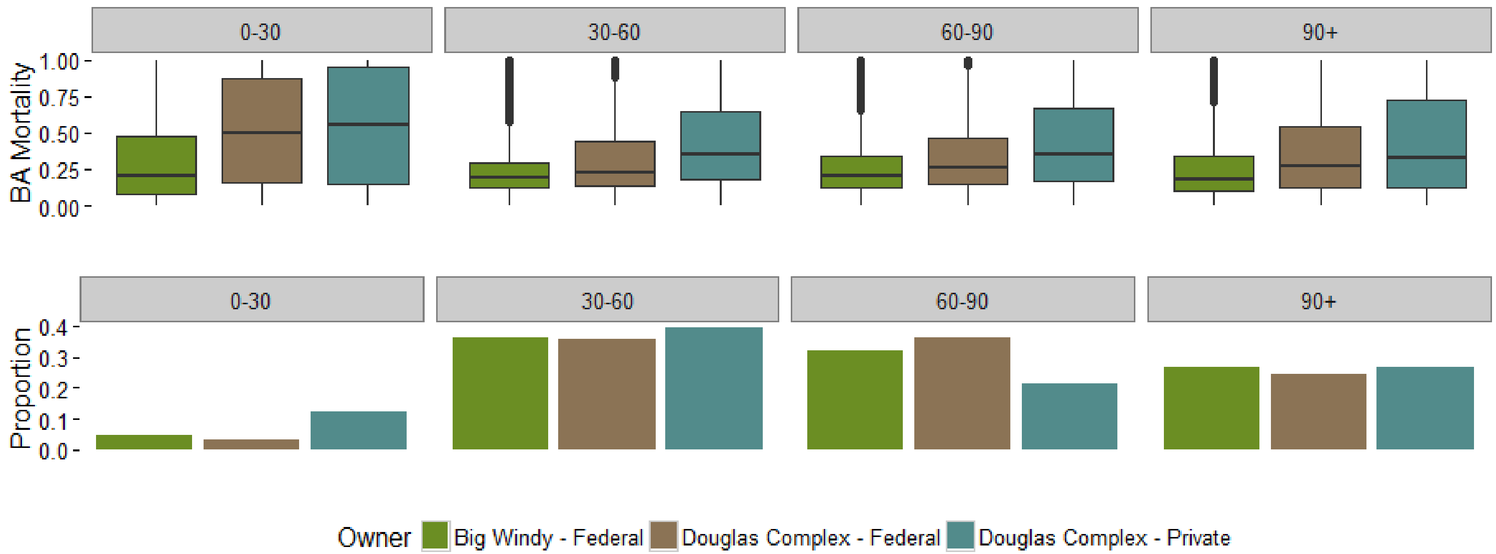

FIGURE 3.9: Comparison of mortality by landowner and basal area class (top) and the proportion of landscape held within each by owner (bottom). Basal area (m^2 ha^{-1}) is broken into discrete groups (0-30, 30-60, 60-90, 90+). Mortality rate was quantified using multi-temporal LiDAR. Pre-fire basal area was modeled using LiDAR data obtained in 2012 and field measurements taken in 2015. Trees experiencing fire-induced mortality were assumed alive in 2012 and included in observed basal area measurents. Trees exhibiting excessive decay were assumed dead before fire (snags), and removed from basal area observations prior to modeling.

TABLE 3.1: BLM Fires LiDAR Acquisition Specs (2012). Data obtained between March 6th and August 16th, 2012 by Watershed Sciences, Inc. (known now as Quantum Spatial).

Aircraft	Partenavia P38, Cessna Caravan 208B
Sensor	Leica ALS 50, Leica ALS 60
Survey Altitude (AGL)	900m / 1300m
Targeted Aircraft Speed	NA
Coverage	100% Overlap with 60% Sidelap
Field of View (FOV)	30 (at 900m) / 28 (at 1300m)
Laser Pulse Rate	52.2 hz (at 900m) / 46.7 hz (at 1300m)
Targeted Pulse Density	> 8 pulses per square meter
Aircraft Position	Monitored twice per second (2 Hz)
Aircraft Alititude	Monitored 200 times per second (200 Hz)

TABLE 3.2: BLM Fires LiDAR Acquisition Specs (2013). Data obtained between September 26th and October 23rd, 2013 by Watershed Sciences, Inc. (known now as Quantum Spatial).

Aircraft	Cessna Caravan 208B
Sensor	Leica ALS 50
Survey Altitude (AGL)	900 m
Targeted Aircraft Speed	105 knots
Coverage	100% Overlap with 65% Sidelap
Field of View (FOV)	30
Laser Pulse Rate	96,000 - 105,900 Hz
Targeted Pulse Density	> 8 pulses per square meter
Aircraft Position	Monitored twice per second (2 Hz)
Aircraft Alititude	Monitored 200 times per second (200 Hz)

TABLE 3.3: LiDAR variables examined during analysis. Variables listed represent raw metrics for pre- and post-fire conditions. Estimates of change were derived by taking the absolute difference (example: dRP_1) between pre- and post-fire conditions; similar to RdNBR and dNBR. Three height bins were used: 1 (0-2m), 2 (2-10m), and 3 (above 10m).

Variable	**Definition**
HT_{max}	Maximum height
$\overline{HT}$	Mean height
HT_{CV}	Coefficient of variation of height
$HT_{.99}$	99th percentile height
$HT_{.95}$	95th percentile height
$HT_{.80}$	80th percentile height
$HT_{.25}$	25th percentile height
$HT_{.01}$	1st percentile height
$Rumple$	Canopy surface (m^2) / ground surface (m^2)
RP_i	Return proportion per height bin_i
$Cover_2$	(Total # of returns above 2 meters / Total # of first returns)*100
CRR	Canopy Relief Ratio ((mean - min)/(max - min))
$Cover_m$	Percentage of first returns above mean
CT	Canopy Transparency ((Total # returns above 10 m)/(Total # returns above 2 m))
$\bar{I}$	Mean intensity value
$\bar{I}_i$	Mean intensity per height bin_i
I_σ	Standard deviation of intensity values
I_{i_σ}	Standard deviation of intensity per height bin_i
I_{CV}	Coefficient of variation of the intensity values
$I_{i_{CV}}$	Coefficient of variation of intensity per height bin_i
$I_{.99}$	99^{th} percentile intensity value
$I_{.80}$	80^{th} percentile intensity value
$I_{.25}$	25^{th} percentile intensity value
$I_{.05}$	5^{th} percentile intensity value
$I_{.01}$	1^{st} percentile intensity value

TABLE 3.4: Summary statistics for top models predicting pre-fire basal area. N = 51.

Summary Statistics

Model	**Bias**	**Bias(%)**	**RMSE**	**RMSE(%)**	**AIC**	**BIC**
$ln(BA) = \beta_0 + \beta_1 I_{25} + \epsilon$	4.30	10.06	22.04	51.59	-53.72	-49.86
$ln(BA) = \beta_0 + \beta_1 I_{05} + \beta_2 CT + \epsilon$	2.93	6.87	18.85	44.12	-92.54	-86.75
$ln(BA) = \beta_0 + \beta_1 I_{05} + \beta_2 CT + \beta_3 \bar{I}_2 + \epsilon$	2.93	6.85	18.25	42.71	-94.16	-86.43
$ln(BA) = \beta_0 + \beta_1 HT_{CV} + \beta_2 HT_{25} + \beta_3 I_\sigma + \beta_4 I_{95} + \epsilon$	2.03	4.74	16.87	39.48	-92.43	-82.77
$ln(BA) = \beta_0 + \beta_1 HT_{CV} + \beta_2 HT_{25} + \beta_3 I_\sigma + \beta_4 I_{95} + \beta_5 CRS_1 + \epsilon$	2.14	5.00	16.13	37.76	-96.42	-84.83

Cross Validated (Leave-One-Out)

Model	**Bias**	**Bias(%)**	**RMSPE**	**RMSPE(%)**
$ln(BA) = \beta_0 + \beta_1 I_{25} + \epsilon$	4.28	10.01	22.61	52.92
$ln(BA) = \beta_0 + \beta_1 I_{05} + \beta_2 CT + \epsilon$	2.90	6.79	19.50	45.65
$ln(BA) = \beta_0 + \beta_1 I_{05} + \beta_2 CT + \beta_3 \bar{I}_2 + \epsilon$	3.08	7.20	19.51	45.67
$ln(BA) = \beta_0 + \beta_1 HT_{CV} + \beta_2 HT_{25} + \beta_3 I_\sigma + \beta_4 I_{95} + \epsilon$	1.63	3.82	18.89	44.21
$ln(BA) = \beta_0 + \beta_1 HT_{CV} + \beta_2 HT_{25} + \beta_3 I_\sigma + \beta_4 I_{95} + \beta_5 CRS_1 + \epsilon$	1.99	4.67	17.76	41.58

TABLE 3.5: Model summaries including coefficient estimates, t-values, p-values, and variance inflation factors for the best performing regressions found during regression analysis.

Variable	β	Estimate	SE	t-value	Pr(>|t|)	VIF
$Intercept$	β_0	4.59E+00	1.33E-01	34.56	4.55E-36	-
I_{P25}	β_1	-3.28E-02	2.79E-03	-11.74	7.53E-16	-
$Intercept$	β_0	2.71E+00	1.44E-01	18.85	8.02E-24	-
I_{P05}	β_1	-3.81E-02	4.36E-03	-8.73	1.79E-11	1.535
CT	β_2	1.62E-02	1.92E-03	8.44	4.88E-11	1.535
$Intercept$	β_0	2.05E+00	3.82E-01	5.35	2.53E-06	-
I_{P05}	β_1	-4.10E-02	4.54E-03	-9.04	7.60E-12	1.746
CT	β_2	1.96E-02	2.62E-03	7.49	1.48E-09	2.992
$\bar{I}_2$	β_3	7.77E-03	4.18E-03	1.86	6.94E-02	3.325
$Intercept$	β_0	1.53E+00	7.81E-01	1.96	5.64E-02	-
HT_{CV}	β_1	6.10E-01	1.96E-01	3.12	3.15E-03	1.563
HT_{25}	β_2	1.57E-02	2.97E-03	5.29	3.28E-06	1.68
I_σ	β_3	1.38E-01	9.39E-03	14.68	5.61E-19	1.436
I_{95}	β_4	-3.67E-02	5.13E-03	-7.16	5.31E-09	1.376
$Intercept$	β_0	1.29E+00	7.52E-01	1.71	9.40E-02	-
HT_{CV}	β_1	8.16E-01	2.06E-01	3.96	2.60E-04	1.903
HT_{25}	β_2	1.40E-02	2.92E-03	4.78	1.92E-05	1.792
I_σ	β_3	1.24E-01	1.07E-02	11.60	4.10E-15	2.048
I_{95}	β_4	-3.04E-02	5.59E-03	-5.43	2.15E-06	1.793
CRS_1	β_5	-6.24E-07	2.63E-07	-2.37	2.22E-02	3.142

TABLE 3.6: Cross validated summary statistics for models chosen during regression analysis when modeling basal area morality using beta regression and change detection. N = 51.

LiDAR Metrics Only

Model	Bias	Bias(%)	RMSPE	RMSPE(%)
$y = \beta_0 + \beta_1 d\bar{I}_2 + \epsilon$	-0.0305	-7.45	0.2145	52.41
$y = \beta_0 + \beta_1 d\bar{I}_2 + \beta_2 dCRSp_3 + \epsilon$	-0.0180	-4.40	0.1548	37.82
$y = \beta_0 + \beta_1 d\bar{I}_2 + \beta_2 dCRSp_3 + \beta_3 dHT_{max} + \epsilon$	-0.0127	-3.10	0.1293	31.59
$y = \beta_0 + \beta_1 d\bar{I}_2 + \beta_2 dCRSp_3 + \beta_3 dHT_{max} + \beta_4 dHT_{CV} + \epsilon$	-0.0097	-2.37	0.1312	32.06
$y = \beta_0 + \beta_1 d\bar{I}_2 + \beta_2 dCRSp_3 + \beta_3 dHT_{max} + \beta_4 dHT_{CV} + \beta_5 dCRS_1 + \epsilon$	-0.0104	-2.54	0.1259	30.76

Combined Metrics

Model	Bias	Bias(%)	RMSPE	RMSPE(%)
$y = \beta_0 + \beta_1 RdNBR + \epsilon$	-0.0325	-7.94	0.2044	49.94
$y = \beta_0 + \beta_1 RdNBR + \beta_2 dRP_1 + \epsilon$	-0.0199	-4.86	0.1675	40.93
$y = \beta_0 + \beta_1 RdNBR + \beta_2 dRP_1 + \beta_3 HT_{CV_{T0}} + \epsilon$	-0.0181	-4.42	0.1511	36.92
$y = \beta_0 + \beta_1 RdNBR + \beta_2 dRP_1 + \beta_3 HT_{CV_{T0}} + \beta_4 RP_{1_{T0}} + \epsilon$	-0.0092	-2.25	0.1347	32.91
$y = \beta_0 + \beta_1 RdNBR + \beta_2 dRP_1 + \beta_3 HT_{CV_{T0}} + \beta_4 RP_{1_{T0}} + \beta_5 dHT_{.95} + \epsilon$	-0.0102	-2.49	0.1333	32.57

TABLE 3.7: Summary data for the number of hectares by owner, area, and basal area class (m^2 ha^{-1}). We provide pre-fire live, post-fire live, and post-fire dead basal area estimates. Only includes data within burn boundary.

Big Windy - Federal Land Only

Basal Area Class	Pre-fire Living BA	Post-fire Living BA	Post-fire Dead BA
0-30	576.09	1808.91	9112.86
30-60	4245.03	5830.11	1472.04
60-90	3714.66	1924.02	397.08
90+	3118.5	2091.24	672.3

Total Hectares: 11654.28

Douglas Complex - Federal

Basal Area Class	Pre-fire Living BA	Post-fire Living BA	Post-fire Dead BA
0-30	339.12	2370.15	6991.47
30-60	3640.32	4975.56	1935.9
60-90	3732.48	1513.8	577.71
90+	2522.43	1374.84	729.27

Total Hectares: 10234.35

Douglas Complex - Non-Federal

Basal Area Class	Pre-fire Living BA	Post-fire Living BA	Post-fire Dead BA
0-30	1159.02	4176.54	5890.95
30-60	3795.48	3144.6	1978.56
60-90	2053.26	838.44	640.71
90+	2569.23	1417.41	1066.77

Total Hectares: 9576.99

TABLE 3.8: Summary data for estimated basal area mortality across ownership and fire area. Only includes data within burn boundary.

Big Windy - Federal Land Only

Basal Area Class	Basal Area Mortality			
	Min	**Mean**	**Max**	**SD**
0-30	0.00	0.3082	1.00	0.2817
30-60	0.00	0.2440	1.00	0.1870
60-90	0.00	0.2627	1.00	0.1959
90+	0.00	0.2531	1.00	0.2211

Douglas Complex - Federal

Basal Area Class	Basal Area Mortality			
	Min	**Mean**	**Max**	**SD**
0-30	0.00	0.5100	1.00	0.3528
30-60	0.00	0.3267	1.00	0.2602
60-90	0.00	0.3420	1.00	0.2565
90+	0.00	0.3614	1.00	0.2892

Douglas Complex - Non-Federal

Basal Area Class	Basal Area Mortality			
	Min	**Mean**	**Max**	**SD**
0-30	0.00	0.5419	1.00	0.3735
30-60	0.00	0.4290	1.00	0.2969
60-90	0.00	0.4308	1.00	0.3056
90+	0.00	0.4271	1.00	0.3310

Multi-temporal LiDAR Analysis of Landscape-scale Fire Effects in Southwestern Oregon

4 Chapter 4

4.1 General Conclusion

Wildfires are natural and effect ecosystems worldwide. While extreme weather events typically drive severity conditions, we know that certain tree species and bio-physical structures tend to be more resistant to fire-induced mortality. Young trees with thin bark and low crowns have a low probability of survival. In contrast, trees with thick bark, deep roots, and high crown base heights have a higher probability for survival. While remote sensing technology has allowed us to assess post-fire landscape effects, we are often limited by the lack of information related to pre-fire forest attributes. This severely inhibits our ability to understand how pre-fire forest conditions contribute to post-fire effects. We require this information if we intend to improve pro-active management practices to reduce risk and loss. Furthermore, with longer fire seasons and extended drought conditions, our ability to make a significant difference is dwindling.

The Douglas Complex and Big Windy fires offer us a unique opportunity to study fire effects across heterogeneous landscapes and disparate management regimes. The checkerboard landscape provides a perfect layout for us to observe the effect of pre-fire forest structures on post-fire basal area mortality. Wildfires within this region are typically driven by weather, topography, and fuels with complex interactions between each resulting in patches of burned, re-burned, and unburned conditions. Due to the checkerboard landscape, we can assume weather and topography to be constant across ownership.

The first part of our study was to test whether multi-temporal LiDAR data could be used to quantify fire effects using change estimation. We defined fire severity as basal area mortality. Estimates of pre-fire forest conditions were reconstructed by omitting snags (dead before fire) from plot level basal area per hectare calculations. Optical estimates of excessive fire scaring, charring, scorch, and levels of decay (by class: 1-5) were used to determine if a tree was killed by fire or dead before fire. Basal area mortality was derived by dividing observed dead basal area by reconstructed pre-fire conditions.

Stratified height bins were used to examine change within the vertical profile of forest canopies. We ultimately selected 3 height bins, 0-2 (m), 2-10 (m), above 10 meters (bins: 1, 2, 3 respectively), after examining several options. Other bins examined include 2 m intervals and geometric breaks of 0-2, 2-5, 5-10, 10-20, 20-40 m. Two meter height breaks were found to be impractical for Oregon forests and were quickly omitted from further analysis. Geometrics breaks were found to be useful, however, it too was removed due to simplicity and applicability when compared to our chosen method.

Statistical analyses were then performed in R using a variety of methods. All metrics were evaluated as differences from pre-fire (2012) to post-fire (2013) data sets and processed in FUSION. In general, models which used only multi-temporal LiDAR metrics outperformed all others. Combined models performed well, but at the cost of an additional variable. Additionally, combined models required metrics related to change pre-fire conditions. The most correlated predictors to basal area mortality were $RdNBR$ (0.84), $d\bar{I}_2$ (0.80), $dCRSp_1$ (-0.79), and dRP_1 (-0.75).

The second part of our study was consciously targeted at improving our understanding of ecological effects of wildfires. We modeled and mapped pre-fire basal area across the burned landscape. We combined pre-fire basal estimates with basal area mortality obtained from our previous study. This allowed us to illustrate several examples which provide a new perspective of post-fire landscapes. Additionally, several of our methods were used consistently between both studies. For example, height bins, re-constructed pre-fire basal area, and model performance assessments were identical between both studies. Whereas, we only use Leaps and Bounds for variable selection processes when modeling pre-fire basal area, as in this study.

Our results suggest that intensity values are very useful when quantifying basal area using LiDAR metrics over highly variable landscapes. While structural covariates were significant, the inclusion of intensity metrics improved model performance consistently. We also found that models with fewer covariates tended to truncate the range of fitted values, creating a disparate relationship between the range of our observations and model estimates. We therefore selected a model which contains 4 covariates (HT_{cv}, HT_{25}, I_{stdv}, I_{95}), has the lowest bias , and fit the range of our observations the best (observed values: 0.4 - 135 m^2/ha, fitted: 0.06 - 120 m^2/ha).

Our ability to understand these highly complex interactions is only limited by the information we use to assess the landscape. As LiDAR data become more available, opportunities like these will be studied and our ability to quantify, assess, and understand landscape fire effects will continue to improve. While we focus on LiDAR technology, many other sources of remotely sensed information have proven valuable in improving our current knowledge. Likewise, we chose to use simple regression techniques to model and predict mortality rates and basal area due to efficiency and personal ability. There are many other forms of modeling and prediction used for landscape analyses that would prove highly valuable, given this data set. For example, studies are using artificial neural networks and machine learning technology, nearest neighbors, random forest permutations, classification and regression trees (CART), and multivariate adaptive regression splines (MARS) to examine large LiDAR data sets. We are certain that more knowledge will be gained given time and abundant data.

Our research provides several key advancements in our ability to analyze post-fire effects by: 1) providing a well defined measurement of fire severity (basal area mortality) and directly measuring it in the field; 2) quantifying pre-fire forest conditions; 3) modeling proportional response using beta regression; and 4) mapping post-fire, live and dead basal area. Our methods address several key shortcomings such as: 1) ecological interpretation of post-fire effects; 2) ability to capture pre-fire forest conditions; 3) model assumptions and extrapolation when using ordinary least squares for a proportional response; and 4) our ability to manage post-fire forested landscapes, assess risk, and prioritize rehabilitation efforts. As our understanding and technology improves, estimates and interpretations will become more precise, and improvements to pro-active land management will become a reality. Research such as this will be invaluable as we begin to prepare for a future with longer wildfire seasons, increased drought conditions, and expanding populations.

Bibliography

Agee, J. K. (1991). Fire history of Douglas-fir forests in the Pacific Northwest. In: Wildlife and Vegetation of Unmanaged Douglas-fir Forests. U.S. Department of Agriculture, Forest Service, Pacific Northwest Research Station, Portland, OR, pp. 25–33.

Agee, J. K. and C. N. Skinner (2005). Basic principles of forest fuel reduction treatments. *Forest ecology and management 211*(1), 83–96.

Ager, A. A., M. A. Finney, B. K. Kerns, and H. Maffei (2007). Modeling wildfire risk to northern spotted owl (strix occidentalis caurina) habitat in central oregon, USA. *Forest Ecology and Management 246*(1), 45–56.

Ager, A. A., N. M. Vaillant, and M. A. Finney (2010). A comparison of landscape fuel treatment strategies to mitigate wildland fire risk in the urban interface and preserve old forest structure. *Forest Ecology and Management 259*(8), 1556–1570.

Ager, A. A., N. M. Vaillant, and A. McMahan (2013). Restoration of fire in managed forests: a model to prioritize landscapes and analyze tradeoffs. *Ecosphere 4*(2), 1–19.

Allen, C. D., A. K. Macalady, H. Chenchouni, D. Bachelet, N. McDowell, M. Vennetier, T. Kitzberger, A. Rigling, D. D. Breshears, E. T. Hogg, et al. (2010). A global overview of drought and heat-induced tree mortality reveals emerging climate change risks for forests. *Forest ecology and management 259*(4), 660–684.

Attiwill, P. and D. Binkley (2013). Exploring the mega-fire reality: a forest ecology and managementconference. *Forest Ecology and Management* (294), 1–3.

Aubry, K. B. and C. M. Raley (2002). The pileated woodpecker as a keystone habitat modifier in the pacific northwest. *USDA Forest Service General Technical Report PSW-GTR-181*, 257–274.

Betts, M., J. C. Hagar, J. W. Rivers, J. Alexander, K. McGarigal, and B. McComb (2010). Thresholds in forest bird occurrence as a function of the amount of early-seral broadleaf forest at landscape scales. *Ecological Applications 20*(8), 2116–2130.

Bolton, D. K., N. C. Coops, and M. A. Wulder (2015). Characterizing residual structure and forest recovery following high-severity fire in the western boreal of Canada using landsat time-series and airborne lidar data. *Remote Sensing of Environment 163*, 48–60.

Bouvier, M., S. Durrieu, R. A. Fournier, and J.-P. Renaud (2015). Generalizing predictive models of forest inventory attributes using an area-based approach with airborne lidar data. *Remote Sensing of Environment 156*, 322–334.

Bowman, D. M., J. K. Balch, P. Artaxo, W. J. Bond, J. M. Carlson, M. A. Cochrane, C. M. DAntonio, R. S. DeFries, J. C. Doyle, S. P. Harrison, et al. (2009). Fire in the earth system. *science 324*(5926), 481–484.

Bright, B. C., A. T. Hudak, R. E. Kennedy, and A. J. Meddens (2014). Landsat time series and lidar as predictors of live and dead basal area across five bark beetle-affected forests. *IEEE Journal of Selected Topics in Applied Earth Observations and Remote Sensing 7*(8), 3440–3452.

Brosofske, K. D., R. E. Froese, M. J. Falkowski, and A. Banskota (2014). A review of methods for mapping and prediction of inventory attributes for operational forest management. *Forest Science 60*(4), 733–756.

Brown, J. K. and J. K. Smith (2000). Wildland fire in ecosystems: effects of fire on flora. U.S. Department of Agriculture, Forest Service, Gen. Tech. Rep. RMRS-GTR-42-vol. 2. Ogden, UT, 2000. 257 p.

Calcagno, V. (2013). *glmulti: Model selection and multimodel inference made easy.* R package version 1.0.7 https://CRAN.R-project.org/package=glmulti.

Calkin, D. E., K. M. Gebert, J. G. Jones, and R. P. Neilson (2005). Forest service large fire area burned and suppression expenditure trends, 1970–2002. *Journal of Forestry 103*(4), 179–183.

Casas, Á., M. García, R. B. Siegel, A. Koltunov, C. Ramírez, and S. Ustin (2016). Burned forest characterization at single-tree level with airborne laser scanning for assessing wildlife habitat. *Remote Sensing of Environment 175*, 231–241.

Clark, D. A., R. G. Anthony, and L. S. Andrews (2011). Survival rates of northern spotted owls in post-fire landscapes of southwest oregon. *Journal of Raptor Research 45*(1), 38–47.

Clark, K. L., N. Skowronski, M. Gallagher, N. Carlo, M. Farrell, and M. R. Maghirang (2010). Assessment of canopy fuel loading across a heterogeneous landscape using lidar. Joint Fire Sciences Program, Project 10-1-02-14, Final Report, U.S. Department of Agriculture, Forest Service, New Lisbon, NJ & Morgantown, WV, 2010.

Cohen, W. B., Z. Yang, and R. Kennedy (2010). Detecting trends in forest disturbance and recovery using yearly landsat time series: 2. timesynctools for calibration and validation. *Remote Sensing of Environment 114*(12), 2911–2924.

Coops, N. C., T. Hilker, M. A. Wulder, B. St-Onge, G. Newnham, A. Siggins, and J. T. Trofymow (2007). Estimating canopy structure of douglas-fir forest stands from discrete-return lidar. *Trees 21*(3), 295–310.

Cribari-Neto, F. and A. Zeileis (2010). Beta regression in R. *Journal of Statistical Software 34*(2), 1–24. http://www.jstatsoft.org/v34/i02/.

Dale, L. (2009). The true cost of wildfire in the western US. *Western Forestry Leadership Coalition*. Available at: http://wflccenter.org/news_pdf/324_pdf.pdf, Accessed: February 18, 2015.

Dewberry (2016). National enhanced elevation assessment final report - appendix F: Benefit cost analysis process. *Dewberry*, 671–686. Accessed: March 15th, 2016. Available at: http://www.dewberry.com/docs/default-source/documents/neea_final-report_revised-3-29-12.pdf?sfvrsn=0.

Dunn, C. J. and J. D. Bailey (2016). Tree mortality and structural change following mixed-severity fire in Pseudotsuga forests of Oregons western cascades, USA. *Forest Ecology and Management 365*, 107–118.

Duren, O. C., P. S. Muir, and P. E. Hosten (2012). Vegetation change from the Euro-American settlement era to the present in relation to environment and disturbance in southwest Oregon. *Northwest Science 86*(4), 310–328.

Erdody, T. L. and L. M. Moskal (2010). Fusion of lidar and imagery for estimating forest canopy fuels. *Remote Sensing of Environment 114*(4), 725–737.

Escuin, S., R. Navarro, and P. Fernandez (2008). Fire severity assessment by using nbr (normalized burn ratio) and ndvi (normalized difference vegetation index) derived from landsat TM/ETM images. *International Journal of Remote Sensing 29*(4), 1053–1073.

Eskelson, B. N., L. Madsen, J. C. Hagar, and H. Temesgen (2011). Estimating riparian understory vegetation cover with beta regression and copula models. *Forest Science 57*(3), 212–221.

Ferrari, S. and F. Cribari-Neto (2004). Beta regression for modelling rates and proportions. *Journal of Applied Statistics 31*(7), 799–815.

Finney, M. A., R. C. Seli, C. W. McHugh, A. A. Ager, B. Bahro, and J. K. Agee (2008). Simulation of long-term landscape-level fuel treatment effects on large wildfires. *International Journal of Wildland Fire 16*(6), 712–727.

Franklin, J., K. Johnson, D. Churchill, K. Hagmann, D. Johnson, and J. Johnston (2013). Restoration of dry forests in eastern oregon: a field guide. *The Nature Conservancy, Portland, OR*, 202 p.

Franklin, J. F. and D. S. DeBell (1988). Thirty-six years of tree population change in an old-growth pseudotsuga-tsuga forest. *Canadian Journal of Forest Research 18*(5), 633–639.

Franklin, J. F. and K. N. Johnson (2012). A restoration framework for federal forests in the pacific northwest. *Journal of Forestry 110*(8), 429–439.

Franklin, J. F., H. Shugart, and M. E. Harmon (1987). Tree death as an ecological process. *BioScience 37*(8), 550–556.

Franklin, J. F., T. A. Spies, R. Van Pelt, A. B. Carey, D. A. Thornburgh, D. R. Berg, D. B. Lindenmayer, M. E. Harmon, W. S. Keeton, D. C. Shaw, et al. (2002). Disturbances and structural development of natural forest ecosystems with silvicultural implications, using douglas-fir forests as an example. *Forest Ecology and Management 155*(1), 399–423.

Fule, P. Z., A. E. Cocke, T. A. Heinlein, and W. W. Covington (2004). Effects of an intense prescribed forest fire: is it ecological restoration? *Restoration Ecology 12*(2), 220–230.

GAO (2009). Wildland fire management: Federal agencies have taken important steps forward, but additional, strategic action is needed to capitalize on those steps. *Report to Congressional Addressees GAO-09-877*.

García, M., D. Riaño, E. Chuvieco, and F. M. Danson (2010). Estimating biomass carbon stocks for a mediterranean forest in central Spain using lidar height and intensity data. *Remote Sensing of Environment 114*(4), 816–830.

Goerndt, M. E., V. J. Monleon, and H. Temesgen (2010). Relating forest attributes with area-and tree-based light detection and ranging metrics for western oregon. *Western Journal of Applied Forestry 25*(3), 105–111.

Graham, R. T., S. McCaffrey, and T. B. Jain (2004). Science basis for changing forest structure to modify wildfire behavior and severity. Gen. Tech. Re. RMRS-GTR-120. Fort Collins, CO: U.S. Department of Agriculture, Forest Service, Rock Mountain Research Station. 43 p.

Guerra-Hernández, J., M. Tomé, and E. González-Ferreiro (2016). Using low density lidar data to map mediterranean forest characteristics by means of an area-based approach and height threshold analysis. *Revista de Teledetección* (46), 103–117.

Gutschick, V. P. and H. BassiriRad (2003). Extreme events as shaping physiology, ecology, and evolution of plants: toward a unified definition and evaluation of their consequences. *New Phytologist 160*(1), 21–42.

Haas, J. R., D. E. Calkin, and M. P. Thompson (2013). A national approach for integrating wildfire simulation modeling into wildland urban interface risk assessments within the united states. *Landscape and Urban Planning 119*, 44–53.

Habib, A. F., Y.-C. Chang, and D. C. Lee (2009). Occlusion-based methodology for the classification of lidar data. *Photogrammetric Engineering & Remote Sensing 75*(6), 703–712.

Hall, S., I. Burke, D. Box, M. Kaufmann, and J. M. Stoker (2005). Estimating stand structure using discrete-return lidar: an example from low density, fire prone ponderosa pine forests. *Forest Ecology and Management 208*(1), 189–209.

Hallum, D. and S. Parent (2014). Developing a business case for statewide light detection and ranging data collection. *Nebraska Department of Natural Resources. Accessed: May 11, 2016*. Accessed: May 10, 2016. Available at: http://watercenter.unl.edu/PRS/PRS2009/Posters/Hallum%20Doug.pdf.

Halofsky, J., D. Donato, D. Hibbs, J. Campbell, M. D. Cannon, J. Fontaine, J. Thompson, R. Anthony, B. Bormann, L. Kayes, et al. (2011). Mixed-severity fire regimes: lessons and hypotheses from the Klamath-Siskiyou ecoregion. *Ecosphere 2*(4), 1–19.

Hammer, R. B., V. C. Radeloff, J. S. Fried, and S. I. Stewart (2007). Wildland–urban interface housing growth during the 1990s in California, Oregon, and Washington. *International Journal of Wildland Fire 16*(3), 255–265.

Harmon, M. E., J. F. Franklin, F. J. Swanson, P. Sollins, S. Gregory, J. Lattin, N. Anderson, S. Cline, N. G. Aumen, J. Sedell, et al. (1986). Ecology of coarse woody debris in temperate ecosystems. *Advances in ecological research 15*, 133–302.

Hessburg, P. F., R. B. Salter, and K. M. James (2007). Re-examining fire severity relations in pre-management era mixed conifer forests: inferences from landscape patterns of forest structure. *Landscape Ecology 22*(1), 5–24.

Hijmans, R. J. (2016). *raster: Geographic Data Analysis and Modeling*. R package version 2.5-8, https://CRAN.R-project.org/package=raster.

Hoe, M. S., C. Dunn, and H. Temesgen (*in preparation*). Improving landscape scale fire severity estimates using multi-temporal lidar and change estimation. *To be submitted to the International Journal of Wildland Fire*.

Hofner, B., A. Mayr, N. Fenske, and M. Schmid (2016). *gamboostLSS: Boosting Methods for GAMLSS Models*. R package version 1.2-1 http://CRAN.R-project.org/package=gamboostLSS.

Hofner, B., A. Mayr, and M. Schmid (2015). gamboostLSS: An R package for model building and variable selection in the GAMLSS framework. *Journal of Statistical Software*. Accepted.

Hudak, A., P. Morgan, M. Bobbitt, A. Smith, S. Lewis, L. Lentile, P. Robichaud, J. Clark, and R. McKinley (2007). The relationship of multispectral satellite imagery to immediate fire effects. fire ecology 3 (1): 64-90. *Fire Ecology Special Issue Vol 3*, 66.

Hudak, A. T., N. L. Crookston, J. S. Evans, M. J. Falkowski, A. M. Smith, P. E. Gessler, and P. Morgan (2006). Regression modeling and mapping of coniferous forest basal area and tree density from discrete-return lidar and multispectral satellite data. *Canadian Journal of Remote Sensing 32*(2), 126–138.

Hudak, A. T., M. A. Lefsky, W. B. Cohen, and M. Berterretche (2002). Integration of lidar and landsat ETM+ data for estimating and mapping forest canopy height. *Remote sensing of Environment 82*(2), 397–416.

InciWeb, I. I. S. (2013). Douglas Complex Incident Information. *USDA Forest Service*. Accessed on February 13, 2014. Available at: http://inciweb.nwcg.gov/incident/3559/.

Johnson, M. C., M. C. Kennedy, and D. L. Peterson (2011). Simulating fuel treatment effects in dry forests of the western united states: testing the principles of a fire-safe forest. *Canadian Journal of Forest Research 41*(5), 1018–1030.

Jolly, W. M., M. A. Cochrane, P. H. Freeborn, Z. A. Holden, T. J. Brown, G. J. Williamson, and D. M. Bowman (2015). Climate-induced variations in global wildfire danger from 1979 to 2013. *Nature communications 6*.

Kane, V. R., C. A. Cansler, N. A. Povak, J. T. Kane, R. J. McGaughey, J. A. Lutz, D. J. Churchill, and M. P. North (2015). Mixed severity fire effects within the rim fire: relative importance of local climate, fire weather, topography, and forest structure. *Forest Ecology and Management 358*, 62–79.

Kane, V. R., J. A. Lutz, S. L. Roberts, D. F. Smith, R. J. McGaughey, N. A. Povak, and M. L. Brooks (2013). Landscape-scale effects of fire severity on mixed-conifer and red fir forest structure in yosemite national park. *Forest Ecology and Management 287*, 17–31.

Kane, V. R., R. J. McGaughey, J. D. Bakker, R. F. Gersonde, J. A. Lutz, and J. F. Franklin (2010). Comparisons between field-and lidar-based measures of stand structural complexity. *Canadian Journal of Forest Research 40*(4), 761–773.

Keeley, J. E. (2009). Fire intensity, fire severity and burn severity: a brief review and suggested usage. *International Journal of Wildland Fire 18*(1), 116–126.

Kennedy, R. E., Z. Yang, and W. B. Cohen (2010). Detecting trends in forest disturbance and recovery using yearly landsat time series: 1. LandTrendrTemporal segmentation algorithms. *Remote Sensing of Environment 114*(12), 2897–2910.

Key, C. and N. Benson (1999). Measuring and remote sensing of burn severity. In L. F. Neuenschwander and K. C. Ryan (Eds.), *Proceedings joint fire science conference and workshop*, Volume 2, Boise, ID, 15-17 June 1999. University of Idaho and International Association of Wildland Fire, pp. 284.

Key, C. and N. Benson (2005). Landscape assessment: remote sensing of severity, the normalized burn ratio and ground measure of severity, the composite burn index. *FIREMON: Fire effects monitoring and inventory system Ogden, Utah: USDA Forest Service, Rocky Mountain Res. Station*. USDA Forest Service Gen. Tech. Rep. RMRS-GTR-164-CD, LA-1-55.

Kohavi, R. et al. (1995). A study of cross-validation and bootstrap for accuracy estimation and model selection. In *International Joint Conference on Artificial Intelligence*, Volume 14, pp. 1137–1145.

Korhonen, L., K. T. Korhonen, P. Stenberg, M. Maltamo, and M. Rautiainen (2007). Local models for forest canopy cover with beta regression. *Silva Fennica 41*(4), 671.

Lefsky, M. A., W. B. Cohen, A. Hudak, S. A. Acker, and J. Ohmann (1999). Integration of lidar, landsat ETM+ and forest inventory data for regional forest mapping. *International Archives of Photogrammetry and Remote Sensing 32*, 119–126.

Lenihan, J. M., D. Bachelet, R. P. Neilson, and R. Drapek (2008). Response of vegetation distribution, ecosystem productivity, and fire to climate change scenarios for California. *Climatic Change 87*(1), 215–230.

Lentile, L. B., Z. A. Holden, A. M. Smith, M. J. Falkowski, A. T. Hudak, P. Morgan, S. A. Lewis, P. E. Gessler, and N. C. Benson (2006). Remote sensing techniques to assess active fire characteristics and post-fire effects. *International Journal of Wildland Fire 15*(3), 319–345.

Lindenmayer, D. B., W. Blanchard, L. McBurney, D. Blair, S. Banks, G. E. Likens, J. F. Franklin, W. F. Laurance, J. A. Stein, and P. Gibbons (2012). Interacting factors driving a major loss of large trees with cavities in a forest ecosystem. *PLoS One 7*(10), e41864.

Littell, J. S., D. McKenzie, D. L. Peterson, and A. L. Westerling (2009). Climate and wildfire area burned in western US ecoprovinces, 1916–2003. *Ecological Applications 19*(4), 1003–1021.

Littell, J. S., E. E. Oneil, D. McKenzie, J. A. Hicke, J. A. Lutz, R. A. Norheim, and M. M. Elsner (2010). Forest ecosystems, disturbance, and climatic change in washington state, USA. *Climatic change 102*(1-2), 129–158.

Liu, Y., S. L. Goodrick, and J. A. Stanturf (2013). Future US wildfire potential trends projected using a dynamically downscaled climate change scenario. *Forest Ecology and Management 294*, 120–135.

Lumley, T. (2009). *leaps: regression subset selection.* R package version 2.9 https://CRAN.R-project.org/package=leaps.

Mallek, C., H. Safford, J. Viers, and J. Miller (2013). Modern departures in fire severity and area vary by forest type, Sierra Nevada and southern Cascades, California, USA. *Ecosphere 4*(12), 1–28.

Marlon, J. R., P. J. Bartlein, D. G. Gavin, C. J. Long, R. S. Anderson, C. E. Briles, K. J. Brown, D. Colombaroli, D. J. Hallett, M. J. Power, et al. (2012). Long-term perspective on wildfires in the western USA. *Proceedings of the National Academy of Sciences 109*(9), E535–E543.

Mayr, A., N. Fenske, B. Hofner, T. Kneib, and M. Schmid (2012). Generalized additive models for location, scale and shape for high-dimensional data - a flexible approach based on boosting. *Journal of the Royal Statistical Society, Series C - Applied Statistics 61*(3), 403–427.

McBride, J. R. (1983). Analysis of tree rings and fire scars to establish fire history. *Tree-Ring Bulletin*. 43:51-67.

McCombs, J. W., S. D. Roberts, and D. L. Evans (2003). Influence of fusing lidar and multispectral imagery on remotely sensed estimates of stand density and mean tree height in a managed loblolly pine plantation. *Forest Science 49*(3), 457–466.

McGaughey, R. J. (2014). Fusion: Providing fast, efficient, and flexible access to lidar, ifsar and terrain datasets. *Pacific Northwest Research Station, USDA Forest Service*. Accessed: Sept. 28, 2014. Available at: http://forsys.cfr.washington.edu/fusion/fusionlatest.html.

Means, J. E., S. A. Acker, D. J. Harding, J. B. Blair, M. A. Lefsky, W. B. Cohen, M. E. Harmon, and W. A. McKee (1999). Use of large-footprint scanning airborne lidar to estimate forest stand characteristics in the western cascades of oregon. *Remote Sensing of Environment 67*(3), 298–308.

Meigs, G. W., R. E. Kennedy, and W. B. Cohen (2011). A landsat time series approach to characterize bark beetle and defoliator impacts on tree mortality and surface fuels in conifer forests. *Remote Sensing of Environment 115*(12), 3707–3718.

Meng, Q. and R. K. Meentemeyer (2011). Modeling of multi-strata forest fire severity using landsat TM data. *International Journal of Applied Earth Observation and Geoinformation 13*(1), 120–126.

Miller, J. D., E. E. Knapp, C. H. Key, C. N. Skinner, C. J. Isbell, R. M. Creasy, and J. W. Sherlock (2009). Calibration and validation of the relative differenced normalized burn ratio (rdnbr) to three measures of fire severity in the Sierra Nevada and Klamath Mountains, California, USA. *Remote Sensing of Environment 113*(3), 645–656.

Miller, J. D. and H. Safford (2012). Trends in wildfire severity: 1984 to 2010 in the Sierra Nevada, Modoc Plateau, and southern Cascades, California, USA. *Fire Ecology 8*(3), 41–57.

Miller, J. D. and A. E. Thode (2007). Quantifying burn severity in a heterogeneous landscape with a relative version of the delta normalized burn ratio (dnbr). *Remote Sensing of Environment 109*(1), 66–80.

Miller, J. D. and S. R. Yool (2002). Mapping forest post-fire canopy consumption in several overstory types using multi-temporal landsat TM and ETM data. *Remote Sensing of Environment 82*(2), 481–496.

Montealegre, A. L., M. T. Lamelas, M. A. Tanase, and J. de la Riva (2014). Forest fire severity assessment using ALS data in a mediterranean environment. *Remote Sensing 6*(5), 4240–4265.

Morgan, P., R. E. Keane, G. K. Dillon, T. B. Jain, A. T. Hudak, E. C. Karau, P. G. Sikkink, Z. A. Holden, and E. K. Strand (2014). Challenges of assessing fire and burn severity using field measures, remote sensing and modeling. *International Journal of Wildland Fire 23*(8), 1045–1060.

MTBS (2014). Monitoring trends in burn severity. *USDA Forest Service*. Accessed: December 2014. Available at: http://www.mtbs.gov.

Næsset, E. (2007). Airborne laser scanning as a method in operational forest inventory: Status of accuracy assessments accomplished in Scandinavia. *Scandinavian Journal of Forest Research 22*(5), 433–442.

Naficy, C., A. Sala, E. G. Keeling, J. Graham, and T. H. DeLuca (2010). Interactive effects of historical logging and fire exclusion on ponderosa pine forest structure in the northern rockies. *Ecological Applications 20*(7), 1851–1864.

Omernik, J. M. and G. E. Griffith (2014). Ecoregions of the conterminous United States: evolution of a hierarchical spatial framework. *Environmental management 54*(6), 1249–1266.

Osborne, J. W. (2010). Improving your data transformations: Applying the box-cox transformation. *Practical Assessment, Research & Evaluation 15*(12), 1–9.

Perry, D. A., P. F. Hessburg, C. N. Skinner, T. A. Spies, S. L. Stephens, A. H. Taylor, J. F. Franklin, B. McComb, and G. Riegel (2011a). The ecology of mixed severity fire regimes in Washington, Oregon, and Northern California. *Forest Ecology and Management 262*(5), 703–717.

Perry, D. A., P. F. Hessburg, C. N. Skinner, T. A. Spies, S. L. Stephens, A. H. Taylor, J. F. Franklin, B. McComb, and G. Riegel (2011b). The ecology of mixed severity fire regimes in Washington, Oregon, and Northern California. *Forest Ecology and Management 262*(5), 703–717.

Persson, A., J. Holmgren, and U. Söderman (2002). Detecting and measuring individual trees using an airborne laser scanner. *Photogrammetric Engineering and Remote Sensing 68*(9), 925–932.

Popescu, S. C. and R. H. Wynne (2004). Seeing the trees in the forest. *Photogrammetric Engineering & Remote Sensing 70*(5), 589–604.

Poudel, K. P. and H. Temesgen (2016). Developing biomass equations for western hemlock and red alder trees in western oregon forests. *Forests 7*(4), 88.

R Core Team (2016). R: A language and environment for statistical computing. *R Foundation for Statistical Computing*. Vienna, Austria. https://www.R-project.org/.

Reilly, M. J., C. J. Dunn, G. W. Meigs, T. A. Spies, R. E. Kennedy, J. D. Bailey, and K. Briggs (*in review*). Contemporary patterns of burn severity in forests of the pacific northwest (1985-2010). *Forest Ecology and Management*.

Ruediger, L. (2014). Big windy fire report: Wildfire on the wild rogue - an analysis of fire effects, fire suppression impacts and management implications. *Klamath Forest Alliance*. Accessed on: August 13, 2016. Available at:http://www.klamathforestalliance.org/documents/Big_Windy_Fire_Report.pdf.

Ryan, K. C. and W. H. Frandsen (1991). Basal injury from smoldering fires in mature pinus ponderosa laws. *International Journal of Wildland Fire 1*(2), 107–118.

Safford, H. D., J. Miller, D. Schmidt, B. Roath, and A. Parsons (2008). BAER soil burn severity maps do not measure fire effects to vegetation: a comment on Odion and Hanson (2006). *Ecosystems 11*(1), 1–11.

Schoennagel, T., T. T. Veblen, and W. H. Romme (2004). The interaction of fire, fuels, and climate across rocky mountain forests. *BioScience 54*(7), 661–676.

Seidl, R., W. Rammer, and T. A. Spies (2014). Disturbance legacies increase the resilience of forest ecosystem structure, composition, and functioning. *Ecological Applications 24*(8), 2063–2077.

Short, K. (2014). A spatial database of wildfires in the United States, 1992-2011. *Earth System Science Data 6*(1), 1–27.

Skinner, C., A. Taylor, and J. Agee (2006). Klammath mountains bioregion. In N. G. Sugihara, J. W. van Wagtendonk, J. Fites-Kaufmann, K. E. Shaffer, and A. E. Thode, editors, *Fire in California's ecosystems*, pp. 170–194. Berkeley, CA: University of California Press.

Skowronski, N., K. Clark, R. Nelson, J. Hom, and M. Patterson (2007). Remotely sensed measurements of forest structure and fuel loads in the pinelands of New Jersey. *Remote Sensing of Environment 108*(2), 123–129.

Skowronski, N. S., K. L. Clark, M. Duveneck, and J. Hom (2011). Three-dimensional canopy fuel loading predicted using upward and downward sensing lidar systems. *Remote Sensing of Environment 115*(2), 703–714.

Smithson, M. and J. Verkuilen (2006). A better lemon squeezer? maximum-likelihood regression with beta-distributed dependent variables. *Psychological methods 11*(1), 54.

Spies, T. A., M. A. Hemstrom, A. Youngblood, and S. Hummel (2006). Conserving old-growth forest diversity in disturbance-prone landscapes. *Conservation Biology 20*(2), 351–362.

Spies, T. A., J. D. Miller, J. B. Buchanan, J. F. Lehmkuhl, J. F. Franklin, S. P. Healey, P. F. Hessburg, H. D. Safford, W. B. Cohen, R. S. Kennedy, et al. (2010). Underestimating risks to the northern spotted owl in fire-prone forests: Response to Hanson et al. *Conservation Biology 24*(1), 330–333.

Sprugel, D. (1983). Correcting for bias in log-transformed allometric equations. *Ecology 64*(1), 209–210.

Stephens, S. L., N. Burrows, A. Buyantuyev, R. W. Gray, R. E. Keane, R. Kubian, S. Liu, F. Seijo, L. Shu, K. G. Tolhurst, et al. (2014). Temperate and boreal forest mega-fires: characteristics and challenges. *Frontiers in Ecology and the Environment 12*(2), 115–122.

Sumnall, M. J., R. A. Hill, and S. A. Hinsley (2016). Comparison of small-footprint discrete return and full waveform airborne lidar data for estimating multiple forest variables. *Remote Sensing of Environment 173*, 214–223.

Taylor, A. H. and C. N. Skinner (1998). Fire history and landscape dynamics in a late-successional reserve, Klamath Mountains, California, USA. *Forest Ecology and Management 111*(2), 285–301.

Thompson, J. R. and T. A. Spies (2009). Vegetation and weather explain variation in crown damage within a large mixed-severity wildfire. *Forest Ecology and Management 258*(7), 1684–1694.

Thompson, J. R. and T. A. Spies (2010). Factors associated with crown damage following recurring mixed-severity wildfires and post-fire management in southwestern oregon. *Landscape Ecology 25*(5), 775–789.

Thompson, M. P., J. R. Haas, M. A. Finney, D. E. Calkin, M. S. Hand, M. J. Browne, M. Halek, K. C. Short, and I. C. Grenfell (2015). Development and application of a probabilistic method for wildfire suppression cost modeling. *Forest Policy and Economics 50*, 249–258.

Turner, M. G., W. L. Baker, C. J. Peterson, and R. K. Peet (1998). Factors influencing succession: lessons from large, infrequent natural disturbances. *Ecosystems 1*(6), 511–523.

Turner, M. G., W. H. Romme, and D. B. Tinker (2003). Surprises and lessons from the 1988 Yellowstone fires. *Frontiers in Ecology and the Environment 1*(7), 351–358.

Verbyla, D. L., E. S. Kasischke, and E. E. Hoy (2008). Seasonal and topographic effects on estimating fire severity from landsat TM/ETM+ data. *International Journal of Wildland Fire 17*(4), 527–534.

Vines, R. (1968). Heat transfer through bark, and the resistance of trees to fire. *Australian Journal of Botany 16*(3), 499–514.

Vogeler, J. C., A. T. Hudak, L. A. Vierling, J. Evans, P. Green, and K. T. Vierling (2014). Terrain and vegetation structural influences on local avian species richness in two mixed-conifer forests. *Remote Sensing of Environment 147*, 13–22.

Vogeler, J. C., Z. Yang, and W. B. Cohen (2016). Mapping post-fire habitat characteristics through the fusion of remote sensing tools. *Remote Sensing of Environment 173*, 294–303.

Warton, D. I. and F. K. C. Hui (2011). The arcsine is asinine: the analysis of proportions in ecology. *Ecology 92*(1), 3–10. http://dx.doi.org/10.1890/10-0340.1.

Westerling, A., B. Bryant, H. Preisler, T. Holmes, H. Hidalgo, T. Das, and S. Shrestha (2011). Climate change and growth scenarios for California wildfire. *Climatic Change 109*(1), 445–463.

Westerling, A. L., H. G. Hidalgo, D. R. Cayan, and T. W. Swetnam (2006). Warming and earlier spring increase western US forest wildfire activity. *Science 313*(5789), 940–943.

Whittier, T. R. and A. N. Gray (2016). Tree mortality based fire severity classification for forest inventories: A pacific northwest national forests example. *Forest Ecology and Management 359*, 199–209.

Wimberly, M. C., M. A. Cochrane, A. D. Baer, and K. Pabst (2009). Assessing fuel treatment effectiveness using satellite imagery and spatial statistics. *Ecological Applications 19*(6), 1377–1384.

Woods, M., D. Pitt, M. Penner, K. Lim, D. Nesbitt, D. Etheridge, and P. Treitz (2011). Operational implementation of a lidar inventory in boreal Ontario. *The Forestry Chronicle 87*(4), 512–528.

Wright, H. A. and A. W. Bailey (1982). *Fire ecology: United States and southern Canada.* John Wiley & Sons. pp 15–22.

Wulder, M., J. White, F. Alvarez, T. Han, J. Rogan, and B. Hawkes (2009). Characterizing boreal forest wildfire with multi-temporal landsat and lidar data. *Remote Sensing of Environment 113*(7), 1540–1555.

Wulder, M. A., T. Han, J. C. White, T. Sweda, and H. Tsuzuki (2007). Integrating profiling lidar with landsat data for regional boreal forest canopy attribute estimation and change characterization. *Remote Sensing of Environment 110*(1), 123–137.

Wulder, M. A., J. C. White, R. F. Nelson, E. Næsset, H. O. Ørka, N. C. Coops, T. Hilker, C. W. Bater, and T. Gobakken (2012). Lidar sampling for large-area forest characterization: A review. *Remote Sensing of Environment 121*, 196–209.

Yan, W. Y. and A. Shaker (2016). Reduction of striping noise in overlapping lidar intensity data by radiometric normalization. *International Archives of the Photogrammetry, Remote Sensing & Spatial Information Sciences 41.*

Young, J. (2014). Maine geolibrary: Cost benefit analysis and typical uses of lidar data. *Maine Library of Geographic Information*. Accessed: May 11, 2016. Available at: http://www.maine.gov/geolib/LiDAR.html.

Zeileis, A. and T. Hothorn (2002). Diagnostic checking in regression relationships. *R News 2*(3), 7–10. http://CRAN.R-project.org/doc/Rnews/.

APPENDICES

A Acronyms

AIC: Akaike information criterion

ALS: airborne laser scanning device or system

ArcMap: GIS software

BIC: Bayesian information criterion

BLM: Bureau of Land Management

CBD: canopy bulk density (kg/m)

CFW: canopy fuel weight (kg)

CRS: canopy reflection sum

CRSp: proportion of CRS

DEM: digital elevation model

dNBR: difference in NBR

HS: high severity

LiDAR: light detection and ranging

LS: low severity

MS: moderate severity

MTBS: Monitoring Trends in Burn Severity

NBR: normalized burn ratio

RdNBR: relative difference in NBR

RMSE: root mean square error

RMSPE: root mean square prediction error.

VIF: variance inflation factor

B Definitions

basal area *the average amount of area occupied by tree stems per hectare.*

burn severity *the proportion of fire-induced basal area mortality.*

canopy bulk density *The mass of foliage, branches, and twigs above ground per unit volume.*

canopy fuel weight *The total mass of above ground foliage.*

canopy reflection sum *As defined by Means et. al. (1999).*

$$\frac{\sum_{i=1}^{N} I_i}{A} \tag{4.1}$$

Where N is the number of observations, A is the area being sampled, and I_i is the intensity value of the i^{th} observation.

canopy reflection sum(%)

$$CRSp_i = \frac{CRS_i}{CRS_T} = \frac{\frac{N_i * \bar{I}_i}{A}}{\frac{N * \bar{I}}{A}} = \frac{N_i}{N} * \frac{\bar{I}_i}{\bar{I}} \tag{4.2}$$

Where CRS_i is the CRS for the observed height bin, CRS_T is the total CRS, and $CRS_i(\%)$ is the ratio of the two. $CRS_i(\%)$ is now expressed as a product of two ratios. The first is the proportion of returns within the observed height bin. The second is the proportion of intensity within the observed height bin.

FUSION *LiDAR processing software developed by the USDA Forest Service.*

mortality *death.*

C Additional Plot Information

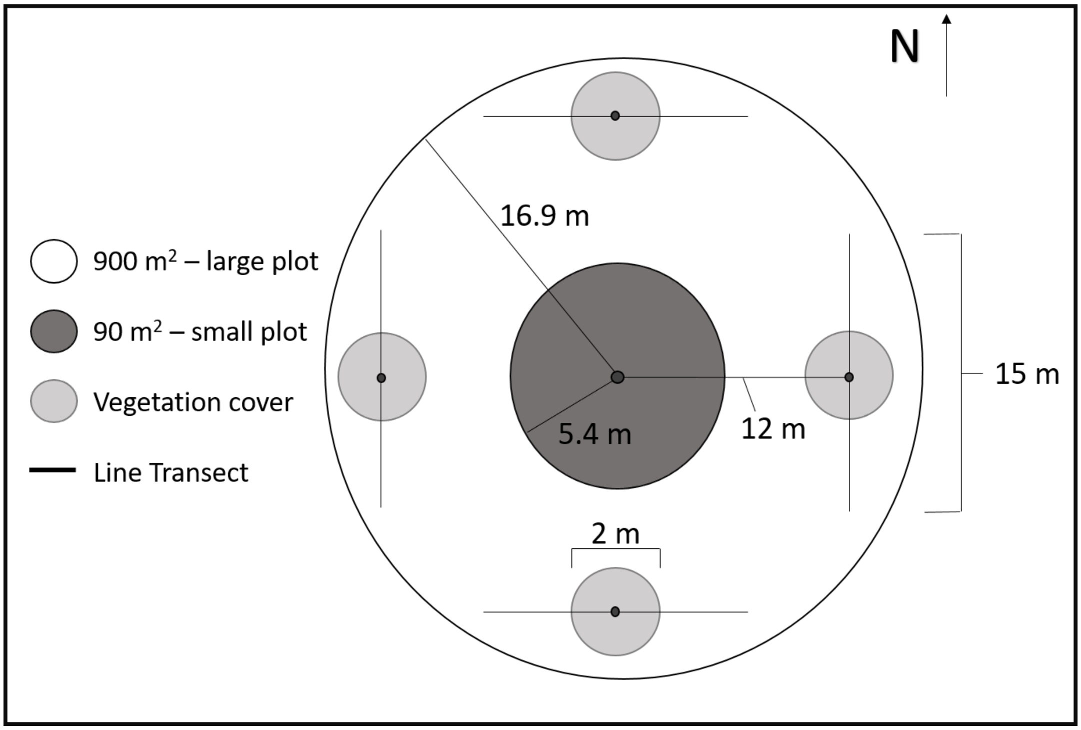

FIGURE C.1: Illustration of calibration plots installed 2-years post-fire. All trees above 10cm were mapped and measured within the large plot. Trees between 2.54 - 10 cm were mapped and measured in the small plot. Additional measurements were taken for fuels, understory vegetation composition, and vegetation cover.

TABLE C.1: Definitions for Table C.2 which summarizes the specific topographical attributes, observed basal area, and RdNBR values. Nested fixed radius plots were used to measure trees (>10 cm - full plot, 2.54-10 cm subplot), snags, shrubs, coarse woody debris (1000 hr), and fine fuels (1, 10, 100 hr). The total area sampled (full plot) is $900m^2$; the size of a LandSAT pixel. UT-20 and UT-27 are low severity and within the burn boundary

Variable	**Definition**
Plot (prefix)	Severity: High(H), Mod-High(MH), Mod-Low(ML), Low(L), Unburned(U)*
Plot (suffix)	Height Class: $> 30m$ (T), $< 30m$ (S)
Area	Big Windy (BW), Dad's Creek (DC), Rabbit Mountain (RM), Outside (OUT)
D(m)	Distance from plot to pixel center derived from MTBS data in meters
Asp	Aspect (°)
Slp	Slope (°)
Elev	Elevation (m)
RdNBR	Relative difference in normalized burn ratio (obtained from MTBS data)
BA_T	Total basal area observed on the plot including live and dead (m^2/ha)
BA_L	Basal area of surviving trees (m^2/ha)
BA_D	Basal area of fire-killed trees (m^2/ha)
M	Proportion of basal area mortality (range: 0-1)

TABLE C.2: Summary of field data taken during the Summer of 2015. Definitions for each attribute are provided in Table C.1. *UT-20 and UT-27 are low severity and inside the burn boundary. Basal area in square meters per hectare.

Plot	Area	D(m)	Asp°	Slp°	Elev(m)	RdNBR	BA_T	BA_L	BA_D	M
HS-10	RM	0.36	139.84	22.64	542.50	919	3.88	0.00	3.88	1.00
HS-22	DC	1.20	271.62	19.77	991.50	813	7.61	1.34	6.27	0.82
HS-23	BW	2.01	137.08	26.21	658.40	734	14.56	4.39	10.16	0.70
HS-24	BW	2.02	335.63	32.19	1074.10	850	0.41	0.00	0.41	1.00
HS-25	DC	1.75	244.90	24.43	358.40	942	9.75	2.66	7.09	0.73
HS-26	DC	3.04	4.71	30.31	486.80	900	2.45	0.00	2.45	1.00
HS-27	DC	1.08	322.73	20.56	684.00	729	14.79	0.00	14.79	1.00
HT-12	RM	1.44	130.40	18.35	495.60	812	13.95	3.27	10.68	0.77
HT-14	RM	9.09	132.47	15.93	423.70	704	33.79	12.44	21.34	0.63
HT-143	BW	11.86	126.30	30.25	1054.30	1018	58.64	0.00	58.64	1.00
HT-182	BW	4.43	82.90	16.36	1097.30	1062	77.91	0.00	77.91	1.00
HT-190	BW	8.64	176.94	27.43	1223.20	846	135.20	0.00	135.20	1.00
HT-204	BW	3.54	95.18	19.23	1072.00	919	7.58	0.00	7.58	1.00
LS-12	DC	6.08	235.63	28.10	539.80	346	42.77	39.33	3.44	0.08
LS-28	DC	2.76	192.54	24.87	604.70	188	51.26	47.03	4.24	0.08
LS-29	DC	3.22	223.12	14.96	1044.90	181	74.52	28.16	46.35	0.62
LS-30	DC	2.84	46.73	15.77	486.20	132	46.08	44.62	1.45	0.03
LT-10	RM	7.56	275.89	24.36	557.20	94	79.03	75.64	3.39	0.04
LT-14	RM	2.88	163.90	34.86	784.60	176	52.12	45.89	6.23	0.12
LT-21	RM	0.45	205.72	4.75	522.40	104	57.77	52.86	4.91	0.08
LT-26	DC	0.80	24.81	19.20	633.10	150	61.03	38.60	22.43	0.37
LT-29	DC	7.04	319.49	33.46	1069.80	62	57.18	50.39	6.80	0.12
MHS-17	RM	3.98	142.71	25.16	386.20	519	10.82	0.00	10.82	1.00
MHS-20	RM	1.83	160.77	20.13	605.60	499	14.15	14.15	0.00	0.00
MHS-581	BW	6.37	61.75	6.22	1178.40	508	93.80	15.89	77.91	0.83
MHS-587	BW	5.55	321.39	18.12	1178.10	515	2.89	2.27	0.63	0.22
MHT-17	BW	1.36	258.94	12.61	1034.20	413	34.73	16.62	18.11	0.52
MHT-22	RM	1.98	164.80	22.12	660.80	615	85.87	65.24	20.63	0.24
MHT-28	DC	13.24	293.51	19.90	673.60	614	24.75	21.77	2.98	0.12
MHT-7	BW	2.40	99.26	17.88	632.50	512	21.66	13.35	8.31	0.38

Continued on next page

TABLE C.2 – continued from previous page

Plot	Area	D(m)	Asp°	Slp°	Elev(m)	RdNBR	BA_T	BA_L	BA_D	M
MLS-14	BW	3.04	0.39	18.07	882.40	291	20.10	14.77	5.33	0.27
MLS-3	RM	1.42	176.19	20.59	819.90	246	78.24	35.03	43.21	0.55
MLS-6	RM	2.82	174.71	29.20	649.80	302	53.89	28.74	25.15	0.47
MLS-767	BW	7.26	121.48	10.13	1047.30	466	45.41	23.99	21.42	0.47
MLS-795	BW	4.93	146.83	14.58	1168.30	340	45.09	27.85	17.24	0.38
MLS-819	BW	6.11	345.35	15.36	1057.70	534	21.89	16.97	4.91	0.22
MLS-951	BW	5.30	325.04	32.89	1122.60	382	44.84	28.82	16.02	0.36
MLT-10	DC	1.42	87.90	22.38	778.20	360	37.12	25.42	11.70	0.32
MLT-4	RM	1.55	199.26	29.55	598.90	363	52.83	43.63	9.20	0.17
MLT-7	RM	4.34	0.72	58.32	716.60	399	57.01	30.81	26.21	0.46
MLT-9	RM	15.82	151.70	20.36	667.80	124	28.02	26.53	1.49	0.05
US-107	OUT	1.90	166.02	21.31	576.40	-3	62.59	62.59	1.63	0.03
US-112	OUT	2.85	175.14	31.33	640.40	16	9.86	9.65	0.46	0.05
US-158	OUT	0.90	131.57	23.72	297.80	-84	20.24	20.24	2.43	0.12
UT-128	OUT	2.07	149.49	28.20	747.70	-5	10.61	10.61	0.00	0.00
UT-145	OUT	2.55	170.31	23.24	475.50	-4	41.99	41.99	0.36	0.01
UT-148	OUT	6.21	170.07	9.57	527.60	-30	90.78	90.08	14.05	0.15
UT-151	OUT	10.49	11.00	4.11	460.90	5	53.40	53.40	0.18	0.00
UT-153	OUT	1.13	43.47	15.80	513.90	3	30.64	30.64	0.27	0.01
UT-20	BW	10.90	357.71	6.13	892.10	59	68.89	64.86	4.03	0.06
UT-27	BW	5.24	67.92	33.75	1303.30	43	114.57	99.41	15.15	0.13

TABLE C.3: Additional information for plot measurements taken. [1] Small and large end for coarse wood larger than 15cm. [2] Trees Only. [3] Shrubs only. [4] Includes vegetation, litter, bare soil, rock, and coarse wood.

Variable	**Full Plot**	**Subplot**	**Regen**	**Transect**
Plot radius or Transect length (m)	16.9	5.6	2	15
Species	*	*	*	*
Diameter[1] (cm)	*	*		*
Height (m)	*	*		
Distance (m)	*	*		
Azimuth (°)	*	*		
Slope (°)				*
Height to live crown[2] (m)	*	*		
Crown width[3] (m)		*		
Cover estimates[4] (%)			*	
Scorch Length (m)	*	*		
Log length (m, 1000hr)	*	*		*
Tree Condition (Live or Dead)	*	*		
Decay class (1-5)	*	*		*
Top Condition (Broken, Fork, Fallen)	*	*		
Fire-killed (Y/N)	*	*		
Foliage present (Y/N)	*	*		
Fuels transect (1hr, 10hr, 100hr)				*
Regeneration (10cm height classes)			*	
Duff & Litter depth[5] (cm)				*

TABLE C.4: List of plot center coordinates for calibration plots installed during the Summer of 2015. Projection: Oregon Statewide Lambert Conformal Conic. Horizontal and Vertical datum: NAD83 (2011), NAVD88 (Geoid 12A).

Plot	**Area**	**X**	**Y**	**Plot**	**Area**	**X**	**Y**
HS-10	RM	482006.45	406644.69	MHS-587	BW	431828.61	329576.85
HS-22	DC	488505.91	357034.58	MHT-17	BW	450120.37	313333.35
HS-23	BW	433588.54	354971.83	MHT-22	RM	475517.20	388629.50
HS-24	BW	425910.55	353490.74	MHT-28	DC	511789.05	359976.09
HS-25	DC	504153.05	353488.51	MHT-7	BW	433585.84	354077.90
HS-26	DC	512725.79	351130.63	MLS-14	BW	420894.06	352317.74
HS-27	DC	509760.95	349948.17	MLS-3	RM	494702.51	403981.99
HT-12	RM	478466.39	401628.20	MLS-6	RM	481707.09	384506.01
HT-14	RM	483751.78	393639.33	MLS-767	BW	459880.22	324837.64
HT-143	BW	425352.98	349650.90	MLS-795	BW	462534.91	323969.94
HT-182	BW	429461.61	345516.21	MLS-819	BW	456632.92	323075.67
HT-190	BW	423275.66	344633.66	MLS-951	BW	445702.57	311850.36
HT-204	BW	422667.76	341974.44	MLT-10	DC	511531.16	381247.26
LS-12	DC	502073.38	349966.36	MLT-4	RM	493815.12	406049.31
LS-28	DC	513017.10	384505.07	MLT-7	RM	493517.32	393048.11
LS-29	DC	483787.78	370319.23	MLT-9	RM	471052.27	383950.11
LS-30	DC	509462.87	366773.80	US-107	OUT	502670.47	392764.58
LT-10	RM	491156.21	406619.48	US-112	OUT	468726.49	378599.27
LT-14	RM	492628.56	403399.71	US-158	OUT	510356.41	342865.51
LT-21	RM	489092.90	391585.91	UT-128	OUT	501785.09	404573.10
LT-26	DC	512718.10	383315.63	UT-145	OUT	492632.35	390692.13
LT-29	DC	496188.81	368531.77	UT-148	OUT	496750.91	389514.80
MHS-17	RM	482020.12	404869.95	UT-151	OUT	491748.18	386894.66
MHS-20	RM	492340.79	391885.97	UT-153	OUT	492935.53	383905.55
MHS-581	BW	429172.97	329866.31	UT-20	BW	428841.84	358545.98
				UT-27	BW	421491.81	247287.42